Molecular dynamics simulation of uni and bi-modal semicrystalline polymers : Nucleation, chain topology and microstructure

Zengqiang Zhai

N°d'ordre NNT: 2019LYSEI069

THESE de DOCTORAT DE L'UNIVERSITE DE LYON
opérée au sein de
L'Institut National des Sciences Appliquées de Lyon

Ecole Doctorale N° EDA 034
Matériaux de Lyon

Spécialité de doctorat: Matériaux

Soutenue publiquement le 30/09/2019, par :
Zengqiang ZHAI

Molecular dynamics simulation of uni and bi-modal semicrystalline polymers: nucleation, chain topology and microstructure

---

Devant le jury composé de :

BARRAT, Jean-Louis	Professeur	Université Grenoble Alpes	Rapporteur
BASCHNAGEL, Jörg	Professeur	Université de Strasbourg	Rapporteur
SOMMER, Jens-Uwe	Professeur	Technische Universität Dresden	Examinateur
CASTAGNET, Sylvie	Directrice de Recherche	Institut Pprime (CNRS)	Examinatrice
LAME, Olivier	Professeur	INSA-LYON	Directeur de thèse
FUSCO, Claudio	Maître de conférences	INSA-LYON	Encadrant
PEREZ, Michel	Professeur	INSA-LYON	Invité
MORTHOMAS, Julien	Maître de conférences	INSA-LYON	Invité

Département FEDORA – INSA Lyon - Ecoles Doctorales – Quinquennal 2016-2020

SIGLE	ECOLE DOCTORALE	NOM ET COORDONNEES DU RESPONSABLE
CHIMIE	**CHIMIE DE LYON** **http://www.edchimie-lyon.fr** Sec. : Renée EL MELHEM Bât. Blaise PASCAL, 3e étage **secretariat@edchimie-lyon.fr** INSA : R. GOURDON	M. Stéphane DANIELE Institut de recherches sur la catalyse et l'environnement de Lyon IRCELYON-UMR 5256 Équipe CDFA 2 Avenue Albert EINSTEIN 69 626 Villeurbanne CEDEX **directeur@edchimie-lyon.fr**
E.E.A.	**ÉLECTRONIQUE, ÉLECTROTECHNIQUE, AUTOMATIQUE** **http://edeea.ec-lyon.fr** Sec. : M.C. HAVGOUDOUKIAN **ecole-doctorale.eea@ec-lyon.fr**	M. Gérard SCORLETTI École Centrale de Lyon 36 Avenue Guy DE COLLONGUE 69 134 Écully Tél : 04.72.18.60.97 Fax 04.78.43.37.17 **gerard.scorletti@ec-lyon.fr**
E2M2	**ÉVOLUTION, ÉCOSYSTÈME, MICROBIOLOGIE, MODÉLISATION** **http://e2m2.universite-lyon.fr** Sec. : Sylvie ROBERJOT Bât. Atrium, UCB Lyon 1 Tél : 04.72.44.83.62 INSA : H. CHARLES **secretariat.e2m2@univ-lyon1.fr**	M. Philippe NORMAND UMR 5557 Lab. d'Ecologie Microbienne Université Claude Bernard Lyon 1 Bâtiment Mendel 43, boulevard du 11 Novembre 1918 69 622 Villeurbanne CEDEX **philippe.normand@univ-lyon1.fr**
EDISS	**INTERDISCIPLINAIRE SCIENCES-SANTÉ** **http://www.ediss-lyon.fr** Sec. : Sylvie ROBERJOT Bât. Atrium, UCB Lyon 1 Tél : 04.72.44.83.62 INSA : M. LAGARDE **secretariat.ediss@univ-lyon1.fr**	Mme Emmanuelle CANET-SOULAS INSERM U1060, CarMeN lab, Univ. Lyon 1 Bâtiment IMBL 11 Avenue Jean CAPELLE INSA de Lyon 69 621 Villeurbanne Tél : 04.72.68.49.09 Fax : 04.72.68.49.16 **emmanuelle.canet@univ-lyon1.fr**
INFOMATHS	**INFORMATIQUE ET MATHÉMATIQUES** **http://edinfomaths.universite-lyon.fr** Sec. : Renée EL MELHEM Bât. Blaise PASCAL, 3e étage Tél : 04.72.43.80.46 **infomaths@univ-lyon1.fr**	M. Luca ZAMBONI Bât. Braconnier 43 Boulevard du 11 novembre 1918 69 622 Villeurbanne CEDEX Tél : 04.26.23.45.52 **zamboni@maths.univ-lyon1.fr**
Matériaux	**MATÉRIAUX DE LYON** **http://ed34.universite-lyon.fr** Sec. : Stéphanie CAUVIN Tél : 04.72.43.71.70 Bât. Direction **ed.materiaux@insa-lyon.fr**	M. Jean-Yves BUFFIÈRE INSA de Lyon MATEIS - Bât. Saint-Exupéry 7 Avenue Jean CAPELLE 69 621 Villeurbanne CEDEX Tél : 04.72.43.71.70 Fax : 04.72.43.85.28 **jean-yves.buffiere@insa-lyon.fr**
MEGA	**MÉCANIQUE, ÉNERGÉTIQUE, GÉNIE CIVIL, ACOUSTIQUE** **http://edmega.universite-lyon.fr** Sec. : Stéphanie CAUVIN Tél : 04.72.43.71.70 Bât. Direction **mega@insa-lyon.fr**	M. Jocelyn BONJOUR INSA de Lyon Laboratoire CETHIL Bâtiment Sadi-Carnot 9, rue de la Physique 69 621 Villeurbanne CEDEX **jocelyn.bonjour@insa-lyon.fr**
ScSo	**ScSo*** **http://ed483.univ-lyon2.fr** Sec. : Véronique GUICHARD INSA : J.Y. TOUSSAINT Tél : 04.78.69.72.76 **veronique.cervantes@univ-lyon2.fr**	M. Christian MONTES Université Lyon 2 86 Rue Pasteur 69 365 Lyon CEDEX 07 **christian.montes@univ-lyon2.fr**

*ScSo : Histoire, Géographie, Aménagement, Urbanisme, Archéologie, Science politique, Sociologie, Anthropologie

Acknowledgement

I would like first to thank my supervisors: Olivier Lame, Michel Perez, Julien Morthomas and Claudio Fusco for their support and help throughout this thesis. Thanks for their patience and advice. I learned a lot, and improved a lot.

Many thanks to the rapporteurs and jury members for reading this manuscript in a very short time, and for participating in the defense.

Many thanks also to all my colleagues from the Matéis laboratory. Thank you for your company. Thank you for the outings and the good atmosphere. During the four years, the thesis had its ups and downs, but the atmosphere was always at the top.

Many thanks to my friends who hang out with me and made lift in Lyon colorful and full of joy.

Many thanks to Chinese Scholarship Council (CSC) for providing a grant for my studies in France.

Finally, I would like to thank my parents, my sister, and my wife for the eternal spiritual support.

Table of contents

Abstract

Semicrystalline polymers (such as polyethylene, polylactic acid, polyamide, *etc*.) are used in a wide range of application (such as automotive, pipes, gearing, *etc.*) due to promoted mechanical properties. There is strong link between the mechanical properties and microstructure of semicrystalline polymer, such as bimodality, molecular topology (the way polymer chains pass through crystalline and amorphous phases), chain entanglements, lamellar thickness, temperature, and so on. However, these microstructure cannot be access quantitatively in experiment. There exists some molecular dynamics investigations, but the homogeneous crystallization is very difficult to achieve and not extensively discussed. Thus, the crystallization mechanism of polymers and the dependence of microstructure remain relatively unclear and controversy.

In this thesis, we have performed the homogeneous crystallization of polymers using a coarse-grained molecular dynamics (CG-MD) model published in our previous article [1], which favors chain alignment and crystallization. The main objective of this thesis is to use CG-MD simulation technique to provide more insights of the homogeneous nucleation and crystal growth behavior of bimodal and unimodal MWD polymers, the influence of bimodality on the molecular topology (loop, tie, cilia) and entanglement concentration, the chain disentanglement process and its influence on lamellar thickening as well the temperature dependence.

First of all, the crystallization behavior and the molecular topology of bimodal molecular weight distribution polymers has been studied using the CG-MD model with varying weight fraction of short and long chains. Extensive simulations of isothermal crystallization have been performed. The interfacial free energy and the incubation time have been obtained using a mean first-passage time analysis (a simulation method to calculate the critical nucleus and incubation time by tracing the nucleus size with time). It has been found that the incubation time has a

maximum value at 30% of long chains which results from the conflicting effect of interfacial free energy and mobility of chain segments. Intra- and inter- molecular nucleation modes are also found to be dependent of molecular weight. It is also discovered that the concentration of loop and tie segments increases with increasing weight fraction of long chains.

Secondly, the homogeneous nucleation of bimodal and unimodal molecular weight distribution (MWD) polymers with equivalent average molecular weight has been addressed. A Growing Probability Method has been proposed to determine the critical nuclei, which is used to calculate the free energy barrier of forming nuclei. This method traces the sizes of all the nuclei growing and shrinking in the process of isothermal treatment, and obtains the critical nucleus size when the probabilities of growing and shrinking are equivalent (*i.e.* 50%). The validity of the classical nucleation theory has been confirmed through the comparison of nucleation rate from molecular dynamics simulations and from classical nucleation theory. Compared with unimodal system, the bimodal system exhibits lower interfacial free energy and consequently lower free energy barrier for nucleation, while the two systems have similar activation energy for diffusion.

Thirdly, the isothermal crystallization of bimodal and unimodal molecular weight distribution (MWD) polymers with the equivalent average molecular weight. Primitive path analysis has been performed, the entanglement evolution has been continuously monitored during the process of crystallization. A quantitative correlation between the degree of disentanglement and crystallinity. The scenario of the whole process of chain disentangling and lamellar thickening in the manner of chain sliding diffusion has been demonstrated. Compared with unimodal system, the disentanglement degree of the bimodal system is more delayed than its crystallinity due to the slower chain sliding of long chain component; the bimodal system reaches a greater lamellar thickness at all temperatures due to the promotion of higher chain sliding mobility of short chain component.

Finally, existing molecular dynamics simulations keep the same interaction potential in both crystalline and amorphous domains, which makes these models not sufficiently realistic. We have built a more realistic semicrystalline polymer model with a larger well depth of Lennard-Jones (LJ) potential for the crystalline phase than the amorphous phase. The validity of this model is confirmed through the promoted stability and elevated yielding stress in the process of tensile test. The evolution of molecular topology and crystalline morphology are monitored during mechanical deformation. This is just an initial test of the idea adapting different LJ potential in crystalline and amorphous phase. Deeper and more extensive work will be done base on this idea in the future.

Résumé étendu

Les polymères semi-cristallins (comme le polyéthylène, l'acide polylactique, le polyamide, *etc*.) sont utilisés dans un large éventail d'applications (automobiles, tuyaux, engrenages, *etc*.) en raison de propriétés mécaniques promues. Il existe un lien étroit entre les propriétés mécaniques et la microstructure du polymère semi-cristallin, comme la bimodalité, la topologie moléculaire (la façon dont les chaînes de polymères passent à travers les phases cristallines et amorphes), les enchevêtrements de chaînes, l'épaisseur lamellar, température, et ainsi de suite. Cependant, ces microstructures ne peuvent pas être accédées quantitativement à l'expérience. Il existe quelques études de dynamique moléculaire, mais la cristallisation homogène est très difficile à réaliser et n'a pas fait l'objet de discussions approfondies. Ainsi, le mécanisme de cristallisation des polymères et la dépendance de la microstructure restent relativement flous et controversés. Le premier chapitre est une introduction de la recherche générale, qui intègre des polymères semi-cristallins, des nucléations et de la cinétique de croissance cristalline, la théorie classique de la nucléation et des simulations numériques.

Dans cette thèse, nous avons effectué la cristallisation homogène des polymères à l'aide d'un modèle de dynamique moléculaire à grain grossier (CG-MD) publié dans notre article précédent, qui favorise l'alignement des chaînes et la cristallisation. L'objectif principal de cette thèse est d'utiliser la technique de simulation CG-MD pour fournir plus d'informations sur la nucléation homogène et le comportement de croissance cristalline des polymères MWD bimodaux et unimod, l'influence de la bimodalité sur la topologie moléculaire (boucle, cravate, cils) et la concentration d'enchevêtrement, le processus de démêlage de chaîne et son influence sur l'épaississement lamellar aussi bien que la dépendance de température.

Tout d'abord, le comportement de cristallisation et la topologie moléculaire des polymères bimodaux de répartition du poids moléculaire ont été étudiés à l'aide du modèle CG-MD avec

une fraction de poids variable des chaînes courtes et longues. Des simulations étendues de cristallisation isothermale ont été effectuées. L'énergie libre interfaciale et le temps d'incubation ont été obtenus à l'aide d'une analyse moyenne du temps de premier passage (méthode de simulation retraçant la taille du noyau avec le temps). Il a été constaté que le temps d'incubation a une valeur maximale à 30% des longues chaînes qui résulte de l'effet contradictoire de l'énergie libre interfaciale et la mobilité des segments de chaîne. Les modes de nucléation intra- et intermoléculaires sont également dépendants du poids moléculaire. On découvre également que la concentration de segments de boucle et de cravate augmente avec la fraction de poids croissante des longues chaînes.

Deuxièmement, la nucléation homogène des polymères de répartition du poids moléculaire bimodale et unimodal (MWD) avec un poids moléculaire moyen équivalent a été abordée. Une méthode de probabilité croissante a été proposée pour déterminer les noyaux critiques, qui est utilisé pour calculer la barrière d'énergie libre de former des noyaux. Cette méthode retrace la taille de tous les noyaux de plus en plus et de rétrécissement dans le processus de traitement isotherme, et obtient la taille du noyau critique lorsque les probabilités de croissance et de rétrécissement sont équivalentes (c.-à-d. 50%). La validité de la théorie classique de la nucléation a été confirmée par le taux de nucléation correspondant aux simulations de dynamique moléculaire. Comparé au système unimodal, le système bimodal présente une énergie libre interfaciale inférieure et, par conséquent, une barrière d'énergie libre plus faible pour la nucléation, tandis que les deux systèmes ont une énergie d'activation similaire pour la diffusion.

Troisièmement, la cristallisation isothermique des polymères de répartition du poids moléculaire bimodale et unimodal (MWD) avec le poids moléculaire moyen équivalent. L'analyse primitive de chemin a été exécutée, l'évolution d'enchevêtrement a été continuellement surveillée pendant le processus de cristallisation. Une corrélation quantitative

entre le degré de démêlement et de cristallinité. Le scénario de l'ensemble du processus de démêlage de chaîne et d'épaississement lamellar à la manière de la diffusion coulissante en chaîne a été démontré. Comparé au système unimodal, le degré de démêlage du système bimodal est plus retardé que sa cristallinité due au glissement plus lent de chaîne du composant de chaîne longue ; le système bimodal atteint une plus grande épaisseur lamellar à toutes les températures en raison de la promotion de la mobilité coulissante à chaîne plus élevée de composant à chaîne courte.

Enfin, les simulations de dynamique moléculaire existantes conservent le même potentiel d'interaction dans les domaines cristallins et amorphes, ce qui rend ces modèles pas suffisamment réalistes. Nous avons construit un modèle de polymère semi-cristallin plus réaliste avec une profondeur de puits plus profonde du potentiel de Lennard-Jones (LJ) pour la phase cristalline que la phase amorphe. La validité de ce modèle est confirmée par la stabilité promue et le stress élevé de rendement dans le processus de test tendu. L'évolution de la topologie moléculaire et de la morphologie cristalline est surveillée lors de la déformation mécanique. Ce n'est qu'un premier test de l'idée d'adapter différents potentiels LJ en phase cristalline et amorphe. Des travaux plus approfondis et plus approfondis seront réalisés sur cette base à l'avenir.

Chapter 1

Literature review

Contents

1.1 Semicrystalline polymers

Researchers have recognized for many years that polymer chains could align and form crystals upon cooling down from a melt, mechanical stretching or solvent evaporation [2]. It should be noted that there is a huge difference between the crystallization behavior of atomic or small molecule systems and macromolecule systems due to the chain-link nature of polymers. Figure 1-1 is a schematic illustration of this difference. In the atomic system, the crystallization is a relatively simple process where each atom or small molecule can be transported to the growth front turning from disordered phase to crystal lattice points. In the polymer system, the crystallization behavior is much more complicated, because the movement of each chain unit should be under the strong restriction of the complete chain, where the polymer chains must not be cut (only covering physical behavior, chemical reaction is excluded here).

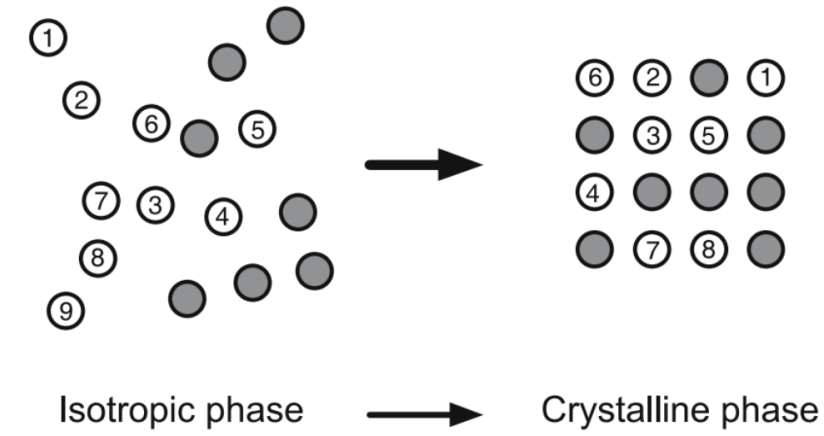

(a) Atomic system

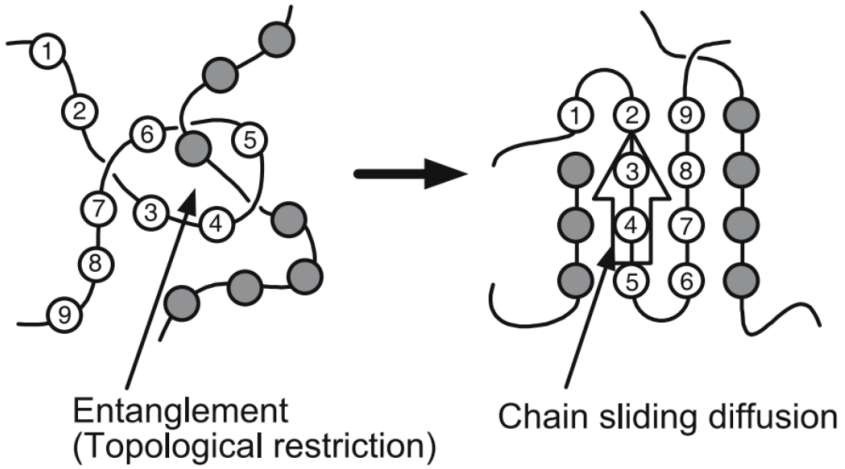

(b) Polymer system

Figure 1-1 Difference in the crystallization process of atomic or low molecular weight system and polymer system. (a) Atomic system, where atoms or small molecules can move to lattice point independently. (b) Polymer system, where the movement of one chain unit would cause the rearrangement of the whole chain. (from ref [2])

Due to the chain-link nature, polymer systems are only able to be partially crystallized, which is what we call semicrystalline polymer. The degree of crystallinity typical ranges between 10% and 80% [3]. Examples of semi-crystalline polymers are linear polyethylene (PE), polyethylene terephthalate (PET), polytetrafluoroethylene (PTFE) or isotactic polypropylene (PP) [4]. Semicrystalline polymer have been exploited commercially in several manufactural fields because of their thermoplastic properties along with a good mechanical performance. Whether or not polymers can crystallize depends on their molecular structure - presence of

straight chains with regularly spaced side groups facilitates crystallization. For example, crystallization occurs much more easily in isotactic than in the atactic polypropylene form. Atactic polymers crystallize when the side groups are very small, as in polyvinyl and do not crystallize in case of large substituents like in rubber or silicones [5].

1.1.1 Morphology of semicrystalline polymers

Semicrystalline polymers have complicated morphologies where crystalline phase are seperated by amorphous regions. These morphologies are called hierarchical structure, consisiting of the crystalline lamella (with a repeating distance in the order of 10^{-1}-10^{0} nm), lamellar morphology (10^{-1}-10^{0} nm), and spherulite structure (>10^{3} nm), as schematically illustrated in Figure 1-2. Under tensile strain, the deformation begins in equatorial zones of the spherulite and then propagates to the polar zones, where the stress is transmitted from hard crystal zones to soft amorphous zones of the material. The strain in the amorphous phase will obviously be much larger than that in the crystal zones, which may even be considered as non deformable. The local deformation is mainly supported by the stress transmitters in the amorphous phase connecting between crystalline phases [6,7]. A variety of experimental techniques are used to observe the lamellar and amorphous morphologies, like wide-angle X-ray diffraction (WAXD), small-angle X-ray scattering (SAXS), small-angle neutron scattering (SANS), or transmission electron microscope (TEM), and optical microscope (OM).

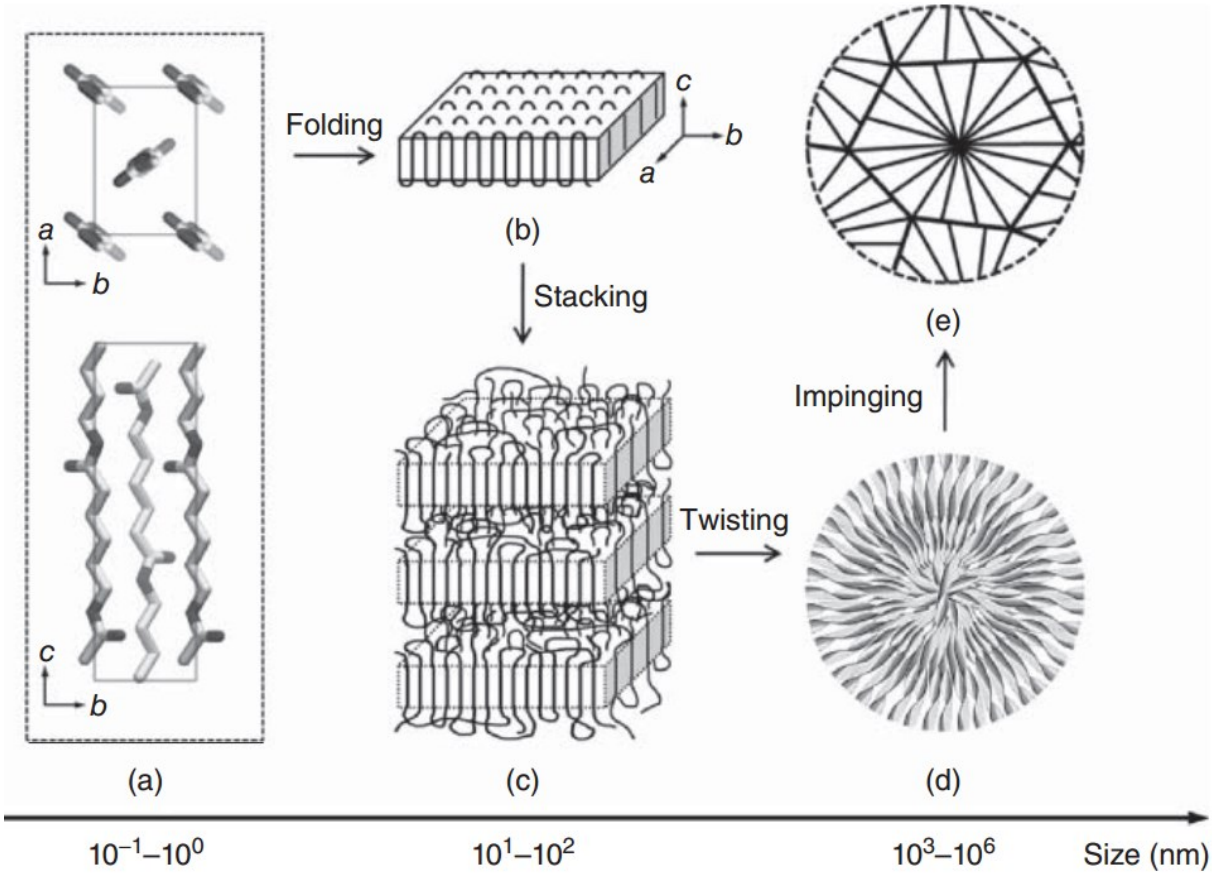

Figure 1-2 Scheme of the hierarchical structure of semicrystalline polymer. (a) Aligned chains, (b) crystal lamella, (c) lamellar stacking morphology, (d) spherulite, and spherulite structure [8].

The lattice of real semicrystalline polymers is not cubic because of the strong difference between the C-C bond length and the weak bond length. As a result, the possible lattices include triclinic, orthorhombic, tetragonal, hexagonal and so on. The molecular conformation of semicrystalline polymer is mainly governed by the intramolecular interaction. For instance, polyethylene presents a planer zig-zag conformation [9] while isotactic polypropylene forms a helical conformation due to steric repulsion between side substituents [10]. The lamellar packing is on the contrary mainly determined by the intermolecular interaction between neighboring chains such as van der Waals interaction and hydrogen bonds (e.g. polyvinyl [11], polyamides [12]). The alternating structure of crystal and amorphous layers are separated by interfacial regions. The thickness of crystal layers and amorphous layers are quantitatively measured by SAXS [13].

Typically the polymer chain length is several times greater than the lamellar thickness and each chain passes through the same and different lamellae several times.

1.1.2 Chain topology and mechanical properties

Earlier studies have shown that the molecular topology of the amorphous phase is extremely important for the tensile or compression behavior of semi-crystalline polymers [14–16]. As illustrated in Figure 1-3, molecular topology of amorphous phase is characterized by the concentration of (i) tie chain segments that span the inter-lamellar region and connect two different crystallites, (ii) loop segments that start from one crystallite and then folding back into the same one, and (iii) cilia segments that start from one crystal face and end in the amorphous region [17,18]. Such topological features and the alternation of crystalline and non-crystalline domains have formed the basis of most molecular level description of the semi-crystalline state [19,20]. Loops belonging to different crystal lamellae that are topologically constrained so that they cannot disentangle from one another are similar mechanically to bridges that run directly from one lamella to the other [21]. A large majority of loop molecules are indeed entangled: two entangled loop chains are then equivalent to two tie molecules [22]. Earlier works [22–24] have reported that tie segments and entangled loop segments which play as stress transmitters, are supposed to contribute most effectively to the mechanical behavior of semi-crystalline polymers.

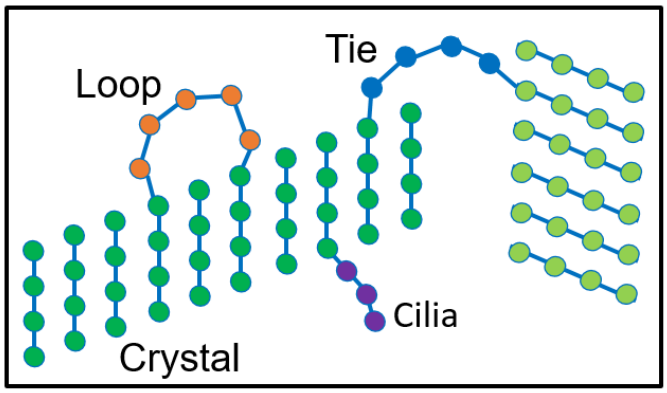

Figure 1-3 Schematic description of the possible polymer chains going in and out of crystallites: loop (orange), tie (blue), cilia (purple). Green and dark green are crystal stems in two different crystallites.

When an amorphous polymer is heated, the temperature at which the polymer structure turns "viscous liquid or rubbery" is called the Glass Transition Temperature (T_g). At the molecular level, at T_g the polymer chains in the amorphous phase gain enough thermal energy to begin sliding at a noticeable rate. The temperature where entire chain movement occurs is called melting temperature (T_m), which is greater than the T_g. Amorphous polymers only have a T_g but semicrystalline polymers consisting of both crystal and amorphous phase have a T_m and a T_g.

A constant force applied to a polymer at temperatures above T_g results in a viscoelastic deformation [8], suggesting that polymer begins to creep. Its elastic modulus changes significantly only at higher temperature [21,22,25]. It also depends on the degree of crystallinity: higher crystallinity results in a harder and more thermally stable, but also more brittle material, whereas both the amorphous and crystal regions provide certain elasticity and impact resistance [26,27].

Above T_g amorphous chains in a semi-crystalline polymer are ductile and are able to deform plastically. Crystalline regions of the polymer are linked by the stress transmitters (tie segments and entangled loop segments) in amorphous regions. The stress transmitters prevent the amorphous and crystalline phases from separating under an applied load. When a tensile

stress is applied to the semi-crystalline polymer, the mechanical response exhibits four main regimes (Figure 1-4): (1) the elastic regime which is correlated with the elastic stretching of amorphous chains, and the crystalline regions also deform elastically and are responsible for the stiffness of the material; (2) the yield regime which corresponds to the onset of plastic deformation of the crystalline regions [28], where the yield is a signature of the cavitation which leads to a progressive destruction of the crystallite network, and the yield point is accompanied with the necking and whitening of the sample; (3) the drawing regime which occurs at constant stress, and corresponds to the propagation of the neck in the sample transforming the local microstructure to fibrils; (4) the strain hardening regime corresponds to the stretching of chains.

The molecular mechanism for semi-crystalline yielding involves the deformation of crystalline regions of the material via dislocation motion. Dislocations result in coarse or fine slips in the polymer and lead to crystalline fragmentation and yielding [29,30]. Fine slip is defined as a small amount of slip occurring on a large number of planes. Conversely, coarse slip is a large amount of slip on few planes. The yield stress is determined by the creation of dislocations and their resistance to motion [14,15,31]. The role of stress transmitters becomes more relevant in the strain hardening regime because of the bridging network of tie segments and entangled loop segments. Several studies [32–34] showed that the increase of the number of stress transmitters would eventually increase the strain hardening modulus of the sample. On the contrary, the decrease of stress transmitters between crystallites leads to a fast stress concentration in the crystalline phases and the damage of the crystallites occurs by chain pullout. This influence was observed with an atomistic simulation model of semicrystalline polyethylene [35] and a specific coarse grained model [36].

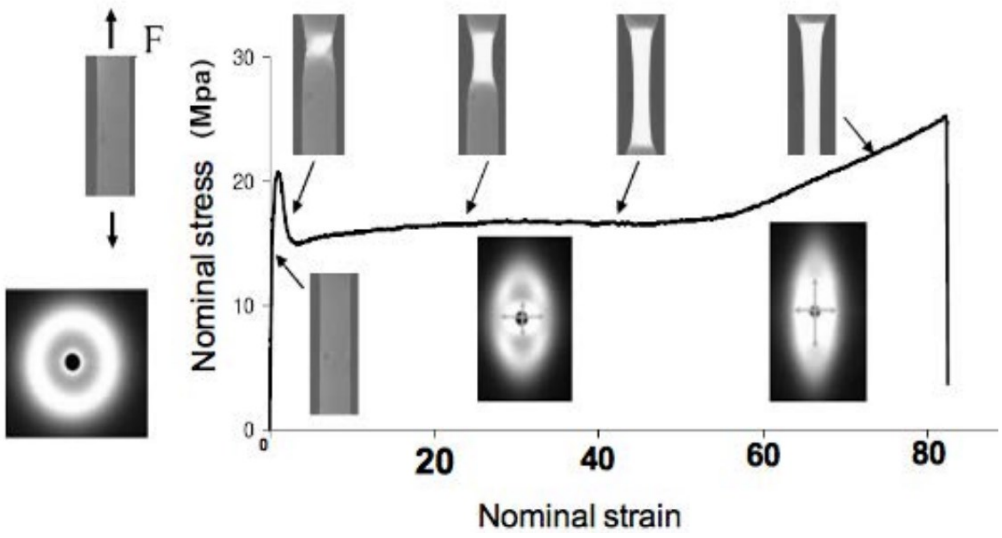

Figure 1-4 Four regime of mechanical test of a typical semicrystalline polymer Polyethylene [6].

Mechanical spectroscopy is a technique used to study and characterize materials. It is most useful for studying the viscoelastic behavior of polymers. A phenomenon related to the plastic response of a semicrystalline polymer is α_c relaxation [37]. It happens when the frequency of an external field matches the rate of flux material crossing the energy barrier: the absorption peak is associated with relaxations within the crystalline phase. α_c relaxation is dipolar and has a molecular origin that has to be sought in the various forms of imperfections: chain loops on the lamellar surface, chain rotations and twisting within the interior of the crystals, discontinuities defects [38,39].

Such defects are identified as thermally activated conformational defects responsible for the α_c relaxation. Seguela *et al.* [40] have shown that the activation of mobile conformational defects in the chain stems of the crystalline lamellae may fairly account for the ability to develop either homogeneous plastic flow or plastic instability, depending on the applied strain rate and temperature. Such defects promote the stepwise migration of the stems by translation jumps along the stem axis. Starting from the lateral surface of crystalline lamellae, this process allows a gradual shear of the crystal via nucleation and propagation of a screw dislocation. The characteristics of defect thermal activation are shown to have a determining part on the dislocation kinetics and, therefore, on the plastic behavior.

The appearance and growth of the α_c relaxation are a direct consequence of the development of the crystalline phase [41,42]. α_c relaxation is observable by static tests, such as stress creep and relaxation, where the material is subjected to constant stress and constant deformation, respectively, or by DMA (Dynamic Mechanical Analysis) tests, where the sample is subject to periodic solicitation. Measurements are carried out with low levels of deformation or stress, so that the relaxation time is independent of it.

1.2 Polymer crystallization

The majority of natural and synthetic polymers are semicrystalline, and such a characteristic structure governs their mechanical, optical and thermal properties. Hence, it is essential to understand the kinetics of polymer crystallization process, which consists of crystal nucleation and crystal growth. The whole process can be influenced by a lot of factors such as molecular weight, chemical structure, temperature, thermal history, *etc*. In this part, we introduce the classical nucleation theory, and the related kinetics theories dominating crystal nucleation and crystal growth.

1.2.1 Crystal nucleation, classical nucleation theory

Polymer crystallization is conventionally initiated by crystal nucleation. Classical nucleation theory method (**CNT**) has been widely used to describe homogeneous nucleation. According to CNT, a crystal nucleus is separated from amorphous phase by an interfacial surface, which consists of two types of crystal interfaces: chain-end surface and side surface. For this reason, a cylinder model is often assumed to describe the shape of nuclei. When temperature is cooled below the melting point, there is a competition between the free energy gain in the bulk of nucleus and the free energy loss in the interfacial surface, which generates a free energy barrier. There exists a critical nucleus size where the free energy gain happens to offset free energy loss, and crystal domains larger than the critical size tend to be more stable.

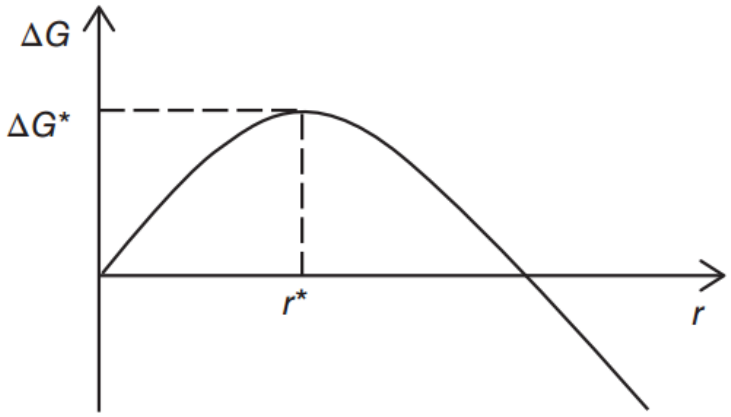

Figure 1-5 Schematic curve of the free energy changes as a function of the radius of nucleus (from ref [8]).

The free energy of formation of a cylindrical crystal nucleus is given by

$$\Delta G = 2\pi r^2 \sigma_e + 2\pi r l \sigma_s - \pi r^2 l \, \Delta G_v \qquad (1.1)$$

where σ_s and σ_e are the interfacial free energies for the side and end surfaces of a cylindrical nucleus of radius r and length l, and ΔG_v is the Gibbs free energy difference per unit volume between the crystal and melt phases. A schematic curve for the free energy change with the increasing radius of nucleus is presented in Figure 1-5. For deep supercooling, an approximation of ΔG_v is [43,44]

$$\Delta G_v \approx \rho_n \Delta H_f T (T_m - T)/T_m^2 \qquad (1.2)$$

where ρ_n is the bead number density, ΔH_f is the melting heat per bead at the thermodynamic equilibrium melting temperature T_m, and T is the crystallization temperature. In fact, to get over the nucleation barrier via thermal fluctuations, the initiation of primary crystal nucleation requires a crystallization temperature T much lower than T_m. Thus, the supercooling for crystallization is defined as

$$\Delta T = T_m - T \qquad (1.3)$$

Maximizing ΔG with respect to r and l gives the critical radius and critical length, respectively:

$$\begin{cases} r^* = 2\sigma_s/\Delta G_v \\ l^* = 4\sigma_e/\Delta G_v \end{cases} \quad (1.4)$$

Inserting r^* and l^* into equation (1.1), the free energy barrier is obtained:

$$\Delta G^* = 8\pi \frac{\sigma_s^2 \sigma_e}{(\Delta G_v)^2} \quad (1.5)$$

The critical nucleus size, measured in number of beads, is

$$n^* = 16\pi \rho_n \frac{\sigma_s^2 \sigma_e}{(\Delta G_v)^3} \quad (1.6)$$

As for mobility of the chains, the diffusion coefficient can be given by

$$D = D_o \exp\left(-\frac{E_d}{RT}\right) \quad (1.7)$$

where D_o is a temperature-independent pre-factor, E_d is the activation energy for chain mobility, which can be obtained from the slope of $\ln D$ versus $1/T$.

According to CNT and transition state theory, Kampmann and Wagner [45] introduced the nucleation rate I (in number of events per volume per time) at the incubation time, leading to the following expression:

$$I = \frac{dN}{dt}\Big|_{nuclei} = A \exp\left(-\frac{E_d}{k_B T}\right) \exp\left(-\frac{\Delta G^*}{k_B T}\right) \quad (1.8)$$

where ΔG^* is critical free energy barrier which mainly results from interfacial free energy, E_d is the activation energy for chain mobility, and A is a temperature independent factor, $dN/dt|_{nuclei}$ is the nucleation rate in number of nuclei formed per unit volume per unit time, which can be obtained from molecular simulations.

Nucleation is a very complex process, because each polymer should be transported and rearranged under the strong restriction that the molecular chain must not be "cut". Nishi *et al.* [2] reported that the primary nucleation is a process of "chain sliding diffusion" within the nucleus which requires disentanglement of molecular chains. It is also natural to consider that the chain sliding diffusion and disentanglement become more difficult with increase in molecular weight. It is widely accepted in experiment and modeling [46,47] that zero rate viscosity is proportional to

the power α of molecular weight, $\eta_0 \propto M_w^{\alpha}$, where the exponent α is 1.0 for unentangled chains and 3.4 for entangled chains. Typically this change or crossover is due to the topological constraints that hinder the overall chain movement. A clear change is detected experimentally [48] in the mechanism of chain dynamics when the molecular weight exceeds a characteristic value, M_e.

Experimentally, a clear change is also seen in the mechanism of chain dynamics (*e.g.* diffusion coefficient). The dynamics of relatively short polymer chain melt ($M<M_e$) is well described by the Rouse model [49], where a chain is envisioned as a set of Brownian particles connected by harmonic springs. The Rouse model is formulated with three parameters: the number of beads, the length of Kuhn segment, and the monomeric friction coefficient. For polymers with $M>M_e$, the reptation theory proposed by de Gennes [50] better describes polymer dynamics. This theory assumes that the motion of an individual chain is restricted by the surrounding chains within a tube defined by the overall chain contour or primitive path. The chain is not allowed to cross the tube but it can move in a snakelike fashion in it. Reptation theory is formulated with the number of beads, the length of Kuhn segment, the monomeric friction coefficient and also the entanglement length. Reptation is actually the process that permits a polymer chain to be removed from the entangled melt by the force of crystallization and be pulled into the growth front. Ibhadon [51] has showed that reptation is responsible for slowing the rate of crystallization in a manner inversely proportional to the molecular weight. As a matter of fact, in nucleation and crystal growth, polymer chains are highly sheared and somewhat disentangled at the local growth front.

1.2.2 Crystal growth

Crystal growth follows primary crystal nucleation, which can be influenced by long-range diffusion and interfacial free energy. Crystal growth can also be separated into two steps, secondary nucleation and thickening forming a wedge-shaped growth front (Figure 1-6).

Lauritzen–Hoffman (LH) theory based on secondary nucleation is a theoretical model which is the most widely used in the kinetics of crystal growth. The LH theory [52,53] is mainly based on the following assumptions: (1) the growth front is smooth; (2) the length of chain-folded crystal stems keeps constant during crystal growth. The energy barrier is gradually compensated by the free energy gain upon depositing neighboring stems with a length slightly beyond a minimum lamellar thickness. According to LH theory, the temperature dependence of the linear growth rate (G) in terms of spherulite radius can be expressed by two exponential factors:

$$G = G_0 \exp\left(-\frac{U}{T-T_0}\right) \exp\left(-\frac{K_g}{T(T_m-T)}\right) \qquad (1.9)$$

G_0 is the rate constant of crystal, U is the transport activation energy, T_0 is a hypothetical temperature (less than T_g) below which chain mobility ceases, K_g is the nucleation kinetics constant. The first exponential factor is attributed to short-range diffusion across the interface, and the second factor is attributed to secondary nucleation barrier.

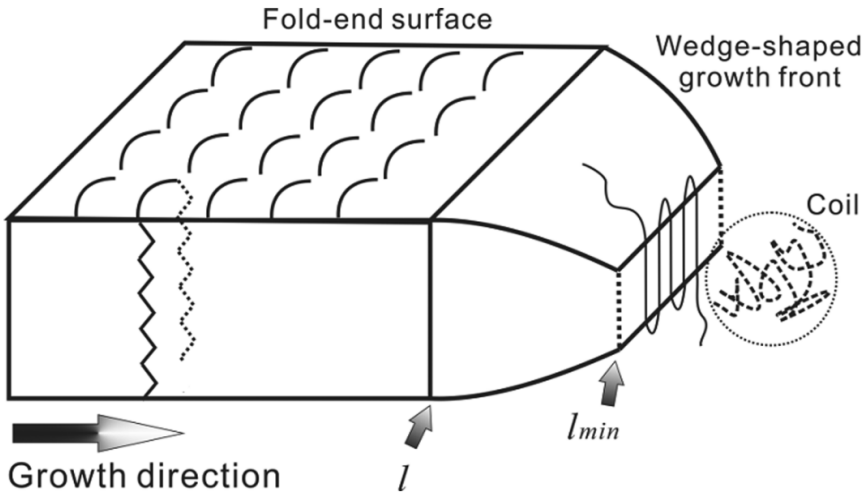

Figure 1-6 Schematic illustration of the side growth front of a wedge-shaped lamellae, indicating that crystal growth consists two stages [54].

From equation (1.9), we can see that these two exponential factors have opposite temperature dependence, producing a maximum growth rate. Many polymeric materials display a bell-shaped temperature dependence of the crystal growth rate. The molecular transport factor is dominant at high supercoolings (low-temperature part of the bell-shaped curve), and will be

very difficult when temperature approaches T_g, and growth rate approaches zero when temperature is below T_g, as shown in Figure 1-7. On the other hand, the secondary nucleation factor becomes more important at low supercoolings (high-temperature part of the bell-shaped curve). Figure 1-7 also shows a schematic comparison of the temperature dependence between primary nucleation rate (I) and growth rate (G). Clearly both nucleation rate and crystal growth rate exhibit a bell-shaped trend with a maximum rate as temperature increases, which can be deduced from equations (1.8) and (1.9). The nucleation rate is more complicated and can be influenced by temperature, presence of nucleation agent, *etc*. The limitation of the LH theory is that the thickening of the crystal stems is omitted during crystal growth. Both molecular simulations [28,55,56] and experimental morphology findings [57–60] have confirmed the wedge-shaped lateral growth front of lamellar crystals. Despite all these criticism lately, the LH thoery is still one of the few models that provides an easy and efficient way of describing the crystallization process.

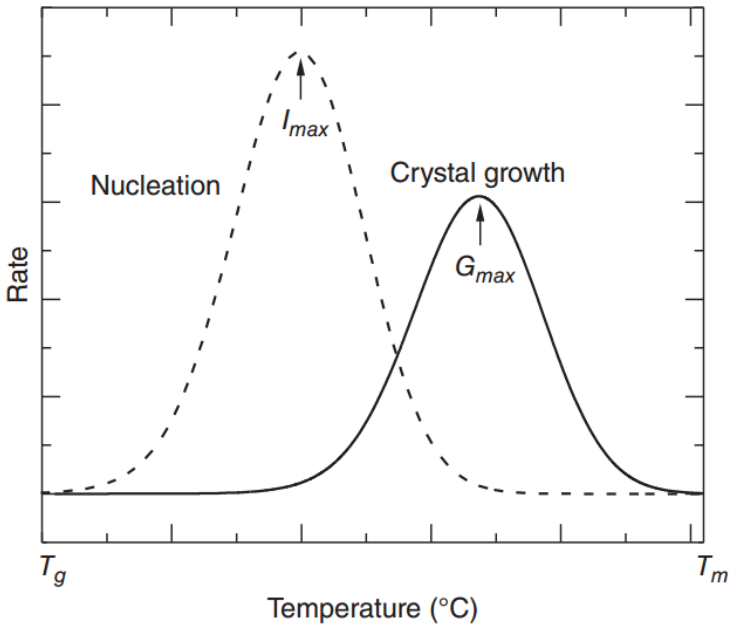

Figure 1-7 Schematic temperature dependence of primary nucleation rate and crystal growth rate [61].

1.3 Bimodal molecular weight distribution polymer

Experimental investigations [15,62–64] have inferred that Molecular Weight Distribution (MWD) is a key factor for the formation of stress transmitters. Nevertheless, unimodal MWD polymer made by traditional catalysis have conflicts between their mechanical properties and processing behaviors: improving mechanical performances by increasing molecular weight (M_w) usually deteriorates the processability because of high melt viscosity.

Bimodal MWD polymer is composed of low- and high- molecular weight contents. More recently, thanks to the development of some novel synthetic techniques, polymers with bimodal MWD have been drawing an increasing attention, for instance the application of bimodal polyethylene (BPE) for the transportation and distribution of water and gas. The bimodal MWD material consisting of both high molecular weight fraction and low molecular weight fraction provides more balanced performances for processing and mechanical behaviors, because the low molecular weight polymer chains promote the melt to flow easily whereas the high molecular weight fraction improve the mechanical properties of the material [65]. At present, there are two methods for directly producing bimodal resins: reactor in series configuration or single reactor with dual site catalysts [17,66]. Generally, it is difficult and expensive to directly prepare bimodal resins in the laboratory [67,68]. A melt blending is better suited to prepare a series of bimodal MWD polymers with variable molecular weight [69,70]. As for bimodal MWD polymers, the research mainly focuses on the synthetic techniques and characterization comparison to unimodal polymers [4,71,72]. Nevertheless, there are only few studies addressing the simulation of crystallization in relation with molecular topology [30,73,74] of bimodal polymers. Moyassari *et al.* [30,73] monitored tie segments and entanglement concentrations during crystallization of PE bimodal blends. Luo *et al.* [74–77] studied the crystallization of unimodal PVA chains and also blends with very short chains (considered as solvent phase), and found a linear relation between lamellar thickness and entanglement length. Anyway crystallization behavior of bimodal MWD

polymers has rarely been reported [67,68,78], and the influence of the MWD on the final molecular topology of the obtained semi-crystalline polymer has not been investigated.

1.4 Numerical simulations

Since about six decades, numerical simulation has progressed and is becoming more and more a leading tool in scientific research and design (Figure 1-8). This field continues to grow thanks to the continuous evolution in computer science (programming languages and techniques, computer, computing clusters, *etc*.). The purpose of the simulation is twofold: on the one hand, to verify the physical hypotheses that make it possible to interpret the simulated phenomenon and to test new ideas making it possible to progress in understanding the local behavior of these systems, and on the other hand to predict the response of a material under complex boundary conditions. Thanks to the considerable progress made in simulation methods, these can be considered as multidisciplinary and multiscale methods. Simulation integrates as an important ingredient in various scientific fields ranging from biology to mechanics to chemistry and physics of materials, also covering a large scale ranging from a few nanometers (in ab-initio methods), up to a few kilometers (in the finite element methods), or even a few tens of light years in the Monte Carlo methods used in the simulation of Galaxies.

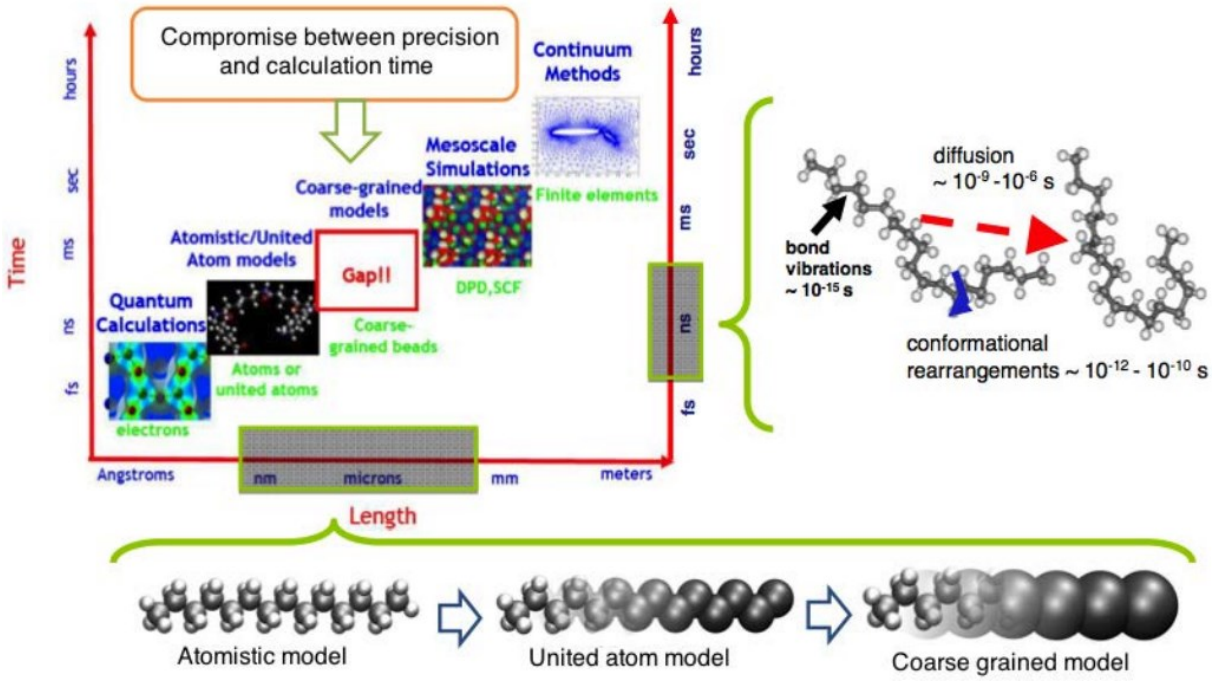

Figure 1-8 The different simulation methods and their characteristic scales (time and distance) (from ref [22]).

In order to optimize the computation time while obtaining the detailed information sought for the studied phenomenon, it is advisable to choose for each simulation the model whose characteristic length corresponds best with the characteristic length of the simulated phenomenon. To carry out our study on the crystallization of polymers, several types of simulation are possible. In our study we are particularly interested in the evolution of the configuration during polymer crystallization.

These configurations are representative enough to observe the events studied (formation of nuclei, chain folding, chain sliding ...), which actually occur on a very small scale (about tens of nanometers). Therefore, the choice of simulation method depends on the length scale on the one hand, and the duration of the phenomena on the other. Molecular dynamics is a particularly suitable method for our study. United-atom (UA) model and coarse-grained (CG) model are widely used in the molecular dynamics simulation of polymer crystallization. UA dynamic simulations [79,80] have been mainly used for short chain systems, and it is not sufficient to simulate the growth of large lamellae. In CG model, the polymer chains consist of beads that

represent a few structural units. The size of the system as well as the time scale involved are large enough to fully address the problems of the size, thickness, and shape of the lamellae as well as the molecular topology. Considering the main purpose of this thesis, which focuses on the crystallization of polymers, it is of limited value to consider chemical details in the simulation model, and complicated models would increase the computational time. Therefore, Coarse-Grained Molecular Dynamics (CG-MD) is the best tool to overcome difficulties of experimental measurements and to study quantitatively the non-equilibrium process of crystallization at the nanoscale.

The most used CG model is the qualitative and not quantitative Kremer-Grest (KG) bead-spring model [81], where the beads are bonded by finite-extensible nonlinear elastic (FENE) potential to prevent chain crossing and non-bonded beads interact by classical Lennard-Jones potential. Even though the KG model has proved to reproduce the experimental behavior of glassy polymer [22,82,83], it fail to undertake homogeneous crystallization. In a previous article [1] of our group, we tested the homogeneous crystallization ability of a simple CG model by optimizing the Lennard-Jones potential parameter. The optimized LJ potential acts as an angular potential that promoted the nucleation of the polymer by aligning of the beads in the same chain. The thermodynamic stability of the optimized LJ potential was verified and homogeneous nucleation ability was confirmed by isothermal crystallization treatment. In this thesis, the optimized LJ potential is employed for all the MD simulations. For the details of this optimized parameters we will explain in section 2.1.

1.5 The objective and organization of this work

Semicrystalline polymers have drawn a wide interest in the academic research and engineering applications due to great mechanical performance. There is strong link between the mechanical properties and microstructure of semicrystalline polymer, such as bimodality, molecular topology (the way polymer chains pass through crystalline and amorphous phases),

chain entanglements, lamellar thickness, temperature, and so on. However, these microstructure cannot be access quantitatively in experiment. There exists some molecular dynamics investigations, but the homogeneous crystallization is very difficult to achieve and not extensively discussed. Thus, in spite of all the previous works on this subject, the crystallization mechanisms of polymers and the dependence of microstructure remain relatively unclear and controversy.

The main objective of this thesis is to use CG-MD simulation technique to provide more insights on the homogeneous nucleation and crystal growth behavior of bimodal and unimodal MWD polymers, the influence of bimodality on the molecular topology (loop, tie, cilia) and entanglement concentration, the chain disentanglement process and its influence on lamellar thickening as well the temperature dependence. Our research will improve the understanding of the crystallization process, and provide instructions to control the microstructure of semicrystalline polymer that the favors engineering application.

The chapters of this thesis are organized and briefly introduced as follows:

- **Chapter 1** is an introduction of general research background, which incorporates semicrystalline polymers, crystallization kinetics and classical nucleation theory, bimodal molecular weight distribution polymer, numerical simulations and the objective of this thesis.
- **Chapter 2** introduces the simulations methods and simulation details. The bonded and non-bonded interactions, the procedure of preparing polymer melts and isothermal crystallization are presented. A hierarchy-clustering method is also presented for post-processing of molecular simulation to calculate the crystallinity and analyze the chain topology of semicrystalline polymer systems.
- **Chapter 3** studies the crystallization behavior and the molecular topology of bimodal molecular weight distribution polymers using a coarse-grained molecular dynamics

model with varying weight fraction of short and long chains. Extensive simulations of isothermal crystallization have been performed. The interfacial free energy and the incubation time have been obtained using a mean first-passage time analysis. The bimodality dependence of molecular topology (loop, tie, cilia) has been discussed.

- **Chapter 4** studies the homogeneous nucleation of bimodal and unimodal molecular weight distribution (MWD) polymers with equivalent average molecular weight. A novel Growing Probability Method has been proposed to determine the critical nuclei, which is used to calculate the free energy barrier of forming nuclei. The validity of the classical nucleation theory has been confirmed through the nucleation rate fitting with molecular dynamics simulations. The influence of bimodality on nucleation rate has been discussed.
- **Chapter 5** also studies the isothermal crystallization of bimodal and unimodal molecular weight distribution (MWD) polymers with the equivalent average molecular weight. Primitive path analysis has been performed, the entanglement evolution has been continuously monitored during the process of crystallization. A quantitative correlation between the degree of disentanglement and crystallinity. The scenario of the whole process of chain disentangling and lamellar thickening in the manner of chain sliding diffusion has been demonstrated. The correlation between the degree of disentanglement and lamellar thickness, and their temperature dependence have also been discussed.
- **Chapter 6** studies the mechanical properties. A novel idea of adopting a stronger Lennard-Jones potential in crystalline phase than in the amorphous phase has been tested and a more realistic model of semicrystalline polymer is built. To perform molecular dynamics simulation of this new model, the potential of beads requires to be adjusted periodically based on their crystallizing and melting, an interface of C++

programming with Lammps has been developed to realize this process. This chapter is an incomplete work due to the limited time of the PhD. The novel idea has been verified to be workable and a new model has been built. Deeper work will be done in the future.

- **Chapter 7** is the summary of the conclusions of the whole thesis, and based on what we have achieved, future research directions have been speculated.

Chapter 2

Methodology

Contents

As explained in section 1.4, we use a coarse-grained (CG) polymer model [1] where polymer chains consist of "beads" representing a few structural units. All simulations are performed in three dimensions using the open-source code LAMMPS [84].

2.1 Interaction potentials

Our CG model is based on two potentials, where energy, length and time units are given by ε_u, σ_u and τ_u respectively (with $\tau_u = \sqrt{m_u \sigma_u^2/\epsilon_u}$ where m_u is the mass unit). All quantities will be expressed in terms of these units. A Finite-Extensible Non-linear Elastic (FENE) potential models intra-chain interactions of bonded beads:

$$V_{FENE}(r) = -0.5kR_0^2\, ln\left[1-\left(\frac{r}{R_0}\right)^2\right] + 4\varepsilon\left[\left(\frac{\sigma_F}{r}\right)^{12} - \left(\frac{\sigma_F}{r}\right)^{6}\right], \qquad (2.1)$$

with classical value of parameters [81]: $k = 30\ \varepsilon_u/{\sigma_u}^2$, $R_0 = 1.5\ \sigma_u$, $\varepsilon = 1\varepsilon_u$ and $\sigma_F = 1.05\ \sigma_u$, chosen so that unphysical bond crossing and chain breaking are avoided. Note that the value of σ_F is chosen such that $V_{FENE}(r = 1\sigma_u)$ is minimum. All other weak interactions are modelled by a simple Lennard-Jones (LJ) potential:

$$V_{LJ}(r) = 4\varepsilon_{LJ}\left[\left(\frac{\sigma_{LJ}}{r}\right)^{12} - \left(\frac{\sigma_{LJ}}{r}\right)^{6}\right] - 4\varepsilon_{LJ}\left[\left(\frac{\sigma_{LJ}}{r_c}\right)^{12} - \left(\frac{\sigma_{LJ}}{r_c}\right)^{6}\right], \qquad (2.2)$$

where $\varepsilon_{LJ} = 1\varepsilon_u$, $r_c = 2.5\sigma_{LJ}$ is the cut-off radius, σ_{LJ} is an adjusted parameter of the potential that favours crystallization and crystal stability for the FENE-LJ model chosen here. Newton's equations of motion are integrated with velocity-Verlet method and a time step is $0.005\tau_u$.

In our previous article [1] of our group,we tested the homogeneous crystallization ability of a simple CG model of linear polymer. The optimal FENE-LJ parameter combinations (ratio between FENE and LJ equilibrium distance) and the optimal lattice parameters were calculated for five different perfect lattices: simple tetragonal, body-centered tetragonal, body-centered orthorhombic, hexagonal primitive and hexagonal close packed. Static ground energy was calculated for perfect crystal structures respectively with these five lattices. It was found that the most energetically favorable structure for homogeneous crystallization for the reason of low lattice energy and stability is the body-centered orthorhombic lattice, furthermore the crystallographic parameters of this lattice was optimized and obtained. The optimal parameter of σ_{LJ} equals $1.888\,\sigma_u$, and the bond length (c) was monitored to be $0.995\,\sigma_u$. As is demonstrated in Figure 2-1, when considering three successive beads in the same chain, the bead number 1 has no effect of LJ potential on the first neighbour (bead number 2), whereas it can interact with the second neighbour (bead number 2). As σ_{LJ} is approximately twice the bond length, the bead number 3 tends to be at a distance of about twice bond length from the bead number 1 for low energy purpose and then three beads tend to be aligned. Actually the optimized LJ potential acts as an angular potential that promoted the nucleation of the polymer by aligning of the beads in the same chain for the low-energy purpose. The thermodynamic stability of the optimized LJ potential was verified and homogeneous nucleation ability was confirmed by isothermal crystallization treatment. The glass transition temperature of our CG model with chain length 100 beads was determined to be 1.4 ϵ_u/k_B through the thermogram of the polymer melt cooling, and the melting temperature was determined to be 3.1 ϵ_u/k_B through

heating of perfect crystal configuration. In this thesis, this optimized LJ potential is employed for all the MD simulations.

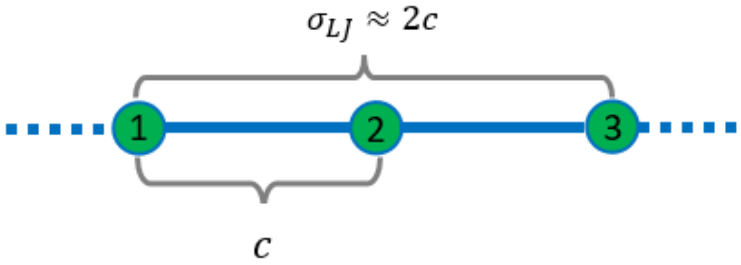

Figure 2-1 Schematic illustration of the angular FENE-LJ potential favorable for chain alignment and crystallization. Green spheres represents three consecutive beads indexing from 1 to 3 in the same chain. σ_{LJ} equals approximately twice of bond length (c).

2.2 Simulation procedure

2.2.1 Preparation of the polymer melts

Polymer chains have been generated and equilibrated using the Radical-Like Polymerization (RLP) method (Figure 2-2) [85,86]. The efficiency of this method relies from its ability to generate and equilibrate the chains simultaneously. As it mimics the central idea of radical polymerization, $AM^* + M \rightarrow AMM^*$, the RLP method builds the chains progressively in an interacting molecular dynamics solvent. As a consequence, the system will be equilibrated while chain growth occurs.

The process of polymerization with RLP method can be described as follows: (1) in the nucleation step, RLP method starts with a Lennard-Jones bath of N_{mon} monomers, M of them being randomly selected as radicals; (2) in the growth step, each radical forms a covalent bond with a new monomer randomly selected from its first nearest monomer neighbors (see Figure 1-1), and transfers the radical to the chosen monomer, thus the chain length is increased by one; (3) relaxation is an essential step of the RLP method, between two successive growth steps, the whole system (created chain fragments and existing monomers) is relaxed with n_{bG} MD steps; (4) in the termination stage, each chain has reached a target size N, for unimodal polymer melt

usually the ratio $\frac{M \times N}{N_{mon}} = 80\%$ is choosen in the first place to accelerate the polymerization process; (5) finally in the equilibration stage, the residual monomers are removed and the system is further relaxed at constant pressure to reach equilibration.

In this thesis, at the end of the RLP method M chains of N units are formed, the system is equilibrated during $5 \times 10^5 \tau_u$ at $T = 3.3\epsilon_u/k_B$ and $P = 0.5\epsilon_u/{\sigma_u}^3$ in the NPT ensemble. The relaxation temperature is well above the melting point ($T_m = 3.1\epsilon_u/k_B$), and we confirmed its efficiency of polymer chains relaxation through initial tests. Mean Square Internal Distance (MSID), radius of gyration, and end-to-end distance are calculated to verify that all systems are well equilibrated. In this way, we are able to create simulation systems of uni- and bimodal MWD polymer melts.

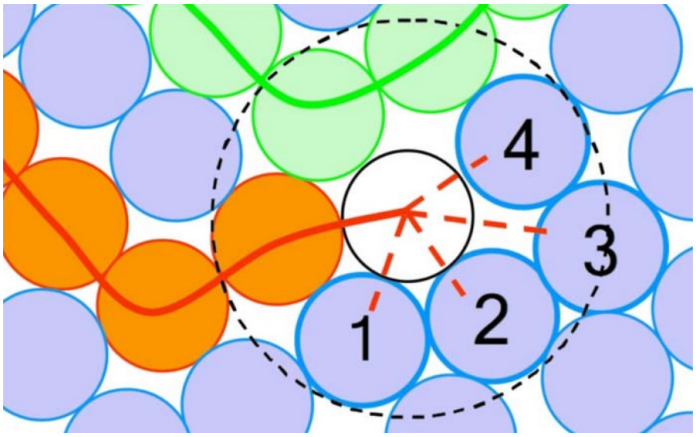

Figure 2-2 Schematic illustration of growth step during the radical-like polymerization method. A radical (white color) is assigned randomly to its closest neighboring monomers (blue color numbered from 1 to 4) to form a new covalent bond and the chain length increases by one more bead (from ref [85]).

2.2.2 Isothermal crystallization treatment

After the preparation of polymer melts, isothermal crystallization study has been carried out on the seven systems according to the following procedure: starting from an equilibrated melt at $T = 3.3\epsilon_u/k_B$, where it was verified that no crystallization occurs, temperature is then cooled down quickly to the desired crystallization temperature of $2.3\epsilon_u/k_B$ during $10^5\ \tau_u$ (cooling rate: $10^{-5}\epsilon_u/k_B/\tau_u$) and maintained during $4 \times 10^5\ \tau_u$. For the snapshots of obtained

semicrystalline polymers, one can refer to Figure 3-3, Figure 4-1 and Figure 5-1. Following Vyazovkin's suggestion [87], a disadvantage of isothermal runs is that quick cooling from melting temperature to a desired temperature is followed by a period of temperature stabilization during which the crystallization kinetics is difficult to estimate. For this reason we use relatively slow cooling before the isothermal process. In our previous article [1], the isothermal temperature ($2.3\epsilon_u/k_B$) has been chosen after an extensive test in order to maximize the size of the crystallites and induce a fast growth of crystallites. To explore the temperature dependence of polymer crystallization and the consequent microstructure, other temperatures are also involved in the specific chapters. For clarity, a flow chart is illustrated in Figure 2-3 for the preparation of melt and isothermal crystallization procedure.

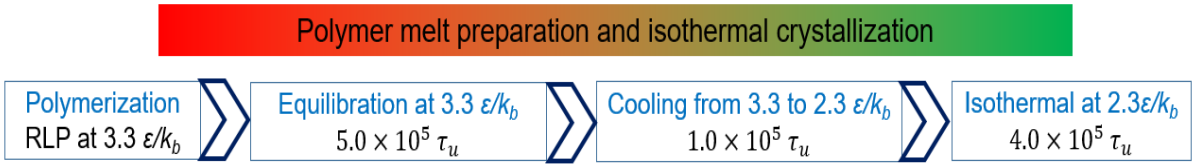

Figure 2-3 Flow chart of polymer melt preparation and isothermal crystallization treatments. $2.3\epsilon_u/k_B$ is the target temperature in this example, and it can be other target temperature.

2.3 Crystallites detection - Hierarchical clustering method

In order to quantify the crystallinity as well as the size distribution of crystallites, our previous article has provided a novel algorithm [1] based on hierarchical clustering. This algorithm seeks to build a hierarchy of crystal clusters and the beads belonging to the same cluster would be detected and integrated. It is actually a bottom-up strategy: each bead starts its own cluster and all the clusters sharing the same orientation are merged as one moves up the tree structure. The orientation of the polymer chain beads is evaluated as follows: neighboring beads i and j belong to the same cluster if their misorentation is lower than 5°. The misorientation between atoms i and j is defined as

$$\Delta \boldsymbol{O}(i,j) = \min[||\boldsymbol{O}(i) + \boldsymbol{O}(j)||, ||\boldsymbol{O}(i) - \boldsymbol{O}(j)||] \quad (2.3)$$

where $\boldsymbol{O}(i)$ is a unit vector giving the chain orientation at the location of the *n*th bead inside a chain with respect to its covalent FENE bonded neighbors:

$$\boldsymbol{O}(n) = \frac{\boldsymbol{r}_{n+1} - \boldsymbol{r}_{n-1}}{||\boldsymbol{r}_{n+1} - \boldsymbol{r}_{n-1}||} \tag{2.4}$$

where $\boldsymbol{r}_n$ is the position of the *n*th bead inside a chain. The orientation of the chain ends is set the same as their bonded neighbor. The crystallinity is defined as the ratio of the number of beads belonging to a crystallite over the total number of beads. In this way, we are able to detect all crystal clusters (*i.e.* crystallites). If the size of a cluster is too small, clearly it is not stable and cannot be treated as a crystallite. We have done some statistics on the size distribution of clusters, and we found that clusters with size less than 50 beads are unstable over time. Moreover, at the end of isothermal treatment, where the crystallization has been fully achieved, very few clusters with size from 50 to 1000 have been detected. There are mainly large crystallites (>1000), and small nuclei (<50) which are far below the critical size. In other words, large orientation clusters tend to form in the process of isothermal crystallization. Evidently, small and unstable clusters are not as important as large ones, and it is not wise to pay much attention on small clusters. As a consequence, we set the critical size of crystallites as 50, and clusters with less than 50 units would be treated as amorphous phase.

2.4 Molecular topology detection

Regarding structure-mechanical property relationships, a very important aspect is the molecular topology (essentially the concentration of loop, tie and cilia segments, see Figure 1-3). More features are added to our hierarchical clustering algorithm to trace each chain going in and out of crystallites and analyse the molecular topology of the systems. Based on the definition of the molecular topology we mentioned in section 1.1.2, loop, tie, and cilia segments can be detected based on trajectories of chain segments attached to the outer surfaces of crystallites. A topological segment is constituted by at least three units. Segments of less than

three beads would be treated as a flaw in this thesis and integrated to the segments ahead and behind it. Loop, tie and cilia have a size equal or higher than three. Apart from the molecular topology, sometimes we also need to mention crystal segment in our following analysis, which is a crystal stem across the edges of the crystallite (see Figure 1-3). Only one exception happens for the identification of loop and tie due to the periodic conditions of MD simulations. From Figure 2-4, we can see that crystallites 1 and 2 are actually one crystal because they are periodically connected. In this case, the blue and red segments both go back to the same crystallites and could therefore be considered as loops. However, the blue segment is better described as a tie. In order to detect this particular case, we consider the two vectors at the ends of a segment entering the same crystallite. If the vectors are in the same direction, it is a loop; if they are opposite, it is a tie. Consequently, all the segments of molecular topology and their sizes are unambiguously recorded for further studies.

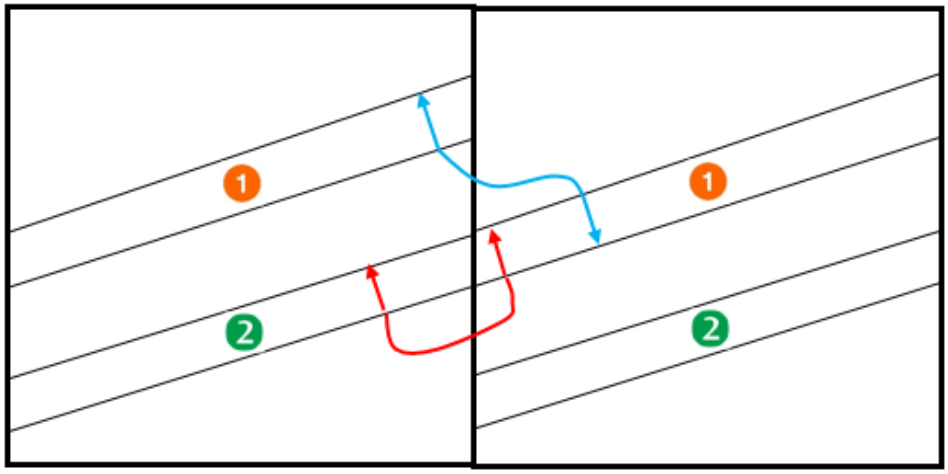

Figure 2-4 Scheme of a particular case due to periodic conditions of the simulation. Block 1 and 2 are crystallites. The blue chain segment is actually a tie and the red one is a loop.

Chapter 3

Crystallization and molecular topology of semicrystalline polymers

Contents

Abstract: In this chapter, the objective is to investigate the homogeneous crystallization mechanism of polymers based on classical nucleation theory, and to discuss the influence of bimodality on crystallization and molecular topology (loop, tie, cilia, *etc.*). This chapter has been published on the journal of Macromolecules (*Macromolecules*, 2019, 52, 11, 4196-4208; DOI: 10.1021/acs.macromol.9b00071), and we adapt this article as chapter 3.

The crystallization behavior and the molecular topology of bimodal molecular weight distribution polymers are studied using a coarse-grained molecular dynamics model with varying weight fraction of short and long chains. Extensive simulations have been performed to prepare polymer melts and obtain semi-crystalline polymer by homogeneous isothermal crystallization. The incubation time (the time elapsed before the establishment of stead-state nucleation) is calculated and the interfacial free energy is obtained using a mean first-passage time analysis, which is a simulation method to calculate the critical nucleus and incubation time by tracing the nucleus size with time. The incubation time first decreases with weight fraction

of long chains, reaches its maximum at 30%, and then turns to increase afterwards. This results from conflicting effects of interfacial free energy and mobility of chain segments. Interfacial free energy decreases with weight fraction of long chains, which is attributed to the transition from intermolecular to intramolecular nucleation, whereas the chain mobility decreases with increasing long chain content. Nevertheless, the growth rate of crystals decrease continuously with weight fraction of long chains, mainly resulting from reduced chain sliding diffusion. We have provided insights into how bimodal molecular weight distribution polymer promotes both nucleation and processability. Moreover, a numerical algorithm has been proposed, tracing each chain going back and forth among crystallites, to access quantitative data of molecular topology (*i.e.* loop, tie and cilia segments). It turns out that the concentration of loop and tie segments increases with increasing weight fraction of long chains. This could be important to understand the mechanical properties of semi-crystalline polymer.

Key words: Semi-crystalline polymer, molecular topology, bimodal molecular weight distribution, inter and intramolecular nucleation, interfacial free energy

3.1 Introduction

Nanostructured polymers such as semi-crystalline polymers are used in a broad range of applications [29,71]. Earlier studies have shown that the molecular topology of the amorphous phase is extremely important for the tensile or compression behavior of semi-crystalline polymers, the fracture toughness and the resistance to slow crack growth [14–16]. Molecular topology is characterized by the concentration of (i) tie chain segments that span the inter-lamellar region and connect two different crystallites, (ii) loop segments that start from one crystallite and then folding back into the same one, and (iii) cilia segments that start from one crystal face and end in the amorphous region [17,18]. Such topological features and the alternation of crystalline and non-crystalline domains have formed the basis of most molecular level description of the semi-crystalline state [19,20]. Earlier works [22–24] have reported that among all

the possible molecular topology, tie segments, linking two adjacent crystallites, are supposed to contribute most effectively to the mechanical behavior of semi-crystalline polymers.

The probability that different segments of a given chain are incorporated into separate lamellae forming tie segments depends on the length scale of the chain in the molten state relative to the inter-lamellar distance. Huang and Brown's statistical approach appears to be the most appropriate one for assessment of TMs and has aroused much interest [15,88,89]. Experimental investigations [15,62–64] have also inferred that Molecular Weight Distribution (MWD) is a key factor for the formation of TMs. Nevertheless, unimodal MWD polymer made by traditional catalysis have conflicts between their mechanical properties and processing behaviors: improving mechanical performances by increasing molecular weight (M_w) usually deteriorates the processability because of high melt viscosity.

More recently, thanks to the development of some novel synthetic techniques, polymers with bimodal MWD have been drawing an increasing attention, for instance the application of bimodal polyethylene (BPE) for the transportation and distribution of water and gas. The bimodal MWD material consisting of both high molecular weight fraction and low molecular weight fraction provides more balanced performances for processing and mechanical behaviors, because the low molecular weight polymer chains promote the melt to flow easily whereas the high molecular weight fraction improve the mechanical properties of the material [65]. At present, there are two methods for directly producing bimodal resins: reactor in series configuration or single reactor with dual site catalysts [17,66]. Generally, it is difficult and expensive to directly prepare bimodal resins in the laboratory [67,68]. A melt blending is better suited to prepare a series of bimodal MWD polymers with variable molecular weight [69,70]. As for bimodal MWD polymers, the research mainly focuses on the synthetic techniques and characterization comparison to unimodal polymers [4,71,72]. However, no experimental technique allows to directly obtain quantitative data for the tie molecule concentration or topology, or to evaluate their exact

contribution to the mechanical behavior. The molecular topology is therefore evaluated only indirectly by mechanical testing [14,90], by molecular simulation [17,73] or statistical analysis [1,71,91,92]. Furthermore, the crystallization behavior of bimodal MWD polymers has rarely been reported [67,68,78], and the influence of the MWD on the final molecular topology of the obtained semi-crystalline polymer has not been investigated.

United-atom (UA) model and coarse-grained (CG) model are widely used in the simulation of polymer crystallization. UA dynamic simulations [79,80] have been performed for short chain (20 methylene units) systems, and it is found that an ordered phase was formed after the induction period. However the induction period was not quantitatively provided in these works. UA model is mainly used with relatively short chain systems, and it is not sufficient to simulate the growth of large lamellae. In CG model, the size of the system as well as the time scale involved are large enough to fully address the problems of the size, thickness, and shape of the lamellae as well as the molecular topology. Coarse-Grained Molecular Dynamics (CG-MD) is also an excellent tool to overcome difficulties of experimental measurements and to study quantitatively the non-equilibrium process of crystallization at the nanoscale. There are only a couple of reports on bimodal MWD using Monte Carlo simulation focused on polymerization [93–95]. To the author's knowledge, very few CG-MD studies focus on the effect of a bimodal MWD on molecular topology and/or mechanical properties. In this chapter, seven uni- and bimodal MWD polymer systems have been prepared using CG-MD. Extensive simulations of isothermal crystallization have been performed, the nucleation behavior and crystal growth have been investigated, and the final influence on the molecular topology of the obtained semi-crystalline polymer have been addressed.

3.2 Modeling systems and MFPT method

The CG-MD model potential is used in this chapter, the simulated polymer melts are prepared using RLP method, the isothermal crystallization treatment is performed to obtain

semicrystalline polymer, and the post-processing is performed using our hierarchical clustering method. All these methods and simulation details have been described in chapter 2, here we just appendix the modeling systems and MFPT method used in this chapter.

3.2.1 Modeling systems

As indicated in Figure 3-1a, experimental bimodal MWD polymers have two dominating chain lengths, a longer one and a shorter one. In order to mimic real bimodal MWD polymer, we incorporate in our CG-MD simulations two types of chains, long chains with 500 units and short chains with 100 units (Figure 3-1b). To investigate the isothermal crystallization mechanism of polymers and get insights of the strength of bimodal MWD polymers, we have created seven systems of uni- and bimodal MWD polymers with varying weight fraction of long chains. For the record, there is the same total number of units in the seven systems, *i.e.* 100,000, (see Table 1).

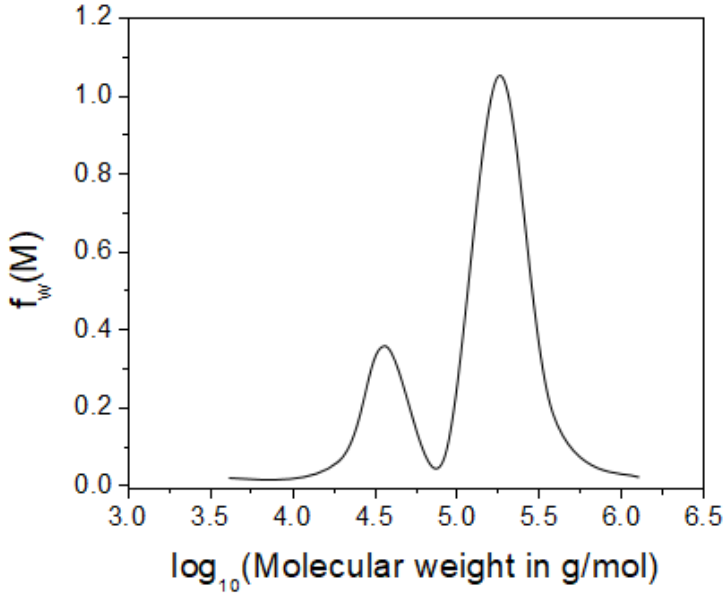

(a)

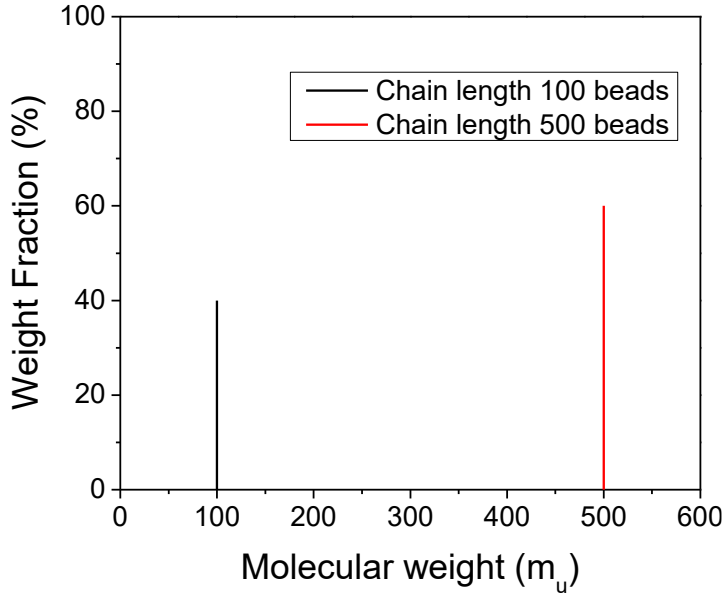

(b)

Figure 3-1 (a) Density distribution, $f_w(M_w)$, as function of the logarithm of chain molecular weight, $log(M_w)$, for the polybutadiene binary blend (from ref[96]). (b) Binary polymer model proposed in this chapter.

Table 1. Seven modeling systems of uni- and bimodal MWD polymers: long-chain length is 500 units, and short-chain length is 100.

Systems	Number of long chains	Number of short chains	Weight fraction of long chains	Average molecular weight ($\overline{M_w}/m_u$)
LC0	0	1000	0%	100
LC10	20	900	10%	108.7
LC30	60	700	30%	131.6
LC50	100	500	50%	166.7
LC70	140	300	70%	227.3
LC90	180	100	90%	357.1
LC100	200	0	100%	500

3.2.2 Mean First Passage Time method

Several methods have been developed to characterize nucleation process from Molecular Dynamics (MD) simulations. The approach by Wedekind *et al.* [97] makes particularly clear the link between the classical nucleation theory and the quantities available by MD simulation. This method has been successfully applied to simulation of nucleation in n-alkanes before [44,98], and is employed here. According to this method, the Mean First Passage Time (MFPT) is the elapsed time of forming largest nucleus in the system. As long as the critical free energy is relatively high ($\Delta G^* \gg k_B T$), MFPT of the largest nucleus size, $\tau(n_{max})$, takes the following form

$$\tau(n_{max}) = 0.5\tau^*\{1 + \mathrm{erf}[Z\sqrt{\pi}(n_{max} - n^*)]\} + 0.5G^{-1}(n_{max} - n^*)[1 + \mathrm{erf}(C(n_{max} - n^*))] \quad (3.1)$$

where τ^* is the average incubation time, n^* is the critical nucleus size, G is the growth rate, Z is the Zeldovich factor and C is a large positive fitting parameter. The second term on the right-hand side accounts for finite crystal growth rates of post-critical nuclei. This method allows us to estimate n^* and τ^* from MD simulations. Then after inserting n^* to equation (1.8), $\sigma_s^2\sigma_e$ will be obtained. Since $\sigma_s^2\sigma_e$ is directly related to free energy barrier (equation (1.6)), we use $\sigma_s^2\sigma_e$

as an indication of interfacial free energy. More details about this method are described in Wedekind [97] and Rutledge [44].

3.3 Results & Discussion

3.3.1 Isothermal crystallization

As explained in section 3.2.1, seven systems of uni- and bimodal polymers have been built, semi-crystalline polymers have been obtained, and analysis of the crystallites and molecular topology has been performed. In this section, we evaluate the ability of these systems to crystallize.

Mean Square Internal Distance (MSID) and Rouse time

Figure 3-2 shows the Mean Square Internal Distance (MSID) after relaxation of $5 \times 10^5 \tau_u$ at $T = 3.3\ \varepsilon_u/k_B$. The convergence of MSID curves indicates that all the seven systems are well equilibrated after period of $5 \times 10^5 \tau_u$ relaxation. There are poor statistics for system LC10, as expected, because of relatively smaller number of long chains. In this process of evolution, the end-to-end vector orientation autocorrelation function ($\langle Ree(t) \cdot Ree(0)/(|Ree(t)| \cdot |Ree(0)|\rangle$) has also been obtained to calculate Rouse time [44,99]. These results are shown in Figure 3-2d. From autocorrelation function versus time, a characteristic relaxation time is obtained. This relaxation time corresponds to the Rouse time τ_R, with the assumption that hydrodynamic interactions are screened in the melt. The inset of Figure 3-2d shows that Rouse time increases dramatically with weight fraction of long chains. And the Rouse times of system LC50 and LC70 are comparable with their incubation time (Figure 3-6a). We have quite fast nucleation here. Rutledge *et al.* [44] have also found the consistence of Rouse time and incubation time in the homogeneous nucleation of polyethylene when the chain length is 150 CH_2 groups.

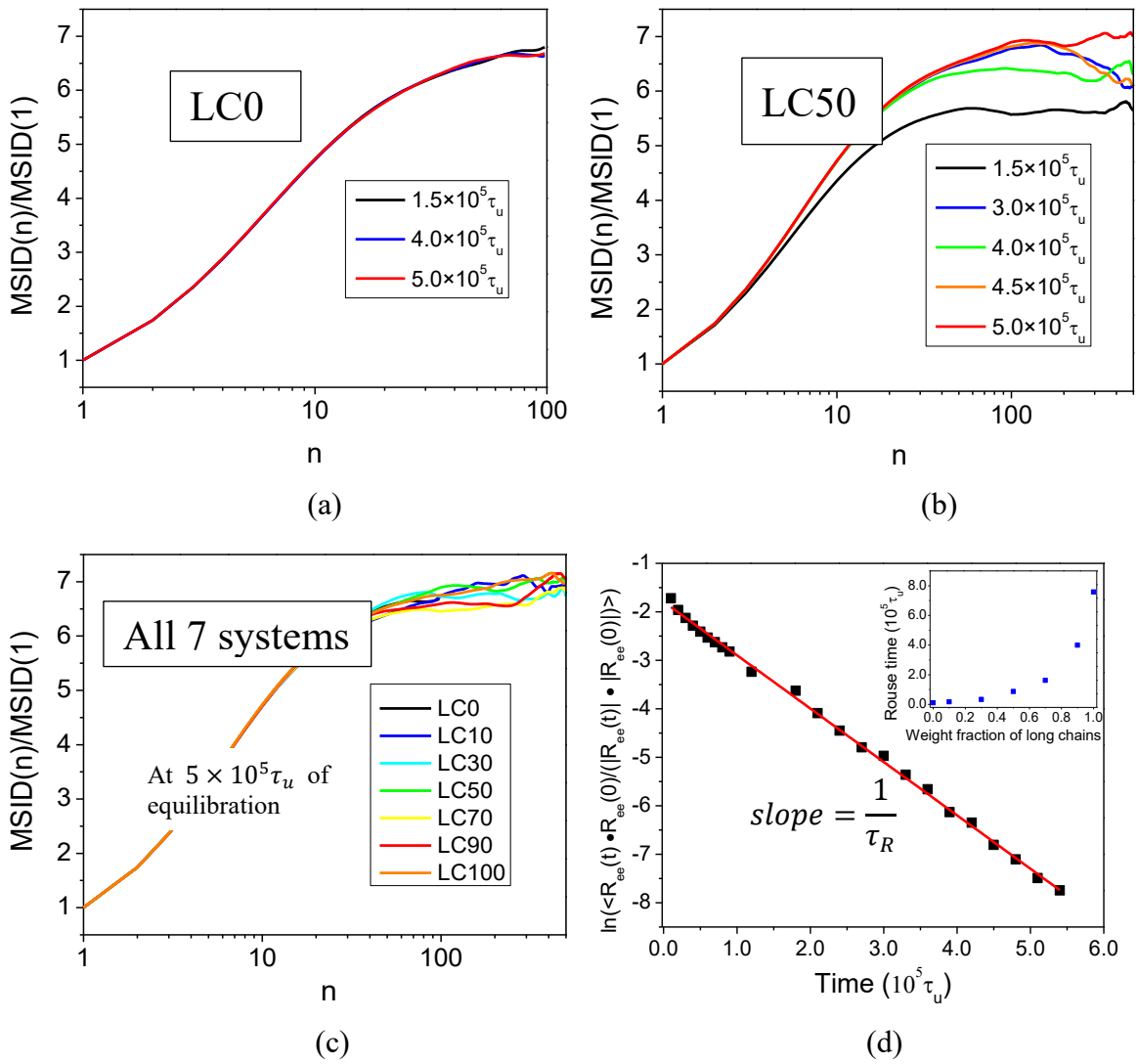

Figure 3-2 Evolution over time of Mean Square Internal Distances (MSID) of polymer melts. (a): system LC0; (b): system LC50; (c): all seven systems at time of $5 \times 10^5 \tau_u$ of equilibration. (d): End-to-end vector orientation autocorrelation function, $\langle Ree(t) \cdot Ree(0)/(|Ree(t)| \cdot |Ree(0)|\rangle$, for system LC50 melt at relaxation temperature of $2.3\epsilon_u/k_B$. (Inset) Rouse time as a function of weight fraction of long chains for the simulated polymer melts.

Overall crystallization and crystallinity

During the cooling stage from $T = 3.3$ to $2.3\epsilon_u/k_B$, the enthalpy varies linearly with time, (see Figure 3-3a), indicating that crystallization is negligible. During the isothermal process at $2.3\epsilon_u/k_B$, after an incubation time crystallization starts and the enthalpy goes down smoothly. The relatively high melting temperature, the significant melting enthalpy as well as the continuous decrease of enthalpy during crystallization are a strong evidence of the thermodynamic stability of the crystal phase for all studied systems. The whole isothermal

process lasts for $4 \times 10^5 \tau_u$, and the enthalpy of all the systems reaches a plateau. At this point all the systems have achieved the maximum of crystallization. Note that system LC100, consisting of only long chains, did not crystallize within fixed isothermal time of $4 \times 10^5 \tau_u$, suggesting that this system is much more difficult to crystallize compared with the other pure short chain and bimodal MWD systems. In the following discussions, we mainly focus on the six crystallized systems. In Figure 3-3(b~e), we also provide four snapshots in the process and at the end of crystallization for systems LC0 and LC50. Large lamellae with tapered edge have been obtained. Yamamoto [100] has also reported tapered shape lamellae between two parallel substrates using CG model.

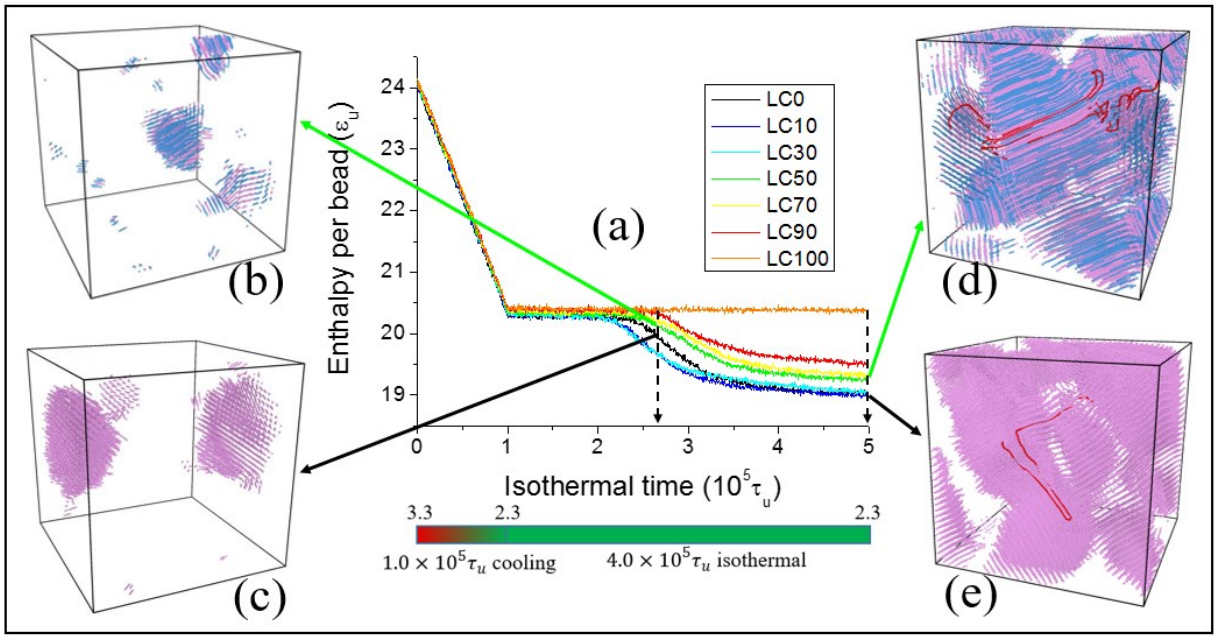

Figure 3-3 (a) Thermogram starting from equilibrated liquid phase, cooling down from $T = 3.3$ to $2.3\epsilon_u/k_B$ and isothermal relaxation at $T = 2.3\epsilon_u/k_B$. (b)&(c) Snapshots of system LC50 and LC0 at time of $2.65 \times 10^5 \tau_u$. (d)&(e) Snapshots of system LC50 and LC0 at the end of isothermal crystallization. The colors in snapshots: pink is crystal atom of short chains, blue is crystal atoms of long chains, red is a typical chain spanning crystalline and amorphous phases.

In order to calculate the achieved crystallinity, we use two methods. The first method is based on the experimental approach on isothermal crystallization [101]. The crystallinity is defined as

$$X_C = -\frac{\Delta H_c}{\Delta H_f^0} \qquad (3.2)$$

where ΔH_c the enthalpy of crystallization and ΔH_f^0 the melting heat of the completely crystalline materials at the equilibrium melting temperature T_m^0. ΔH_f^0 has been calculated in our previous article [1] during melting, yielding $\Delta H_f^0 = 1.9\ \varepsilon_u$. Figure 3-4 shows that the calculated crystallinity goes down from 0.66 to 0.46 with the weight fraction of long chains at the end of isothermal treatment, since long chains make it more difficult for the polymer chains to crystallize from the entangled melts. This is consistent with Li *et al.* [102] who reported that the crystallization enthalpy (ΔH_c) would decrease with the increased molecular weight. Krumme *et al.* [68] have also drawn a conclusion that fully achieved crystallinity decreases linearly with the molecular average weight in their experimental study of bimodal MWD polyethylene. Moreover, Triandafilidi *et al*. [103] have found a faster decrease of crystallinity with chain length of monodisperse polymer melts in MD simulations.

Nevertheless, there are distinct crystal characteristics of polymer compared with other materials. Measurement of the density and other properties of polymer crystals have shown that they are not perfect crystals. The density of the crystals is always less than the theoretical density, which means that non-crystalline material must also be present in the crystal. It is clear that crystalline polymers are by no means perfect from a structural viewpoint (defects with chain fold). They contain crystalline and amorphous region and probably also areas, which are partially disordered. The method of equation (3.2) is a result of enthalpy change, which incorporates crystallization and defects. It is not geometrical crystal and amorphous analysis. On the other hand, to detect the molecular topology of the semi-crystalline system, we also need to locate the geometrical crystals to trace the chains going back and forth of the crystallites.

Given this, we have proposed the hierarchical-clustering method, as illustrated in section 2.3, to calculate crystallinity using our algorithm. The comparison of the two methods is shown in Figure 3-4. It is clear that the results are consistent. Thus, algorithm illustrated in section 2.3

and 2.4 will be used to analyze the topological structure of semi-crystalline systems in the following sections in this chapter.

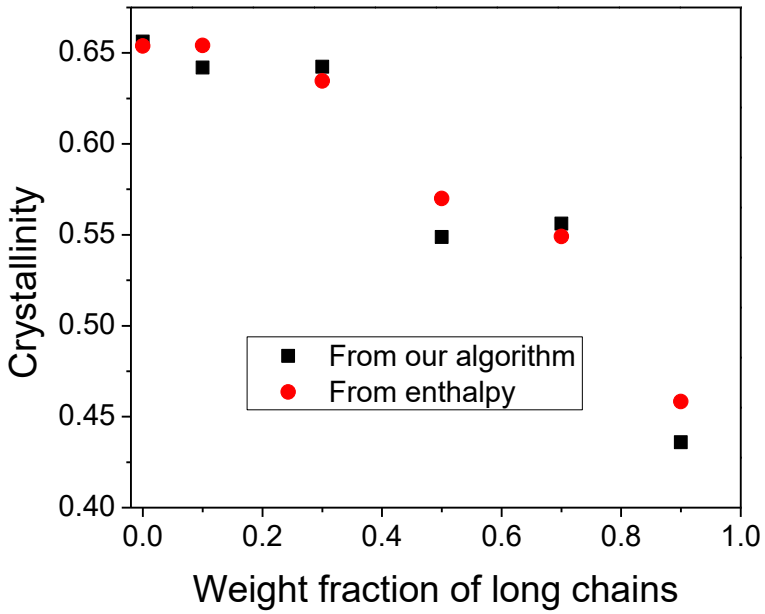

Figure 3-4 Calculated crystallinity from enthalpy and from hierarchical-clustering method versus weight fraction of long chains.

Homogeneous Nucleation

The crystallization of a polymer arises from nucleation and crystal growth: the combination of these two processes dominates the crystallization rate. When the melt has been cooled and becomes supercooled, the nucleation starts and nuclei appear. Thermal fluctuations should be large enough in order to overcome the enthalpy barrier for nucleation. Once the nucleus is larger than the critical size it will grow spontaneously as this will cause the Gibbs free energy to decrease [104]. According to CNT, the nucleation rate I is given by equation (1.8). Here we just want to demonstrate that at a given temperature, nucleation rate depends on interfacial free energy and the movement of chain segments. We will discuss nucleation behavior of uni- and bimodal MWD systems in these two decisive perspectives.

The mean first-passage time method of n_{max}, as explained in section 3.2.2, is obtained using independent starting configurations for all the crystallized systems. Three trajectories for all the systems are collected. To be concise and explicit, here we only plot systems LC0 and

LC50, see Figure 3-5. Equation (3.1) is fitted to each of these curves, as shown in Figure 3-6a. Then we obtain the incubation time τ^* and the critical nucleus size n^*. After inserting n^* into equation (1.6), we can obtain the interfacial free energy $\sigma_s^2\sigma_e$. We plot incubation time (Figure 3-6a) and interfacial free energy $\sigma_s^2\sigma_e$ with critical nucleus size n^* (Figure 3-6b) respectively versus weight fraction of long chains.

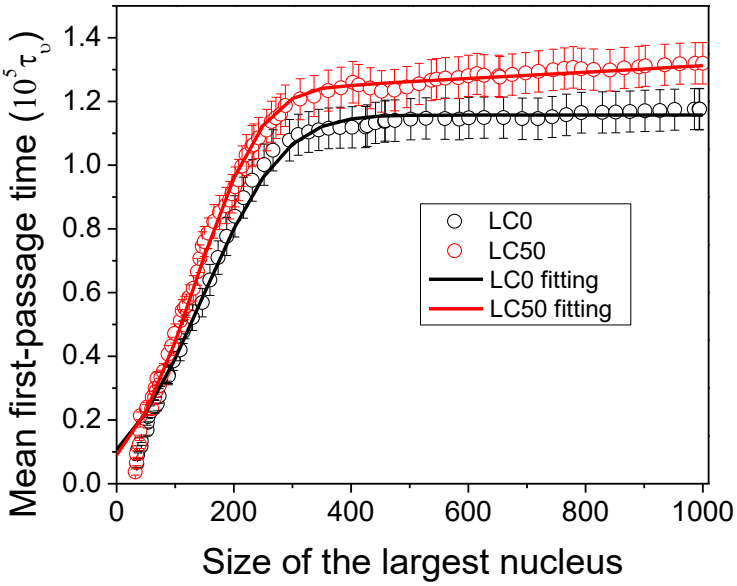

Figure 3-5 Mean first-passage time of maximum nucleus size (n_{max}), and fitting curves of function (3.1).

The incubation time τ^* is the time elapsed before the establishment of stead-state nucleation in the bulk. The nucleation rate I is equal to the inverse of the product of the incubation time and the volume of the system[105] : $I = 1/(\tau^* * V)$, where V is the volume of the system. From Figure 3-6a we can see that the incubation time varies between $0.9 \times 10^5\tau_u$ and $1.7 \times 10^5\tau_u$ for the six crystallized system. It first decreases with weight fraction of long chains, and reaches a minimum at 30%, then it turns to grow rapidly. System LC90 takes the longest time before the initiation of crystallization, whereas system LC30 takes shortest time instead of LC0. Clearly bimodal MWD system would promote the nucleation of isothermal process.

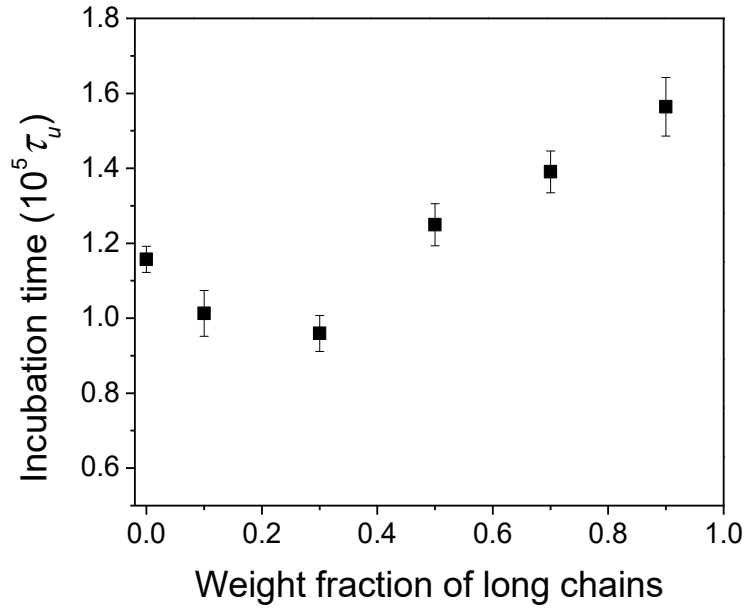

(a)

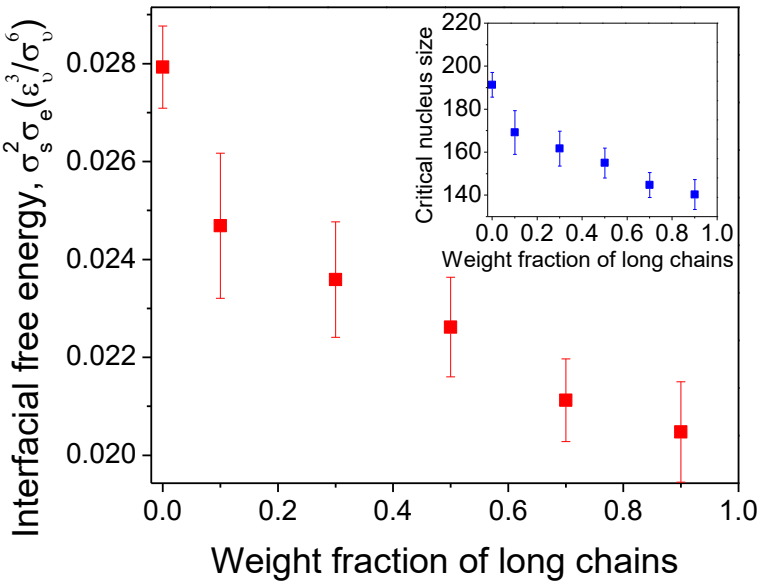

(b)

Figure 3-6 (a) Incubation time versus weight fraction of long chains. (b) Calculated interfacial free energies versus weight fraction of long chains. (Inset) Critical nucleus size versus weight fraction of long chains.

First of all, we explore the nucleation in the perspective of interfacial free energy**.** From Figure 3-6b we can see that interfacial free energy exhibits a drop from pure short chain system LC0 to system LC10 with 10% of long chains. And then interfacial free energy keeps going down until system LC90. According to equation (1.5), the free energy barrier would follow the same trend as interfacial free energy. Apparently, it turns out that the long chain content would

clearly promote the nucleation of the whole system in the perspective of free energy barrier. Song *et al*. [4] have also indicated that high molecular weight component can lower the fold surface free energy (σ_e) of bimodal high density polyethylene (HDPE). They observed promoted nucleation rate during isothermal crystallization experiment, and thereby concluded that high molecular weight component may act as an effective nucleation agent in HDPE matrix. Achilias *et al*. [106] have also indicated that long chains exhibit easier nucleation. We believe that the decreasing interfacial free energy could result from the role of chain-folding (more chain folding with long chains) in the process of nucleation.

Chain-like connection brings an intrinsic anisotropy to the shape of macromolecules, which favors parallel packing the crystalline states [28,107]. Therefore, polymers can perform two typical modes of crystal nucleation, one is chain-folding configuration for a parallel alignment of consecutive strands along each chain, named *intramolecular* crystal nucleation. Another is the fringed-micelle configuration for a parallel alignment of several strands from different chains named *intermolecular* crystal nucleation [28], as illustrated in Figure 3-7a. Flory [108] has estimated the free energy change of intermolecular nucleation of polyethylene, and Zachmann found its stem-end surface free energy around 280 mJ/m^2 [109,110]. In contrast, Hoffman and Miller estimated the fold-end surface free energy of polyethylene around 90 mJ/m^2 [111]. In the overcrowded surface of the fringed-micelle crystalline system, the amorphous segments would encounter significant entropy loss. That can result in high-end surface free energy of fringed-micelle crystals. Since the interfacial free energy is responsible for the nucleation barrier, the chain-folding mode will have a much lower free energy barrier than the fringed-micelle mode in both primary and secondary crystal nucleation. There always exists a competition between two modes of crystal nucleation during polymer crystallization.

As we can see in Figure 3-7a, intramolecular nucleation occurs when a chain forms a tight loop. In this case the fold-end surface free energy will be lower than that of stem-end. In order

to determine the critical size of a tight loop we have looked at the influence of the thickness of the interfacial region on the energy per bead. It turns out that the energy per bead is influenced by the interface up to a distance of five bonds and that it remains constant for larger distances. This is also consistent with the LJ cutoff radius which is in our case approximately equal to $5\sigma_u$. From this analysis we set the critical length of a tight loop as 11 beads. We have found that the majority of loops are tight ones. Meyer *et al.* [112] used a simplified version of model for poly(vinyl alcohol) (PVA), and also found that most chains reenter the same lamellar by tight loop, resulting in chain-folded lamellae of polymer crystal.

By inspecting Figure 3-7a we see the intramolecular nucleation of a tight- folded chain gives rise either to one tight loop with two crystal segments or two tight loops and three crystal segments, so that the ratio $\mathfrak{R}$ between the number of tight loops and crystal segments will be $\mathfrak{R}$=1/2 or higher $\mathfrak{R}$=2/3 in this case. For the intermolecular nucleation there are no tight loops, so that $\mathfrak{R}$=0. In this way can establish the occurrence of intra- or intermolecular nucleation by quantifying the ratio $\mathfrak{R}$ between the number of tight loops and crystal segments.

Thanks to our algorithm explained in section 2.3, we are able to calculate the ratio $\mathfrak{R}$ of tight loop/crystal in the process of nucleation. In Figure 3-7b, we plot the ratio $\mathfrak{R}$ of tight loop/crystal in the nucleation process. For clarity's sake, we only plot four crystallized systems instead of six. We can see that the ratio $\mathfrak{R}$ for system LC0 is very close to 0, which indicates that intermolecular nucleation dominates system LC0. This ratio $\mathfrak{R}$ gradually increases to system LC90, showing that the chain-folded nucleation becomes important as the weight fraction of long chains increases. Figure 3-7b shows what happens during the nucleation process (before growth), where the crystallinity is very low. In this regime, crystallinity may fluctuate with time. In the nucleation process, the ratio of tight loop over crystal segments is fairly constant with crystallinity, and the different systems clearly exhibit different ratios, leading to different nucleation mechanisms (intra- or inter-, see Figure 3-7a). However, this ratio is totally

in different situations during the crystal growth and at the end of the crystallization, which results from crystal thickening and growth mechanisms.

In some MD simulations [113,114], researchers assumed that only intramolecular nucleation happens in their monodisperse polymer system, and they have concluded that the free energy barrier is independent of chain length. In some experimental works[2,115], it has also been concluded that the free energy barrier for nucleation is independent of molar mass. Umemoto *et al*. [116] have also reported that there is a transition from intermolecular to intramolecular nucleation when molecular weight is increased to around 3000 Da. According to these experimental and numerical works, it is believed that free energy barrier of uni-modal polymers is insensitive to molecular weight within the intramolecular nucleation region (*i.e*. long-chain region) and within the intermolecular nucleation region (*i.e*. short-chain region), but differs between the two regions.

In the current chapter, we have used chain length of 500 beads and 100 beads. According to Figure 3-7b, the ratio of tight loop/crystal segments of system LC0 (100-bead length) is very close to zero, which indicates that intermolecular nucleation dominates. In systems LC10/LC50/LC90, this ratio increases with rising content of long chains (500 beads). Therefore the chain length 100 is in intermolecular nucleation region, and that of 500 is in intramolecular nucleation region. Consequently, in our bimodal systems, the interfacial free energy variation results from a competition between inter- and intra- molecular nucleation. Then the decreasing interfacial free energy with weight fraction of long chains results from rising fraction of chain-folded nucleation.

Even if the quantitative details of the results could depend on the specific values of the chain lengths used for our bimodal systems, the same general conclusions would still hold as long as the two types of chains are in intra- and inter- molecular nucleation regions respectively.

MD simulations [113,114] have suggested that the free energy barrier for nucleation in single polymers is independent of chain length in the intramolecular nucleation region. Experimental works [2,115] on the primary nucleation of polyethylene also reported that the free energy barrier for nucleation is independent of molar mass within the intermolecular nucleation and within intramolecular nucleation respectively. Indeed, it seems that the intra and intermolecular nucleation are respectively insensitive to chain length. Hence, we believe that the decreasing interfacial free energy with weight fraction of long chains results from rising fraction of chain-folded nucleation.

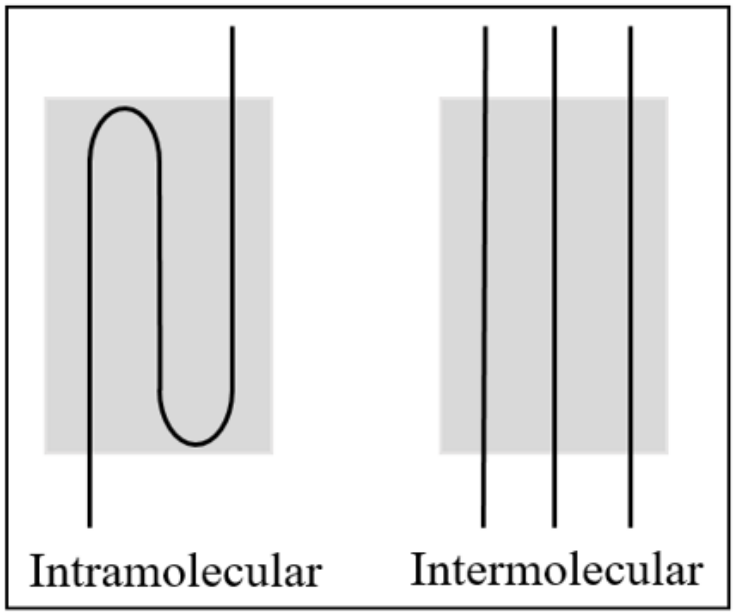

(a)

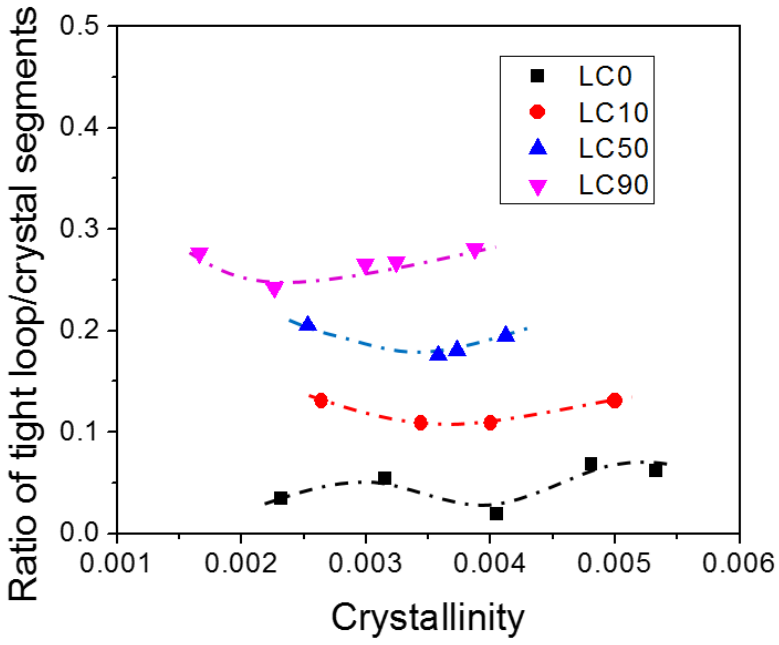

(b)

Figure 3-7 **(a)** Illustration of intramolecular chain-folding mode and intermolecular fringed-micelle mode of crystal nucleation of polymers. **(b)** Ratio ($\Re$) of the number of tight loops and crystal segments.

Afterwards, we explore the nucleation in the perspective of the movement of chain segments. In equation (1.8), E_d is the activation energy for processes that transport chain segments. Here we include shear viscosity η as an indicator of E_d.

Nucleation is a very complex process, because each polymer should be transported and rearranged under the strong restriction that the molecular chain must not be "cut". Nishi *et al.* [2] reported that the primary nucleation is a process of "chain sliding diffusion" within the nucleus which requires disentanglement of molecular chains. It is also natural to consider that the chain sliding diffusion and disentanglement become more difficult with increase in molecular weight. As a matter of fact, in nucleation and crystal growth, polymer chains are highly sheared and somewhat disentangled at the local growth front. Instead of estimating zero-shear viscosity, we believe that a shear viscosity is more meaningful in exploring chain movements in the process of nucleation.

We calculate the shear viscosity with reverse non-equilibrium molecular dynamics (RNEMD) method of Muller-Plathe [117]. Compared to the traditional NEMD techniques, the main advantage of RNEMD is the fact that no energy is added to the system, and hence no energy needs to be removed by an external thermostat. By constant swapping the largest momentum components in the $+x$ and $-x$ directions, a gradient ($\partial v_x/\partial z$) of x component of the melt velocity (v_x) is formed with respect to z direction. It is also denoted as the shear rate. The momentum flux $j_z(p_x)$ is the x component of the momentum p_x transported in z direction per given time and per unit area. The shear viscosity η is also defined as: $j_z(p_x) = -\eta(\partial v_x/\partial z)$. We obtained the shear viscosity for all the seven systems at the shear rate around $9.5 \times 10^{-3}\tau_u^{-1}$ at the isothermal temperature of 2.3 ϵ_u/k_B, at the beginning of the isothermal treatment before the crystallization started. As in RNEMD, chain sliding and disentanglement would occur in the sheared systems, which also happens in the process of nucleation.

Figure 3-8a shows the shear viscosity as a function of the weight fraction of long chains at isothermal temperature of 2.3 ϵ_u/k_B. As in reference [118], logarithmic shear viscosity increases linearly with average molecular weight. Evidently viscosity jumps up fast with increasing weight fraction of long chains. It is widely accepted in experiment and modeling [46,47] that zero

rate viscosity is proportional to the power α of molecular weight, $\eta_0 \propto M_w^{\alpha}$, where the exponent α is 1.0 for unentangled chains and 3.4 for entangled chains. In this chapter, we found that the shear viscosity $\eta \propto {M_w}^{1.317}$, which is reasonable because a proportion of chains disentangle and align as we mentioned above in the process of shearing. Figure 3-8b shows the configuration of a disentangled single long chain of system LC50 under shear rate. This indicates that the polymer chains are somehow disentangled in the process of shearing. That accounts for the depression of power-law exponent.

According to equation (1.8), E_d, the activation energy for the movement of chain segments, would be highly promoted as weight fraction of long chains goes up. As a result, the nucleation rate will decrease. From this analysis, increasing the weight fraction of long chains has two conflicting effects in the nucleation rate, which is promotion of interfacial free energy and decrease of chain diffusion. Interestingly, as we have seen for the incubation time in Figure 3-6a, interfacial free energy dominates the low M_w part, and then reaches a minimum value at 30% of long chains. Afterwards, the incubation time increases continuously, whereas viscosity increases a lot and turns to dominate nucleation.

Some experimental studies [115,119] of polymer crystallization have been used to argue that nucleation rate is inversely proportional to molecular weight. Gee *et al*. [120] have also reported that the time required for the onset of nucleation decreases with the number of monomers in the polymer. Essentially, long chains help the formation of critical nuclei for short chains. When blending a small proportion of long chains (under 30% in our case), the free energy barrier strongly decreases because of reduced interfacial free energy, whereas the movement of chain segments is just slightly lowered. We have provided insights into how bimodal MWD polymer promotes both nucleation and processability.

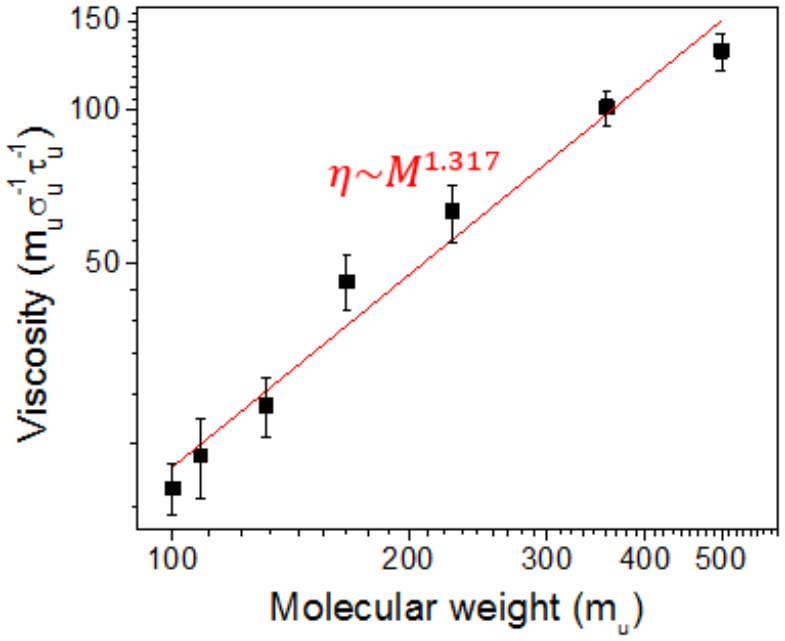

(a)

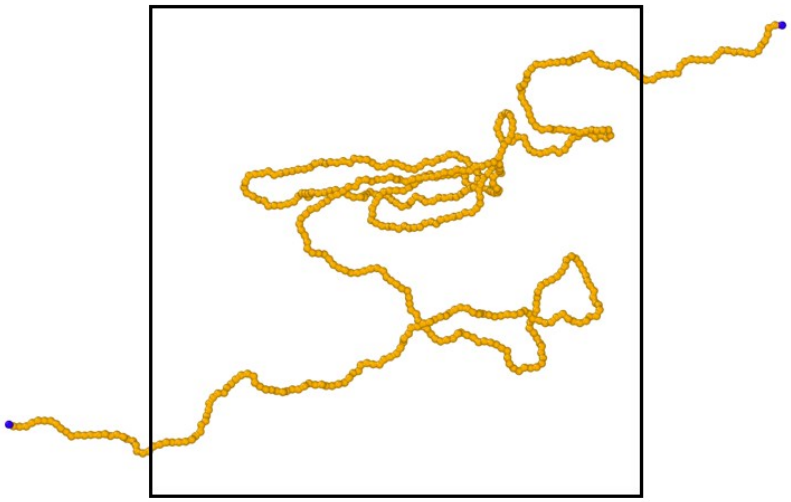

(b)

Figure 3-8 (a) Shear viscosity with average molecular weight, with the shear rate around $9.5 \times 10^{-3}\tau_u^{-3}$ and at the isothermal temperature of 2.3 ϵ_u/k_B. (b) Configuration of individual long chain under shear rate of System LC50.

Crystal growth

As we explained above, we can calculate crystallinity at any time by the decrement of enthalpy using equation (3.2). We make the approximation that the relative crystallinity X_t equals crystallization divided by the fully achieved crystallinity within our isothermal time of $4 \times 10^5\ \tau_u$. The relative degree of crystallinity (X_t) of system LC50 versus crystallization time

at the isothermal temperature is plotted in Figure 3-9a. The tangent line at $X_t = 0.5$ is plotted: the gradient slope of this line is equal to the maximum rate of crystallization, which is an indication of general crystallization rate [3].

We have obtained the max rate of crystallization for all the six crystallized systems and plotted versus different fraction of long chains are presented in Figure 3-9b. In contrast to the nucleation rate, the growth rate decreases continuously with weight fraction of long chains. The growth rate goes down slowly at the beginning, and then undergoes an abrupt drop around 40% of long chains, after that the growth rate keeps decreasing fast until the end. Gee *et al.* [120] have also reported that growth rate of the crystal decreases with the number of monomers in the polymer. It turns out that the transport activation energy dominates the max rate of crystallization. However, from system LC0 to LC90, the molecular weight increases by 3.57 times, and max rate of crystallization only decreases by 20%. Evidently there are other factors that could also influence crystallization rate, like surface free energy, thickness of crystallite, melting enthalpy [43,121], which we do not consider in this chapter. Nevertheless, we believe that bimodal MWD is also another key factor that influences crystallization rate. Krumme *et al.* [68] and Shen *et al.* [78] have both found that the crystallization half-time is not strongly changed with increasing molecular weight in their studies of bimodal MWD polyethylene.

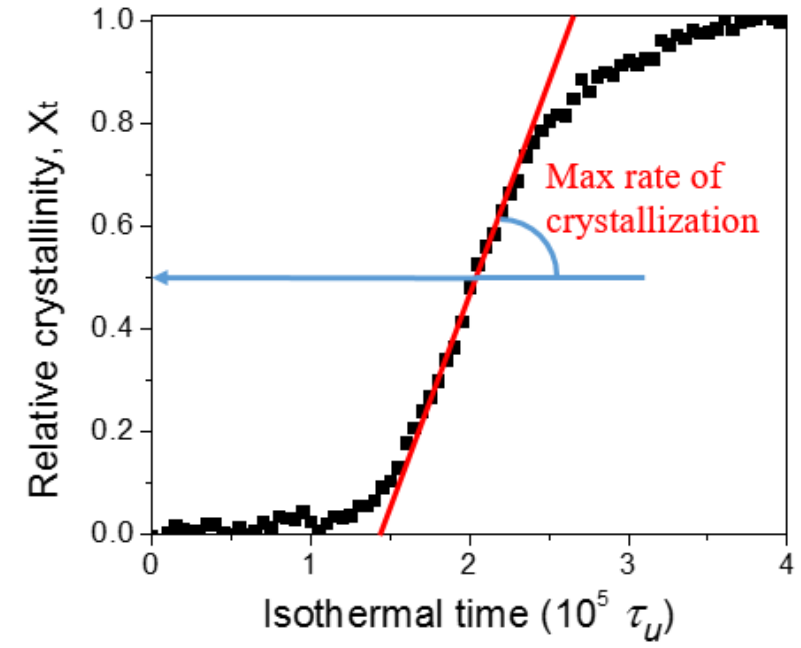

(a)

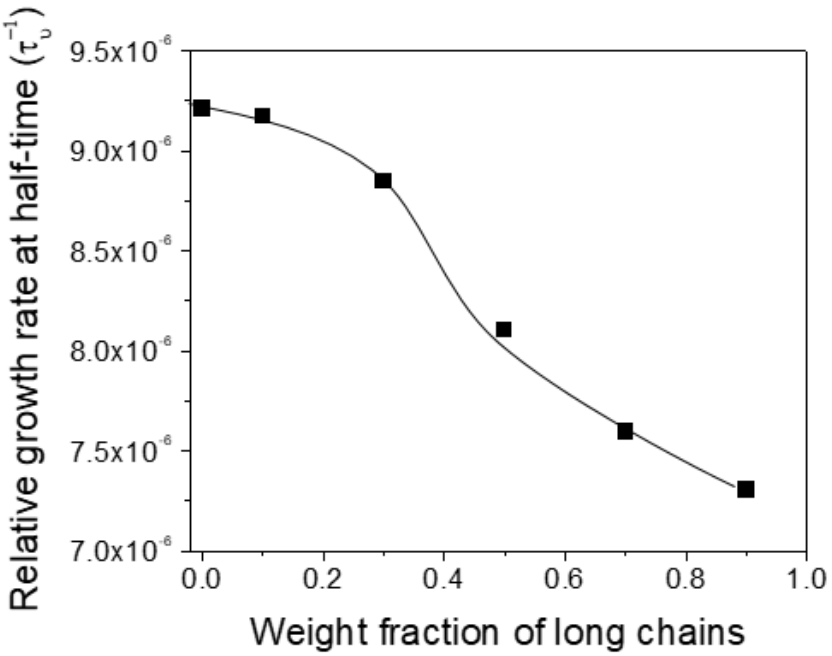

(b)

Figure 3-9 (a) Relative crystallinity of system LC50 with isothermal time, definition of max rate of crystallization. (b) Relative growth rate at half-time of crystallization as a function of weight fraction of long chains.

3.3.2 Molecular topology: tracing back to the same crystallinity (X_c =43%)

It was suggested that the chain topology that governs the distribution of the stress at a local scale on the crystalline lamella surface plays a major role in the propagation of microcracks from which are formed the crystal blocks [90]. Obviously, we are not able to compare the topology of the different systems because of the different crystallinities. Therefore, we assume that we can compare the chain topology if we trace all the systems back to the same crystallinity. We use system LC90 as a reference since it has the lowest crystallinity (43%) at the end of the crystallization: we analyze the topology of all the systems at this value of the crystallinity.

In order to link the topological state to the crystallinity, we performed extended isothermal MD steps for system LC50 after the end of the crystallization. We can see from Figure 3-10 that from $3 \times 10^5 \tau_u$ to $5.5 \times 10^5 \tau_u$, the crystallinity is almost constant and the molecular topology also slightly fluctuates around a plateau. This suggests that the topology does not significantly change if the crystallinity has saturated. Based on the results of Figure 3-10, we have reasons to speculate that crystallinity is representative of the corresponding topology (loop, tie, cilia). Given this speculation, we traced the systems back to the same crystallinity of around 43% and compare their topology.

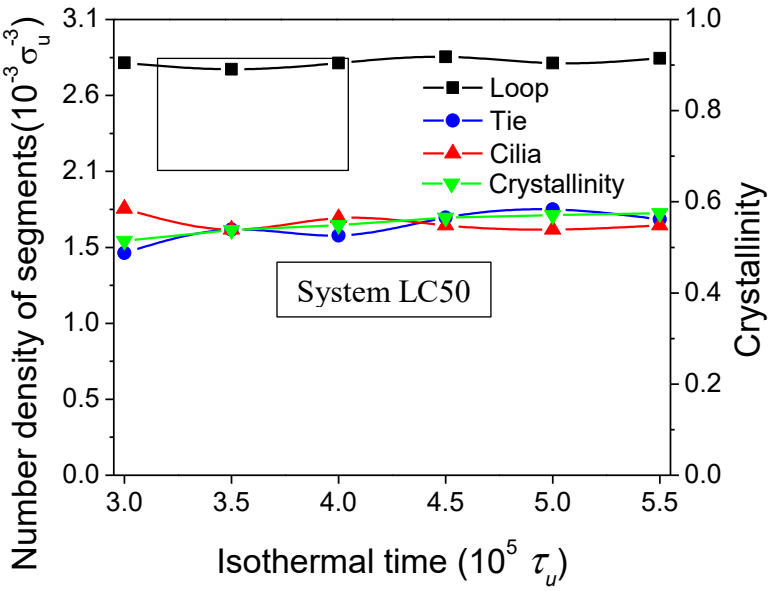

Figure 3-10 Extended isothermal crystallization procedure of system LC50.

Figure 3-11 shows the molecular topology (loop, tie, cilia) for different weight fraction of long chains, of all the system at the same crystallinity (43%). We can see that the number density of loops (Figure 3-11a) approximately increases with long-chain fraction. This results from the increasing chain length. Clearly long chains are more likely to go out of a crystallite and fold back to the same one, forming loop segments. Besides, we argue that the number of crystallites is also a factor that promotes the formation of loops. This would explain the drop of the loop curve at the beginning. There are three crystallites in system LC0, while only one in system LC10. Even with shorter chain length, LC0 has more loop segments than LC10.

Tie segments play an important role in mechanical properties, fracture toughness and resistance to slow crack growth of semi-crystalline polymers. Previous research has proved [20] that the thickness of the amorphous layer (L_a) has a stronger impact than the crystal thickness (L_c) on the tie chain concentration. In other words, the distance between crystallites is a key factor for the formation of tie segment. For our systems, there are different numbers of crystallites in the simulation box resulting in different distances between crystallites. It is reasonable to compare the number density of tie segments between systems with the same number of crystallites (see Figure 3-11b). For our systems with the same number of crystallites, tie segments also increase with long-chain weight fraction. Fundamentally, longer chains are more probable to span the amorphous phase and connect two crystallites. The probability of forming tie molecules decreases with increasing L_a [14,122]. As for cilias, it is clear that the number density decreases from LC0 to LC10. Since the number of chains also decreases from LC0 to LC10, consequently the number density of chain ends decreases, leading to reduced probability of forming cilias.

Rutledge *et al*. [21,26,123] created semicrystalline samples with alternate crystal and amorphous stacks. And the noncrystalline regions were subjected to equilibration by an interphase Monte Carlo (IMC) method that included both local rearrangements and alterations of chain topology.

Out of the total number density of loop/tie/cilia segments in our simulations, the loop segments vary between 34.5%~66.5% and the cilia segments vary between 53.2%~20.9%, from systems LC0 to LC90 at the crystallinity of ~43%. Whereas Rutledge *et al.* [26] obtained 63.9% of loops and 33.3% of cilias in their systems at the average crystallinity of 53.7%. Kubo *et al.* [27] have also built coarse-grained models with chain length of 1000 beads, where forces were applied to promote crystallization. They obtained 43.1% of loops in average at the crystallinity of 76%, more percentage of ties and less cilias than in the current chapter. Compared with Kubo *et al.*, the lower percentage of tie segments and increase of cilia segments could be attributed to the short chains in our systems.

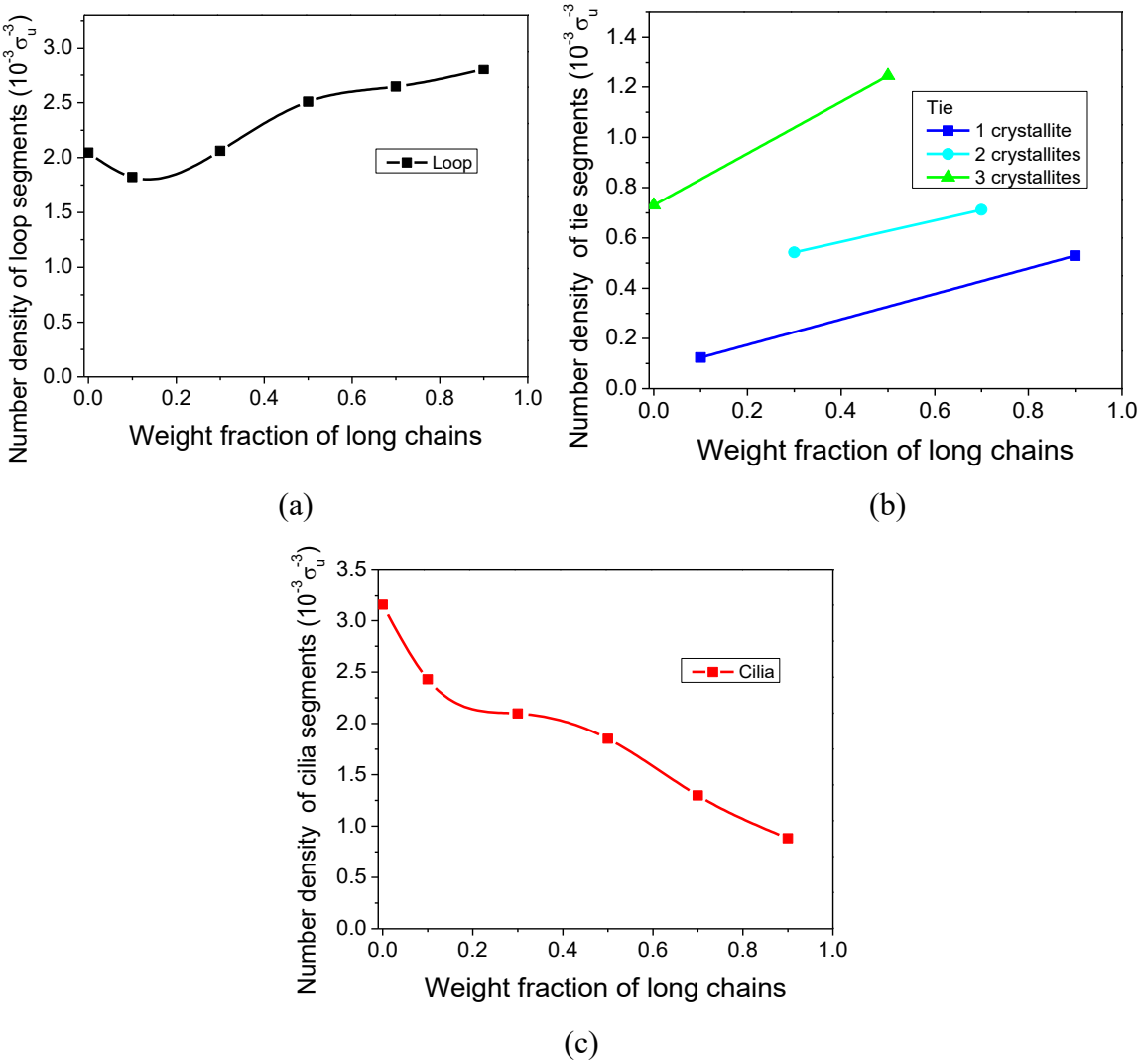

Figure 3-11 Molecular topology of 6 crystallized systems: comparison at the same crystallinity of 43%. Number density of **(a)** loop, **(b)** tie **(c)** cilia as a function of weight fraction of long chains.

Figure 3-12 shows the average thickness of crystallites for all the simulation systems at the same crystallinity of 43%. When it comes to MD simulation, the boundary effect would be a key factor for crystal thickness, because the small distance between crystallites would hinder crystal thickening. Similar with the tie-segment case above, it is also reasonable to compare the average thickness of crystallites between systems with the same number of crystallites (see Figure 3-12). We can see that the average thickness drops from 1-crystallite case to 3-crystallite case, proving the evident boundary effect of MD simulation. This phenomenon is opposite to the behavior of the number density of tie chains (see Figure 3-11b) which are promoted by the number of crystallites instead. For the situations with the same number of crystallites, the average thickness decreases with long chain content. It seems that crystal thickness is promoted by short-chain content, which happens to be the inverse of the number density of tie segments (Figure 3-11b). This conclusion is consistent with experimental results [20,124] in a certain range. Sun *et al.* [124] found that the lamella thickness increased with short chain content in their crystallization studies of bimodal blends. Fujiwara *et al.* [125] indicated that lamellar thickening growth occurred through chain sliding diffusion, which is the sliding motion along the chain axes.

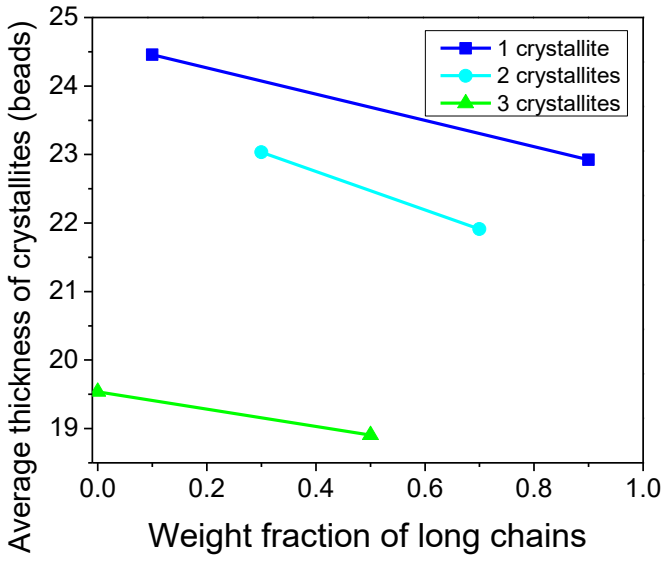

Figure 3-12 Average thickness of crystallites for 6 simulation systems: comparison at the same crystallinity of 43%.

3.4 Conclusions

In this chapter, we have investigated the crystallization and molecular topology of bimodal MWD polymer by MD simulation. We have found that the incubation time of nucleation decreases with rising weight fraction of long chains, and that the long-chain content has opposite effects on nucleation in the perspective of interfacial free energy and chain segment diffusion. Interfacial free energy decreases with weight fraction of long chains, which we attribute to the competition of chain-folded and chain-extended nucleation. We have provided insights into how bimodal MWD polymer promotes both nucleation and processability, which has been rarely addressed before.

Furthermore, we have proposed a novel hierarchical-clustering method to quantitatively access molecular topology of semi-crystalline systems. It has been proved that the number of loop and tie segments increases with rising weight fraction of long chain content. Topological features such as the tie segment population in semicrystalline polymers are believed to play an important role in the mechanical properties. Whereas direct experimental measurement of the molecular topology is not easy, especially during deformation. However, there are already a few frontier researches [21,26,27,123] that have addressed the effect of molecular topology on mechanical properties by molecular dynamics simulation. It has been found that an increase in stress transmitters, which are molecular networks, such as tie segments and bridging entanglements, increases the yielding stress and decreases the generation of voids. As expected, bridging entanglements are stretched, and these persistent bridging entanglements behave similarly to tie segments during deformation. However, the evolution of molecular topology in the process of semicrystalline polymer deformation would be also very interesting, and it has never been investigated to the author's knowledge. Further work on this point can enhance the molecular understanding of the mechanical properties of bimodal MWD semi-crystalline polymers.

Chapter 4

Nucleation and verification of classical nucleation theory

Contents

Abstract: In chapter 3, we have discussed the nucleation of polymers based on the hypothesis that classical nucleation theory is applicable to polymer nucleation. To the author's knowledge, all the researchers used this hypothesis, and its validity has never been quantitatively proved. The objective of this chapter is to verify the validity of classical nucleation theory to polymer nucleation, and to discuss the influence of bimodality and temperature on polymer homogeneous nucleation.

Coarse-grained dynamics simulations have been performed to study the homogeneous nucleation of bimodal and unimodal molecular weight distribution (MWD) polymers with equivalent average molecular weight. A Growing Probability Method has been proposed to determine the critical nuclei, which is used to calculate the free energy barrier to form nuclei. This method traces the sizes of all the nuclei growing and shrinking in the process of isothermal treatment, and obtains the critical nucleus size when the probabilities of growing and shrinking are equivalent (*i.e.* 50%). The activation energy of diffusion has also been obtained through the temperature dependence of diffusion coefficient. The validity of the classical nucleation theory (CNT) has been confirmed through our molecular dynamics simulations of the nucleation rate. Compared with unimodal system, the bimodal system exhibits lower interfacial free energy and

consequently lower free energy barrier for nucleation, while the two systems have similar activation energy for diffusion. This suggests that the promoted nucleation rate of bimodal MWD polymer is a result of the reduction of interfacial free energy, which is eventually a result of chain-folding nucleation of long chain component.

Key words: homogeneous nucleation, bimodal MWD polymer, interfacial free energy, classical nucleation theory

4.1 Introduction

Polymer crystallization consists of two stages: homogeneous nucleation and crystal growth. Extensive investigations [4,14,126–128] have been done on the second stage using both experimental and simulation techniques. Yi *et al*. [44] have calculated the nucleation rate of polyethylene and found that the nucleation rate is insensitive to the chain length within the investigated molecular weight region. Gee *et al*. [129] have investigated the phase separation and morphology of polymer melts in the early ordering stages before crystallization. However, the initial stage involving nucleation has drawn less attention and remains relatively poorly understood.

The nucleation rate strongly depends on the free energy barrier of a critical nucleus. The formation of crystal nuclei is governed by a competition between the loss in free energy of the nucleus, and the gain in free energy of the crystal-melt interface. The interfacial free energy is therefore essential to calculate the free energy barrier for crystal nucleation.

Experimental measurement of polymer crystal−melt surface tension is challenging, and homogeneous nucleation experiments are quite difficult to carry out. Only a few experiments [119,130,131] have been performed in pure droplets with an emulsion of molten polymer, where homogeneous crystallization is monitored by in-situ microscopy or by wide-angle X-ray scattering. Surface tensions then have been obtained by fitting classical nucleation theory (CNT) to experimental results [119,132,133].

Analytical theory and molecular simulation provide an alternative way for obtaining the polymer interfacial free energies. Self-consistent field theory [134] has been used to analytically obtain interfacial free energy from the equilibrium crystal−melt interface of polyethylene, by assuming the chain end surface to be a grafted brush of chain folds in a self-consistent pressure field. Wedekind *et al.* [97] and some other researchers [44,135,136] calculated the size of critical nuclei using a mean first-passage time analysis by tracing the growth of nuclei. Whereas these methods assume the validity of CNT.

However, only a few researches [4,137,138] have addressed the nucleation of bimodal polymers, which remains poorly understood compared to unimodal polymers. Qi *et al*. [138] showed that the free energy barrier using self-consistent field theory, as well as the critical nucleus is sensitive to the polydispersity. Some other researchers [4,106] found that blending long chains to a short chain melt could promote the nucleation rate, and they attributed this effect to long chains. However, the average molecular weight was also promoted with blending of long chains. In order to avoid the effect of molecular weight, we have simulated bimodal and unimodal systems with the same average molecular weight.

In this chapter, to avoid the effect of molecular weight, we have created simulation systems of bimodal and unimodal MWD with an equivalent average molecular weight. Coarse-grained MD simulations have been performed to investigate the isothermal nucleation behavior at several temperatures. A direct Growing Probability Method has been presented for computing the size of critical nuclei. Interfacial free energy has been calculated from critical nuclei based on CNT (equation (1.6)), and the activation energy of diffusion has also been obtained by the temperature dependence of the diffusion coefficient (equation (1.7)). With interfacial free energy and activation energy, nucleation rate can be calculated by CNT with equations (1.5) and (1.8). The nucleation rate which represents the number of nuclei (larger than critical size)

formed per time per volume, can be also obtained directly from MD simulations, and fitted with CNT to prove if the theory is applicable.

4.2 Modeling systems

The CG-MD model potential is also used in this chapter, the simulated polymer melts are prepared using RLP method, the isothermal crystallization treatment is performed to obtain semicrystalline polymer, and the size of the nuclei is traced with our hierarchical clustering method. All these methods and simulation details have been described in chapter 2, here we just appendix the modeling systems.

In this chapter, we created a bimodal system (namely LC50) with 100 long chains (chain length is 500 beads) and 500 short chains (chain length is 100 beads), which makes 50% of weight fraction of long chain content. This system is identical with the LC50 in chapter 3. The average molecular weight of system LC50 is $166.7m_u$. To avoid the effect of average molecular weight, we have created the second system (namely S166) with 600 chains of length 166 beads, with the same molecular weight and total number of beads as system LC50. Extensive simulation and comparison have been done on systems LC50 and S166 in this chapter.

Then the systems LC50 and S166 are submitted to a fast cooling process (cooling rate: $10^{-5}\epsilon_u/k_B/\tau_u$) to the desired crystallization temperature, followed with isothermal treatment until the crystallization of each system saturates. We have selected temperatures of 2.3, 2.1, 2.0, 1.9 and 1.7 ϵ_u/k_B, because the glass transition temperature is 1.39 ϵ_u/k_B, and 2.3 ϵ_u/k_B is the maximum temperature at which homogeneous crystallization can be obtained within acceptable computational time [135].

4.3 Results & Discussion

The two systems LC50 and S166 are relaxed for a long time of $5.0 \times 10^5\ \tau_u$. Then the systems are submitted to a fast cooling process (cooling rate: $10^{-5}\epsilon_u/k_B/\tau_u$) to the target

temperatures 2.3, 2.1, 2.0, 1.9 and 1.7 ϵ_u/k_B respectively. Afterwards, the system temperatures are maintained constant for the isothermal treatment, until the crystallization of each system saturates. Figure 4-1a shows the enthalpies as a function of isothermal time just after the cooling. We can see that only at temperature 2.3 ϵ_u/k_B the enthalpy shows an incubation time and then starts to decrease indicating the onset of crystallization, while the crystallization occurs almost instantly at lower temperatures. Interestingly, the decrease of enthalpy of system LC50 occurs faster than that of system S166 at all simulated temperatures, even though the difference is minor. The whole isothermal process lasts for $4.0 \times 10^5\ \tau_u$, and the enthalpy of all the systems reaches a plateau, indicating that all the systems have reached the maximum crystallinities. In Figure 4-1(b~e), we also provide four snapshots at the early stage and at the end of crystallization for systems LC50 at temperatures 2.3 and 1.9 ϵ_u/k_B respectively. Large lamellae with tapered edge have been obtained at high temperature of 2.3 ϵ_u/k_B, whereas numerous small crystallites are detected at lower temperature of 1.9 ϵ_u/k_B.

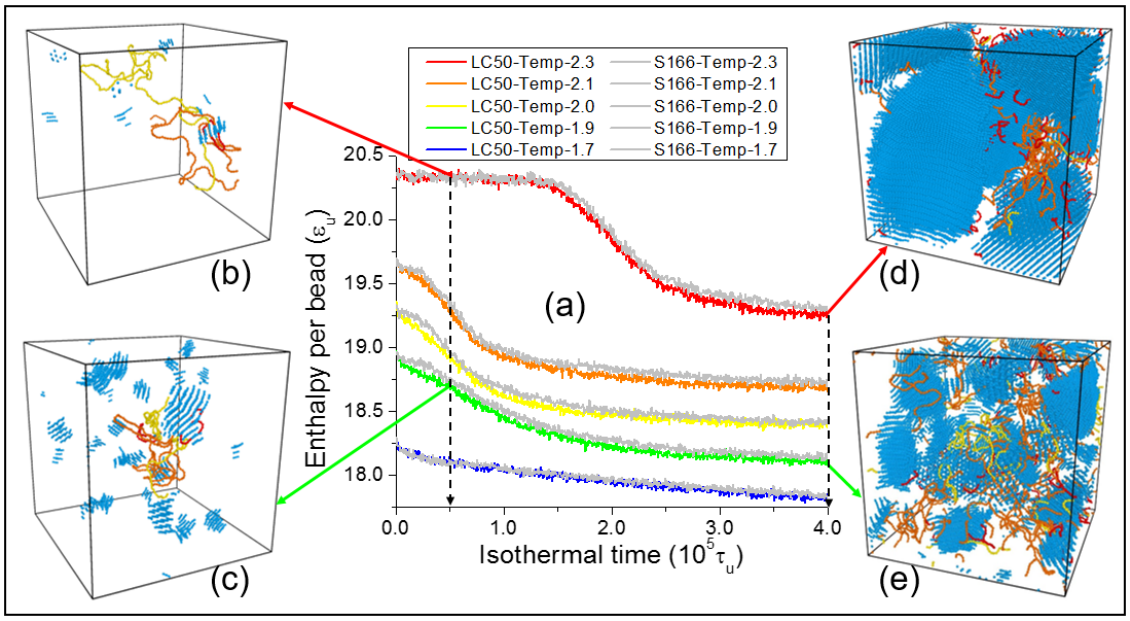

Figure 4-1 (a) Thermograms of isothermal treatment of systems LC50 and S166, at constant temperatures 2.3, 2.1, 1.9 and 1.7 ϵ_u/k_B respectively for a period of $4.0 \times 10^5\ \tau_u$. (b)&(c) Snapshots of system LC50 after $0.5 \times 10^5 \tau_u$ of crystallization with isothermal temperatures of 2.3 and 1.9 ϵ_u/k_B, respectively. (d)&(e) Snapshots of system LC50 at the end of isothermal treatment with isothermal temperatures of 2.3 and 1.9 ϵ_u/k_B, respectively. The colors in snapshots (b~e): blue represents the crystal phase, red represents loop segments, orange represents tie segments, and yellow represents cilia segments.

In order to obtain the critical size of nucleus n^*, we have developed a novel Growing Probability Method based on the growing and shrinking of the nucleus size. According to CNT, the critical size of a nucleus is a point of unstable equilibrium, with equal probability for a nucleus to either grow or shrink (50% of growing probability). In the Growing Probability Method, we trace the sizes of all the nuclei growing and shrinking in the process of isothermal treatment. The configurations are taken every Δt. Assume that a nucleus at time t contains A_t beads, and a nucleus at time $t + \Delta t$ contains $A_{t+\Delta t}$; if these two nuclei have more than $A_t/2$ common beads (every bead has an index), they are considered as the same nucleus. If the same nucleus is not found at $t + \Delta t$, it means that the size of this nucleus $A_{t+\Delta t}$ shrinks to zero. Thus, all the nuclei at time t are compared with those at time $t + \Delta t$ and we are able to trace all the nuclei growing and shrinking. If $A_t \leq A_{t+\Delta t}$, it means a growing event occurs, and the number of growing events is increased by 1: $G(A_t) = G(A_t) + 1$; otherwise the number of shrinking events is $S(A_t) = S(A_t) + 1$. After obtaining a large statistics, the growing probability of a nucleus, $P(A)$ with size A would be $\frac{G(A)}{G(A)+S(A)}$. In this way, the probability of growing $P(A)$ as a function of nucleus size A will be obtained (*e.g.* Figure 4-2a). As mentioned above, the critical nucleus size would be obtained at the growing probability of $P(A)$ =50%.

Figure 4-2a shows the growing probability of nucleus of system LC50 at temperature 2.1 ϵ_u/k_B, with Δt equal to $100\tau_u$, $500\tau_u$ and $1000\tau_u$ respectively. As Δt increases, the curve gets a sharper increase around probability of 50% and the statistics get worse. Interestingly, the three curves at different Δt share a point of intersection at probability of 50%. For the purpose of better statistics, we choose Δt as $100\tau_u$ to perform further analysis. The curve of the growing probability ($\Delta t = 100\tau_u$) of a nucleus as a function of the nucleus size can be fitted by an exponential function of $y = \beta \cdot e^{-\alpha/x}$. For the case in Figure 4-2a, we obtain $\alpha = 127.71, \beta = 1.262$ from the fitting. The critical size of nucleus of system LC50 (obtained from $P(A)$ =50%) at temperature 2.1 ϵ_u/k_B is 135 beads. Using the mean first passage method in chapter 3, the

critical size of a nucleus in the same case was determined to be 129. The difference is within 5%, which verifies the validity of the Growing Probability Method. This Growing Probability Method will be employed in the following calculation of critical size of nucleus. In this way, we have determined the critical nucleus size of systems LC50 and S166 at several temperatures.

As shown in Figure 4-2b, the critical nucleus size as a function of temperature follows an empirical form $n^* = a + b/T\Delta T$ as presented by Yi *et al.* [44], where the supercooling ΔT=$T_m - T$, the fitting parameters for LC50 are: $a_1 = 669.02, b_1 = -202.92$, for S166 are: $a_2 = 658.90, b_2 = -185.03$. Our systems fit this empirical form well. According equation (1.6), in order to follow this equation, the interfacial free energy should be linear dependent of $(T\Delta T)^{-2}$. This contrasts with the linear dependence on $(T\Delta T)^{-3}$ observed for crystallization of the simple Lennard-Jones systems, where the interfacial free energies are temperature independent [139]. Figure 4-2c shows the interfacial free energy $\sigma_s^2\sigma_e$ (defined in section 1.2.1, equations (1.5) and (1.6)) as a function of temperature calculated from the data of Figure 4-2b.This relation is extrapolated up to temperature of 2.95 ϵ_u/k_B (close to T_m=3.1 ϵ_u/k_B) using the empirical form above. This indicates that the interfacial free energy decreases with temperature, and that this decrease trend gets even faster when the temperature is increased up to 2.1 ϵ_u/k_B. One possible explanation is that at low temperature there is significant entropy contribution arising from the onset of chain folding and looping. Loops give rise to some overcrowding in the interface and in the internal energy contributions to the interfacial free energy. While at high temperature the topological entropy due to the introduction of loops becomes important, eventually offsetting the internal energy contributions so that the effective interfacial free energy decreases at high temperature. The interfacial free energy of bimodal system LC50 is lower than that of unimodal system S166 because of the chain-folding nucleation of long-chain content, as it has been demonstrated in chapter 3 [135]. Short chains tend to undertake intramolecular nucleation and long chains tend to undertake intermolecular nucleation (Figure 3-7). It has been proved in chapter

3 that the intramolecular nucleation forms chain-folded crystal surface and exhibits lower crystal-amorphous interfacial free energy than the intermolecular nucleation. Clearly in system LC50, there exists a larger proportion of intramolecular nucleation, and the interfacial free energy is lower than that of system S166, and then the critical size of nucleus and free energy barrier for nucleation is relatively lower according to equation (1.5) and (1.6).

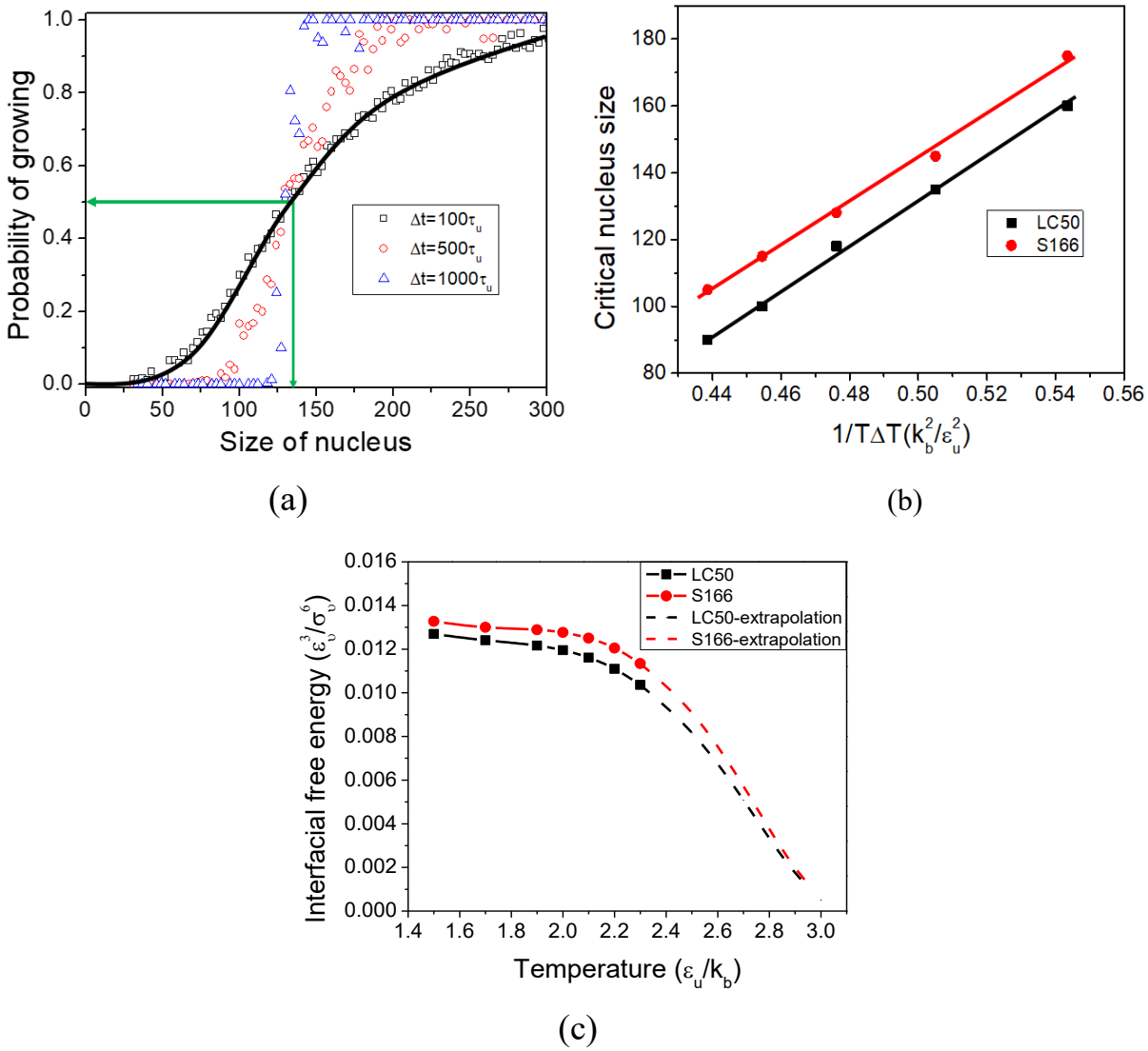

Figure 4-2 (a) Probability of nucleus growing as a function of nucleus size, system LC50 at temperature 2.1 ϵ_u/k_B. (b) Critical nucleus size of system LC50 as a function of $1/T\Delta T$. (c) Interfacial free energy ($\sigma_s^2\sigma_e$) of system LC50 as a function of temperature.

MD simulations have been performed on systems LC50 and S166 at different temperatures to calculate the mean square displacement (MSD) of the centers of mass of the chains, as described by Harmandaris *et al.* [99] These results are calculated at the beginning of isothermal

treatment with a time span of 5% of isothermal time. From the MSD $< r^2(t) >$ we calculate the self-diffusion coefficient, $< r^2(t) > = 6Dt^{\nu}$ according to Einstein's relation [48]. The self-diffusion coefficients D obtained by simulations at several temperatures from 1.7~2.3 ϵ_u/k_B are fitted, as shown in Figure 4-3b. The activation energy E_d for chain mobility can be obtained from the slope of lnD versus $1/T$, according to equation (1.7) explained in section 1.2.1. Our results show that E_d of bimodal system LC50 is $E_d(LC50) = 14.28\varepsilon_u$, and for unimodal system is $E_d(S166) = 14.14\varepsilon_u$. This suggests that E_d is not sensitive to bimodality if average molecular weight is the same, and the bimodality dependence of diffusion coefficient is mainly controlled by the parameter D_0. However, the diffusion coefficient of bimodal system LC50 is larger than that of unimodal system S166, and the difference increases with temperature. We believe that the diffusion coefficient of LC50 is promoted by the short-chain component.

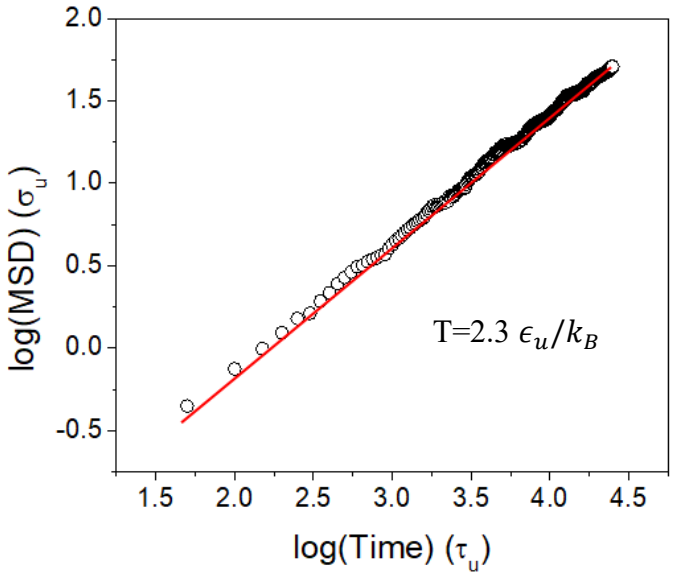

(a)

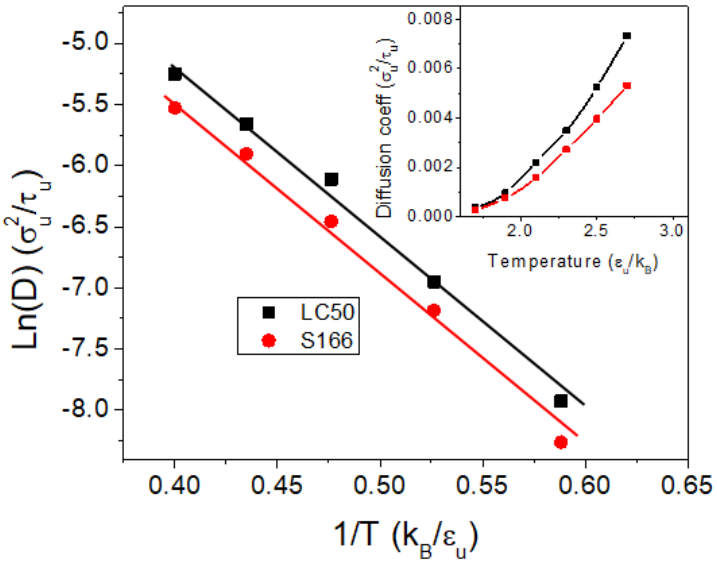

(b)

Figure 4-3 (a) Mean square displacement of mass center of chains as a function of time for LC50 at temp 2.3 ϵ_u/k_B. (b) Diffusion coefficient of Systems LC50 and S166 as a function of inverse temperature, and linear fitting. (Inset) Diffusion coefficient of LC50 and S166 as a function of temperature.

According to equation (1.8), the nucleation rate expressed as number of nuclei formed per unit volume per unit time at incubation time can be calculated from MD simulation. Thanks to our Hierarchical clustering method, we are able to trace the number of nuclei as a function of isothermal time. The nucleation rate at the incubation time has been calculated at different temperatures (Figure 4-4). The points are obtained directly from the MD simulations. To

compare CNT with these points, we only require the values of ΔG^* and E_d. E_d has already been calculated from the data in Figure 4-3b and shown to be bimodality independent, and ΔG^* can be calculated from $\sigma_s^2\sigma_e$ (Figure 4-2c) and equation (1.5). The nucleation rate curve based on CNT of equation (1.8) is plotted in Figure 4-4 and extrapolated up to temperature 2.95 ϵ_u/k_B (close to T_m). We can see that the nucleation rate calculated from MD simulations fit well with that calculated from CNT, which proves the validity of the CNT. According to equation (1.8) in section 1.2.1, the temperature dependence of the nucleation rate can be expressed by two exponential factors: the molecular transport term and the energy barrier term. It has been shown [61,116,140] that these two terms have opposite temperature dependence behavior thereby producing a bell-shaped curve with a maximum rate at the crystallization temperature. For the two uni and bimodal system, the maximum occurs at the similar temperature around 2.1 ϵ_u/k_B. From studies of the crystallization behavior of several polymeric materials, it has been demonstrated that the molecular transport term is of considerable importance at high supercooling (low temperature). While the polymer chain diffusion will become very difficult as temperature approaches the glass transition temperature, and the nucleation rate decreases to zero near or below T_g. The energy barrier term has the opposite dependence of temperature, where the higher supercooling leads to more favorable thermodynamic conditions for nuclei generation. Whereas the nucleation rate decreases to zero when the temperature increases close to T_m, because the energy barrier becomes very high to surpass.

The effect of temperature has been widely investigated on the unimodal polymers, whereas rarely mentioned on bimodal polymers. Interestingly, the nucleation rate-temperature curve of LC50 is always on top of that of S166, indicating that the nucleation rate is promoted with bimodality. As the two systems have the similar activation energy, the nucleation rate difference of bimodal and unimodal mainly comes from the critical nucleus, which is eventually a result of chain-folding nucleation of long chain component as discussed in chapter 3 for the

intramolecular nucleation. Umemono *et al.* [116] also indicated that the fast nucleation rate of bimodal system is due to intramolecular nucleation mode of long chains in system LC50. Song *et al.* [4] found that ultra-high molecular weight polyethylene (UHMWPE), could obviously promote the nucleation rate of high density polyethylene (HDPE), acting as an effective nucleating agent. Kornfield *et al.* [141] have also shown that the long chains in the blend melt controlled the formation of oriented nuclei. As a consequence, we attribute the promoted nucleation rate of bimodal system to its lower energy barrier resulted from the intramolecular nucleation mode of its long chain content; the high mobility of the short chains doesn't contribute a lot but may promote the crystal growth rate instead. The crystal growth is not the focus of this chapter and may be further discussed in the future.

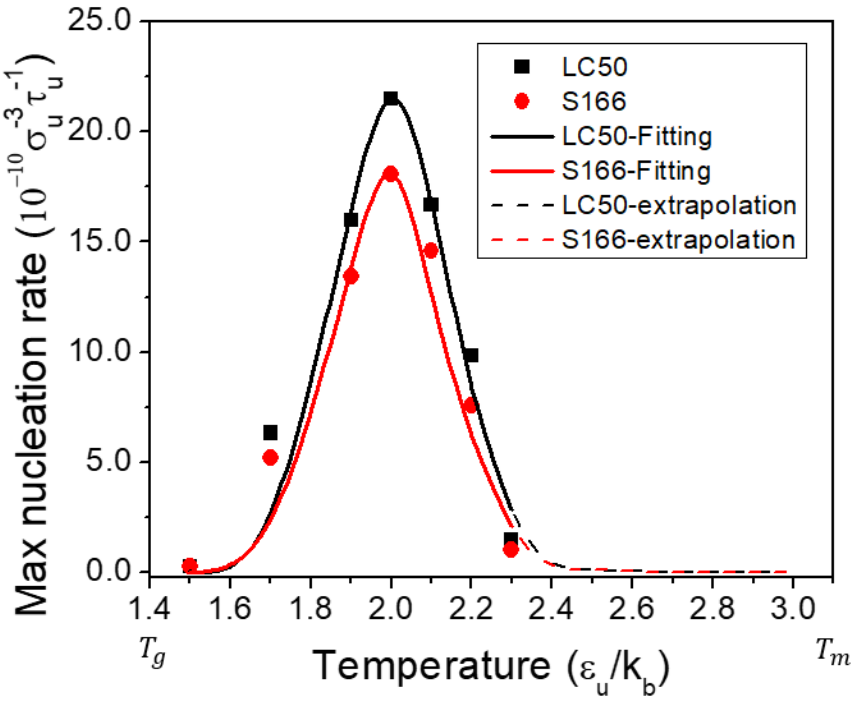

Figure 4-4 Temperature dependence of the nucleation rate at incubation time, the points are nucleation calculated from MD simulations by $dN/dt|_{nuclei}$ (described in equation (1.8)), the smooth curves are plotted by the classical nucleation theory.

4.4 Conclusions

In this chapter, we have simulated the nucleation of bimodal system and unimodal system with equivalent average molecular weight. A Growing Probability Method has been proposed

to calculate the critical size of nucleus over a range of temperatures. The interfacial free energy is calculated using a cylinder model and found to decrease with temperature. We have calculated the free energy barrier and activation energy of diffusion, and compared the nucleation rate with classical nucleation theory, which proves the validity of CNT. Compared to unimodal polymers, the bimodal system exhibits higher nucleation rate. We attribute the promoted nucleation rate of bimodal system to its lower energy barrier resulted from the intramolecular nucleation mode of its long chain content; the high mobility of the short chains doesn't contribute a lot but may promote the crystal growth rate instead. The crystal growth is not the focus of this chapter and may be further discussed in the future. The simulations and theoretical analysis performed in this chapter not only reveal the molecular mechanisms of nucleation of bimodal and unimodal polymers, but also generate meaningful methods that can be used for engineering.

Chapter 5

Entanglements and lamellar thickening of linear polymers during crystallization

Contents

Abstract: In chapter 3 and chapter 4, the crystallization (mainly nucleation) of uni and bimodal molecular weight distribution polymers has been investigated, and the bimodality effects on molecular topology have been discussed. In the current chapter, the focus is the other aspects of microstructure of semicrystalline polymers, *i.e.* entanglements and lamellar thickness, which also play important role in mechanical properties of semicrystalline polymers. The objective of this chapter is to investigate the bimodality influence on the entanglement concentration, and the process of lamellar thickening in the perspective of chain disentanglement at different temperatures. This chapter has been summited to the journal Acs Nano, and currently we are working on reviewers' the comments from this journal.

Coarse-grained molecular dynamics simulations are performed to study the isothermal crystallization of bimodal and unimodal molecular weight distribution (MWD) polymers with equivalent average molecular weight. Primitive path analysis has been performed, the entanglement evolution has been continuously monitored during the process of crystallization. We have discovered a quantitative correlation between the degree of disentanglement and

crystallinity, indicating that chain disentanglement drives the process of crystallization. Such a quantitative correlation is the first to the best of the author's knowledge. In addition, lamellar thickness also displays a linear relation with the degree of disentanglement, and this rule maintains even for the thickness at different temperatures. Based on the observation in our simulations, we are able to elaborate the scenario of the whole process of chain disentangling and lamellar thickening in the manner of chain sliding diffusion. And we have enough evidence to infer that the temperature dependence of lamellar thickness is basically a result of temperature dependence of chain sliding diffusion. Our observations also underlie Hikosaka's sliding diffusion theory. Compared with unimodal system, the disentanglement degree of the bimodal system is more delayed than its crystallinity due to the slower chain sliding of long chain component; the bimodal system reaches a larger lamellar thickness at all temperatures due to the promotion of higher chain sliding mobility of short chain component.

Key words: Bimodal polymer, degree of entanglement, chain sliding diffusion, lamellar thickening

5.1 Introduction

Semicrystalline polymers with bimodal Molecular Weight Distribution (MWD) have a wide application because of the improved processability along with promoted mechanical performance [142]. Bimodal MWD polymer is composed of low- and high- molecular weight contents. Some researchers [4,124,127,141,143] have prepared bimodal polymer blends in experiment and found that bimodal melts have promoted nucleation rate and processability of the material. The relationship between property and micro-structure of bimodal polyethylene (PE) has been studied [31,144,145], and it is believed that the entanglements play an essential role for the outstanding properties of bimodal PE.

Molecular Dynamics simulations have also been used to study crystallization [30,44,73,76,146,147] and microstructure [27,123,148–150] of semicrystaline polymers. Nevertheless, there are only few studies addressing the simulation of crystallization in relation with entanglements [30,73,74] of bimodal polymers. Moyassari *et al.* [30,73] monitored entanglement concentrations during crystallization of PE bimodal blends. Luo *et al.* [74–77] studied the crystallization of unimodal PVA chains and also blends with very short chains (considered as solvent phase), and found a linear relation between lamellar thickness and entanglement length. It is worth noting that these contributions all attributed the promoted nucleation rate of bimodal system to the increased proportion of long chain content, and neglected the fact that the average molecular weight also increased. However, the question remains: what is the main factor for the crystallization and lamellar thickening of bimodal polymers? The increased long chain content or the increased average molecular weight? Therefore, to avoid the effect of molecular weight, we have created bimodal and unimodal systems with the equivalent average molecular weight.

In this chapter, we have studied systems of bimodal and unimodal MWD with an equivalent average molecular weight. Coarse-grained MD simulations have been performed to investigate the isothermal crystallization behavior of these systems at various temperatures. The

entanglements have been continuously monitored in the process of crystallization. The crystal growth and thickening process were described and discussed afterwards.

5.2 Entanglement analysis

The CG-MD model potential is also used in this chapter, the simulated polymer melts are prepared using RLP method, the isothermal crystallization treatment is performed to obtain semicrystalline polymer, and the size of the nuclei is monitored with our hierarchical clustering method. All these methods and simulation details have been described in chapter 2.

In this chapter we have simulated two systems that are exactly the same as in chapter 4, which are a bimodal system LC50 and a unimodal system S166 with equivalent average molecular weight of $166.7m_u$. Here we just explain the method of entanglement analysis.

For semicrystalline systems, the entanglement analysis methods that use pure geometrical criteria to examine the primitive path network of a polymer system, are more efficient. In this chapter, we use the Z1 algorithm [151] to analyze the entanglements. The Z1 code extracts the primitive path of a given trajectory configuration, and determines several entanglement properties, of which we are mainly interested in Z, the number of entanglements (number of interior kinks) in each polymer chain, and $N_{e,kink}$, the entanglement length. As the conformations of polymer chains no longer obey Gaussian statistics in melts near crystallization, we use the directly measured number of beads in a straight primitive path segments between two adjacent kinks as the entanglement length. Thus,

$$Z = \frac{N}{N_{e,kink}} - \frac{N}{N-1} \qquad (5.1)$$

$$N_{e,kink} = \frac{N(N-1)}{Z(N-1)+N} \qquad (5.2)$$

where N is the chain length (*i.e.* number of beads).

5.3 Results & Discussion

5.3.1 Isothermal crystallization

Figure 5-1a shows the enthalpies as a function of isothermal time. We can see that only at temperature 2.3 ϵ_u/k_B the enthalpy shows an incubation time before crystallization and then starts to decrease indicating the onset of crystallization, while the crystallization occurs almost instantly at lower temperatures. Interestingly, the decrease of enthalpy of occurs faster than that of system S166 at all simulated temperatures, even if the difference is minor. The whole isothermal process lasts for 4.0×10^5 τ_u, and the enthalpy of all the systems reaches a plateau, indicating that all the systems have reached maximum crystallinities. In Figure 5-1(b~e), we also provide four snapshots at the early stage and at the end of crystallization for systems LC50 at temperatures 2.3 and 1.9 ϵ_u/k_B respectively. At the early stage, much more nuclei have been formed at temperature of 1.9 ϵ_u/k_B than at high temperature of 2.3 ϵ_u/k_B, which is consistent with experimental observations [28,152]. At the end, large lamellae with tapered edge have been obtained at high temperature of 2.3 ϵ_u/k_B, whereas numerous small crystallites are detected at lower temperature of 1.9 ϵ_u/k_B.

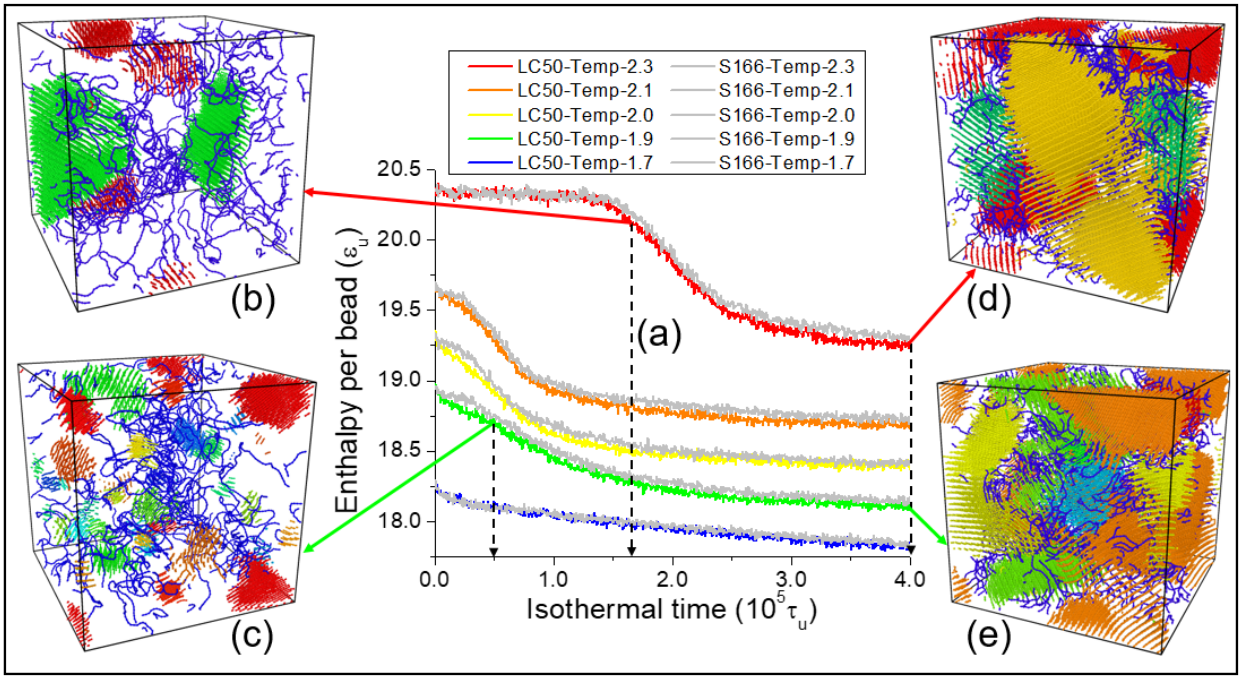

Figure 5-1 (a) Thermograms of isothermal treatment of systems LC50 and S166, at constant temperatures 1.7 to 2.3 ϵ_u/k_B respectively for a period of 4.0×10^5 τ_u. (b)(c) Snapshots of system LC50 at the early stage of crystallization with isothermal temperatures of 2.3 and 1.9 ϵ_u/k_B, respectively. (d)(e) Snapshots of system LC50 at the end of isothermal treatment with isothermal temperatures of 2.3 and 1.9 ϵ_u/k_B, respectively. The colors in snapshots (b~e): blue represents several complete chains traveling through amorphous and crystal phases, the other colors represent different crystallites (one color for each crystallite).

In order to quantify the crystallinity, we have used our hierarchical-clustering method. With this method, we are also able to calculate the crystallinity of systems LC50 and S166, as well as the long-chain crystallinity and short-chain crystallinity. For example, the crystallinity of long chains in LC50 is defined as the number of long-chain beads in crystal phase divided by total number of long-chain beads. From Figure 5-2a, we can see that after an incubation time system LC50 crystallizes earlier than S166, following a faster growth rate and then reaches a plateau, and the final crystallinity is also slightly higher than that of S166. However, the crystallinity-time curves of LC50 and S166 are only weakly different. It is the same case for the final crystallinities at all investigated temperatures (Figure 5-2b). It seems that the final crystallinity is determined by the average molecular weight (M_w) and independent of bimodality. Krumme *et al.* [67,68] and Shen *et al.* [46,78] have also found that the bimodal blends of

PE behaved insensitive to bimodality, with respect to microscopic properties like crystallinity and density.

The crystallinities of long-chain and short-chain components of system LC50 are also plotted in Figure 5-2a. The crystallinities of the two components show the same trend as the overall crystallinity. Short-chain crystallinity is always higher than that of long-chain component, because short chains diffuse and align faster. This indicates that short chains promote the crystallization during the crystal growth process, while long chains hinder it instead. The overall crystallinity of LC50, close to that of unimodal system S166, is a compromise between that of the short and long chains. Triandafilidi *et al.* [103] have also reported a similar conclusion in the crystallization competition of the two components. In Figure 5-2c, we have plotted the ratio of final long-chain crystallinity divided by short-chain crystallinity at various temperatures. This ratio decreases with temperature, indicating that the difference of crystallization rate between short chains and long chains becomes larger at high temperatures. This mainly results from the increasing difference of diffusion behavior between short and long chains and from the fact that the diffusion coefficient increases exponentially with temperature [153,154]. Cosgrove *et al.* [155] reported that the diffusion coefficient of long chains and short chains enlarges with increasing temperature.

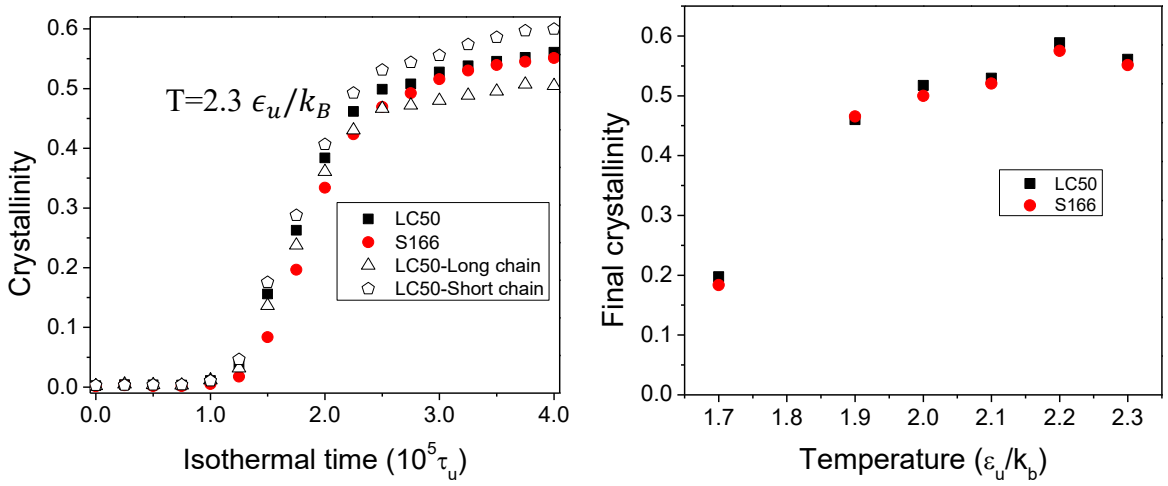

(a) (b)

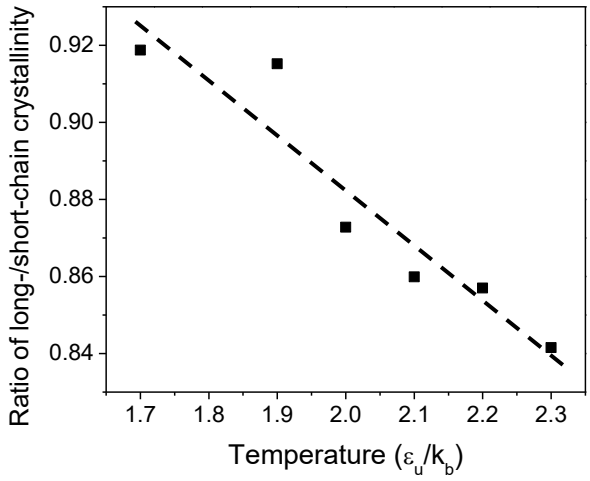

(c)

Figure 5-2 (a) Evolution of crystallinity of systems LC50 (overall/long-chain/short-chain) and S166 at temp 2.3 ϵ_u/k_B, as a function of isothermal time. (b) Final crystallinity at the end of isothermal treatment of systems LC50 and S166, as a function of temperature. (c) Ratio of long-chain crystallinity divided by short-chain crystallinity as a function of temperature.

5.3.2 Entanglement evolution

As shown in some experimental studies [156–158], entanglement characteristics in the polymer melt play an important role for the crystallization selection of morphology and crystal thickening. Therefore it is essential to trace the evolution of entanglements during the crystallization process. For easier comparison, here we use <Z> per bead as an indication of entanglement concentration, *i.e.* average number of entanglements per chain divided by chain length. Figure 5-3a shows the entanglement concentration of systems LC50 and S166 as a

function of isothermal time at temperature 2.3 ϵ_u/k_B. The entanglement concentrations of LC50 and S166 first lightly drop at the beginning of isothermal treatment, which is considered to be the delayed reaction to the preceding fast cooling. Then the <Z> per bead increases slowly during the incubation time which is caused by the increase of chain stiffness. This increase during incubation is consistent with previous simulation studies and theoretical models [83,159,160]. Afterwards, with the onset of crystal growth, the concentration of entanglements rapidly decreases, indicating a disentanglement process. Finally the crystallization saturates and disentanglement reaches a plateau at the end of isothermal treatment. Interestingly, the <Z> per bead of LC50 is very similar to that of S166 during the incubation period, but at the end it drops with a smaller degree compared to S166. Clearly systems LC50 and S166 hold similar crystallinities (Figure 5-2b) even when they disentangles differently, which will be further discussed later. Figure 5-3a also shows the disentanglement process of long/short chains in bimodal system of LC50. Long chains exhibit higher entanglement concentration than short chains, and eventually achieve different decreases of entanglements. These observations also hold for crystallization process at other temperatures, except that no evident incubation period is detected.

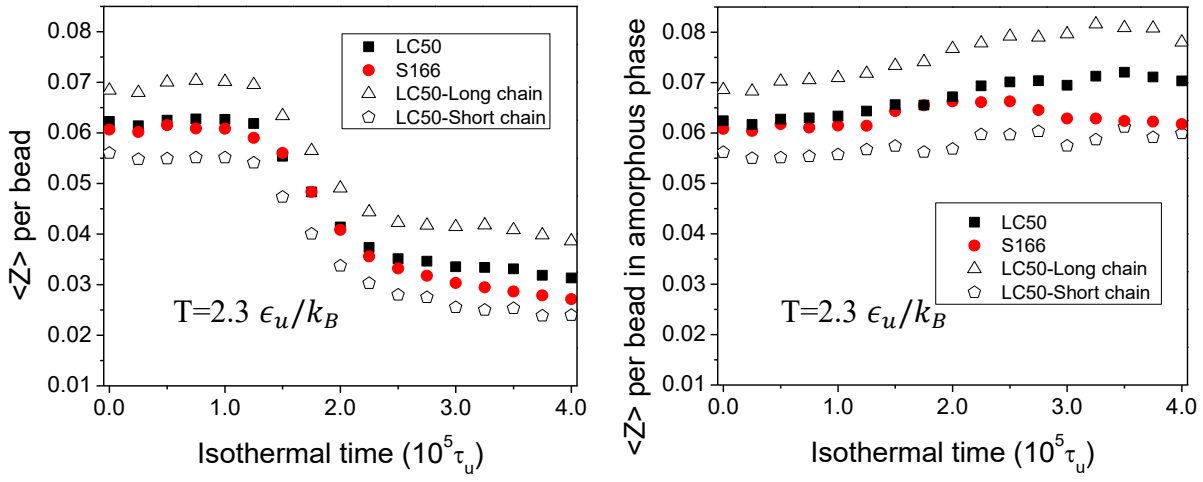

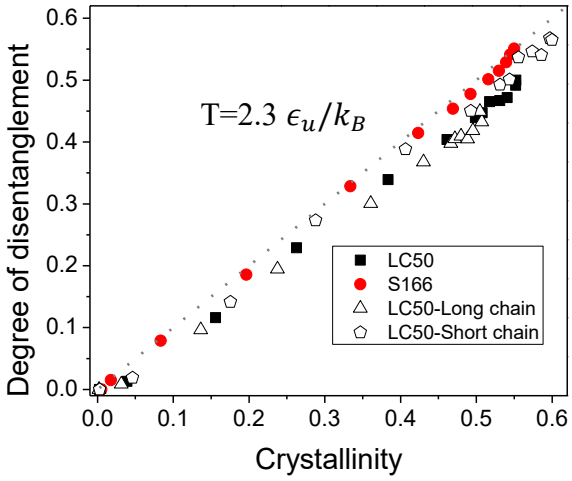

Figure 5-3 (a) The number of entanglements per bead as a function of isothermal time at Temp 2.3 ϵ_u/k_B. (b) The number of entanglements per bead in amorphous phase as a function of isothermal time at Temp 2.3 ϵ_u/k_B. (c) Decrement of <Z> per bead as a function of crystallinity, at Temp 2.3 ϵ_u/k_B.

The role of entanglements and possible mechanisms of disentanglement during polymer crystallization has been debated in literature [161–164], but experimental investigation on entanglement properties is difficult [157,162]. No quantitative relations between the degree of entanglement and crystallization processes have been made. In order to quantify the degree of disentanglement, we define it as $\frac{<Z>(t_0)-<Z>(t)}{<Z>(t_0)}$, where $< Z > (t)$ is the entanglement concentration of the system at time t of isothermal period and t_0 is the incubation time, *i.e.* the time when crystallization starts. Based on the calculation of incubation time in chapter 3 [135], t_0

for system LC50 is $1.22 \times 10^5\ \tau_u$ and for system S166 it is $1.26 \times 10^5\ \tau_u$. With this definition, we are able to plot the degree of disentanglement of systems LC50 and S166, as well as that of long chains and short chains of LC50, as a function of crystallinity (Figure 5-3c).

It needs to be clarified that in Figure 5-3c each component correlates with its own crystallinity. For example, the disentanglement degree of LC50 is a function of average crystallinity of system LC50, and that of long chains is a function of long-chain crystallinity of system LC50. The dashed line is $y = x$. From Figure 5-3c, we can see that the degrees of disentanglement of all the systems and components always follow their own crystallinities. Hence we conclude that the crystallization process is fundamentally a process of chain disentangling, and that the crystallinity is basically the degree of chain disentanglement. We have provided a quantitative correlation between crystallinity and degree of disentanglement. Researchers have debated about the relationship between polymer crystallization and disentanglement [30,126,161,162,165], nevertheless to the best of the author's knowledge, we have never seen similar quantitative reports. For system S166, the entanglement degree always follows its crystallinity. As for system LC50, the average degree of disentanglement is a bit delayed with crystallinity, and long-chain component is similarly delayed while short chains keep close to its crystallinity. It seems that in system LC50, long-chain component dominates the delay of disentanglement degree. Why does this delay exist in bimodal systems, and especially in the long-chain component? In order to answer this question, we monitor the degree of entanglements in the amorphous phase (Figure 5-3b).

As there are few entangled defects in the crystalline domain, we assume that for a specific chain the entanglements are spread along the amorphous fragment, and we assume that the length of this amorphous fragment is $N \cdot (1 - X_c)$ (N is chain length and X_c is crystallinity). With this assumption, we replot the entanglement concentration in amorphous phase (defined as $< Z >_{amorph}$) as a function of isothermal time (Figure 5-3b). We can see that $< Z >_{amorph}$

per bead has an evident increase during the crystal growth for both systems LC50 and S166. The difference is that S166 drops back to similar levels as before crystallization, whereas the drop of LC50 is slower and still in progress at the end of isothermal. As for long chains of LC50, the increase of $< Z >_{amorph}$ is even more evident and draws back slower than S166 and the average value of LC50, while short chains of LC50 exhibits no evident increase or decrease in the whole process of crystallization. Luo *et al.* [74,76,77] have observed that entanglements are almost preserved during crystallization in the amorphous melts in their PVA simulations. Figure 5-3b brings to a similar conclusion, but in our case, the entanglement of amorphous phase increases slightly and draws back at the end. For long chains, the withdrawing is slow and long processing, as confirmed in the extended simulation of system LC50. Moyassari *et al.* [30,126] also reported that entanglements were less preserved for the short chains than the long chains in the process of crystallization. It seems that the delay of disentanglement degree of bimodal system LC50 (compared to its crystallinity) is due to the slow reaction of long-chain component in amorphous phase. This will be further proved later in this chapter.

5.3.3 Lamellar thickening

Another fundamental question concerning polymer crystallization is the effect of bimodal MWD and temperature on lamellar thickness. In general, low crystallization temperatures lead to thinner lamellae and faster growth rate. In Figure 5-4a, we show a linear relation between the final lamellar thickness and degree of disentanglement for systems LC50 and S166 at temperature of 2.3 ϵ_u/k_B. This indicates that crystal thickening is also controlled by disentanglement process of the chains. Luo *et al.* have found a linear relation between the entanglement length at the beginning of crystallization and the resulting crystal thickness [74–76]. These works pointed out the memory effect of entanglements on final crystal thickness, but neglected the disentangling process during crystallization. In this chapter, we focus on the steps

preceding of crystallization and provide more insights into the chain disentangling and chain sliding.

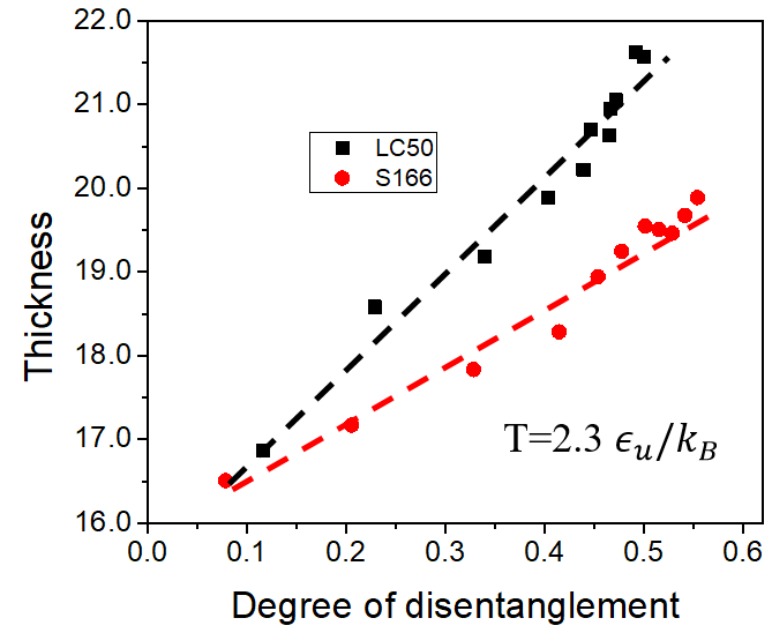

(a)

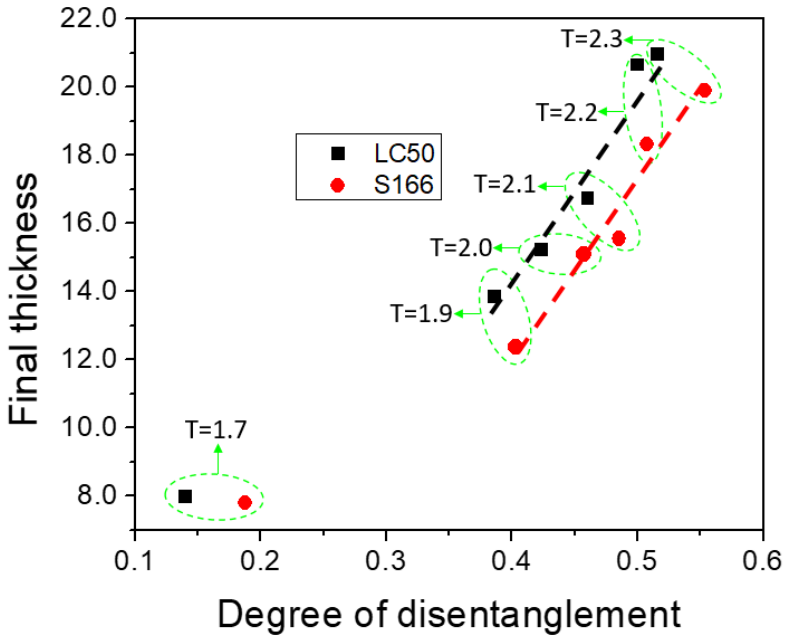

(b)

Figure 5-4 (a) Average thickness as a function disentanglement degree of systems LC50 and S166, at temp 2.3 ϵ_u/k_B. (b) Average thickness at the end of crystallization for different temperatures (unit of temperature labels is ϵ_u/k_B), as a function disentanglement degree of systems LC50 and S166.

Based on Figure 5-3 and Figure 5-4a, we are now able to explain the scenario of the whole process of crystallization. Crystallization is a process where polymer chains disentangle within the interface between a crystallite and the melt, and then rearrange into large crystals via chain diffusion. Apparently there exists two types of diffusion of the chains: sliding diffusion, which is diffusion of a polymer chain along its own axis, and lateral diffusion, which is the displacement of a chain fragment in the lateral direction. Luo *et al.* [76] indicated that the process of polymer crystallization is accompanied by the sliding and folding of chain fragments, which are also the two modes of chain disentangling. Basically the chains fold to the growth front through lateral diffusion forming short crystal stems, and then the stems thicken through chain sliding. This could also be visually observed in Figure 5-5, in which the entanglement evolution of two individual chains of LC50 (a long and a short chain) is presented. The number of kinks (representing entanglements) for the two chains decreases in the process of chain folding and crystal thickening, and most of the kinks fall in the interfacial and amorphous regions indicating that no entanglements exist in the crystal phase. Besides, the short chain disentangles with a larger degree because of the high sliding mobility, in agreement with the work of Lacevic *et al.* [166], who calculated the sliding diffusion coefficient and found that the chain sliding decreases with increasing molecular weight. It is worth noticing that the entanglements do not completely disappeare on the crystal interface of crystallite and melt, which can be seen from the increase of entanglement concentration in amorphous phase (Figure 5-3b) especially for long chains of LC50. In other words, entanglements are pushed from crystal phase to the interface, the majority disappears and the rest is transmitted to the amorphous phase. This transmission is more evident for long chains because of the low chain sliding mobility. This explains the delay of disentanglement degree of long-chain component in system LC50 (Figure 5-3c) and the fact that the lamellar thickness of LC50 is larger than that of S166 (Figure 5-4a). In fact, due to the higher sliding mobility of short chains in LC50, the thickness of bimodal system LC50 is

promoted by the short chains, and long-chain low mobility makes the disentanglement degree of long chains more delayed. Here we have provided insights to the disentangling and lamellar thickening process, and found evidence to support the chain sliding theory of polymer crystallization proposed by Hikosaka [153,154] as well as verified its applicability to bimodal MWD polymers.

Figure 5-4b shows that the final lamellar thickness of system LC50 and S166 at various temperatures also exhibits a linear relation with disentanglement degree. This indicates that the relation between disentanglement and crystal thickness has nothing to do with temperature. It is generally accepted that lower crystallization temperature leads to thinner lamellae, which is simply because lower temperature leads to slower chain sliding and consequently lower degree of disentanglement. This observation leads to the conclusion that the temperature dependence of the lamellar thickness can be the result of the temperature dependence of the disentangling process which is mainly controlled by chain sliding. This conclusion is consistent with Luo *et al.* [75] who have reported an inference that the temperature dependence of lamellar thickness can be simply the result of the entanglement length, which is eventually a result of chain sliding mobility.

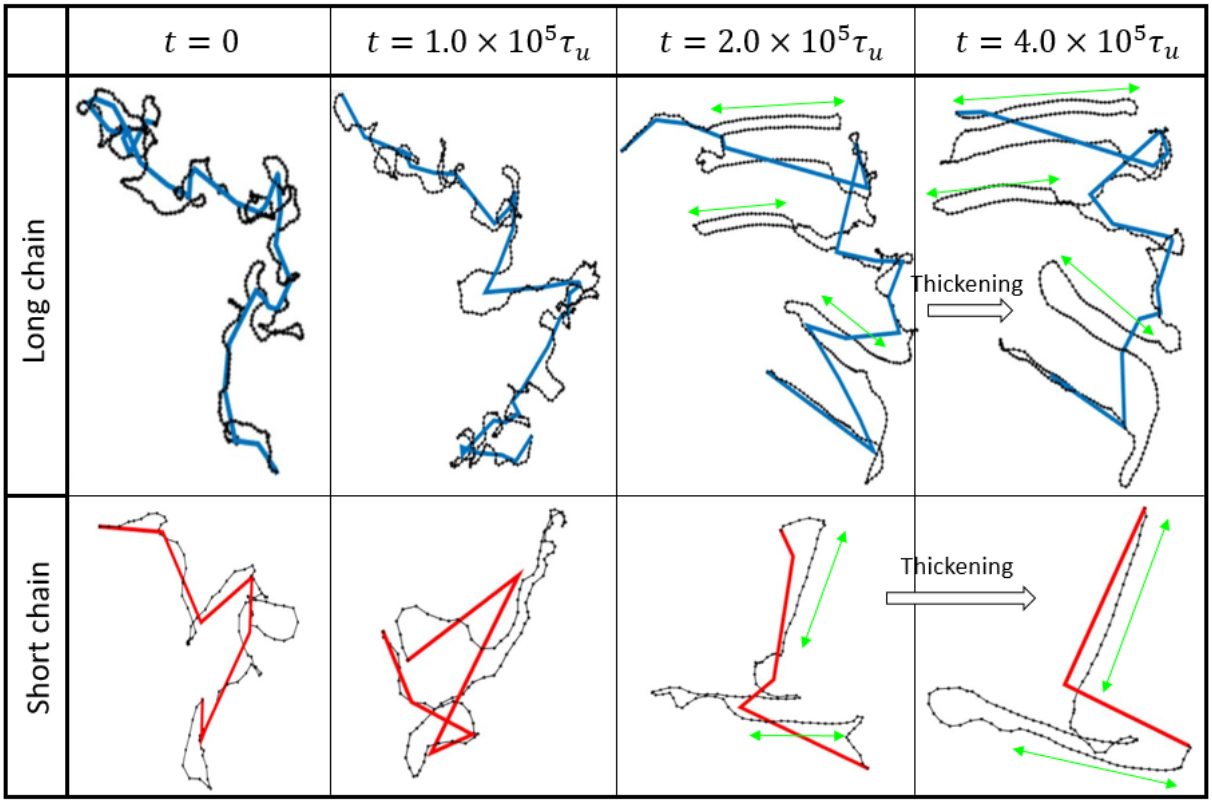

Figure 5-5 Configurations and Primitive Paths (PP) of two individual chains of system LC 50 (one is long chain, the other is short chain), during isothermal crystallization at temperature 2.3 ϵ_u/k_B. The black thin lines are the real configurations, the red and blue thick straight lines are the PP given by Z1 algorithm.

5.4 Conclusions

In this chapter, we have investigated the crystallization of bimodal and unimodal MWD polymers with the same average molecular weight, at various temperatures. Through the primitive path analysis, the entanglement evolution has been continuously monitored during crystallization. We have proved that the crystallization process is driven by chain disentangling, and shown a quantitative correlation between disentanglement degree and the crystallinity. Crystallinity is more of a universal result of average molecular weight, and it makes no evident difference for bimodal and unimodal systems. With the advantage of molecular simulation, we have described polymer crystallization as a process of chain disentangling on the interface of crystal and melted phases in the manner of chain sliding diffusion. Lamellar thickness also displays a linear relation with the degree of disentanglement at all referred temperatures, and

the temperature dependence of lamellar thickness is simply a result of temperature dependence of chain sliding diffusion. Bimodal system LC50 exhibits a higher lamellar thickness than unimodal system S166, also because low molecular weight component has a promotion to lamellar thickness because of high sliding mobility. Our observations provide direct proof of Hikosaka's sliding diffusion theory. Compared with unimodal system, the bimodal system reaches a larger lamellar thickness at all temperatures due to the promotion of short chain component. Observing entanglement restriction is difficult in experiments. Our observations with MD simulation provides a quantitative analysis of the long-term debate on chain disentanglement and lamellar thickening, which is sensitive to bimodality as a result of high chain sliding mobility of the short chain component. The important role of entanglements and chain sliding diffusion sheds a light on deeper understanding of polymer crystallization.

Chapter 6

A novel model for mechanical deformation of semicrystalline polymers

Contents

Abstract: In the previous five chapters, we have investigated the crystallization behavior and the resulting microstructure of molecular topology (loop, tie, cilia), entanglement concentration and lamellar thickness. All these microstructure is believed to play important roles in the mechanical performance of semicrystalline polymers. In this chapter, the objective is to build a realistic model, and investigate the relationship between mechanical properties of semicrystalline polymers and different microstructures.

Existing molecular dynamics simulations keep the same interaction potential in both crystalline and amorphous domains, which makes these models not sufficiently realistic. In this chapter, we have built a more realistic semicrystalline polymer model with a larger well depth of Lennard-Jones (LJ) potential for the crystalline phase than the amorphous phase. The validity of this model is confirmed through the promoted stability and elevated yield stress in the process of tensile test. The evolution of molecular topology and crystalline morphology are monitored during mechanical deformation. This chapter is just an initial test of the idea adapting different LJ potential in crystalline and amorphous phase. Deeper and more extensive work will be done based on this idea in the future.

Key words: Bimodal polymer, mechanical properties, molecular topology

6.1 Introduction

The mechanical behavior of semi-crystalline polymers strongly depends on the crystalline and amorphous phases that are nanoscale. It is currently impossible to directly measure the number of tie chains or entanglements in a semicrystalline polymer experimentally, and this makes it difficult to determine the change in amount of these phase during mechanical deformation. However, with molecular-level simulations, such as Monte Carlo (MC) or molecular dynamics (MD) simulations, it is possible to capture these changes. There are already a few frontier researches [21,26,27,123] that have addressed the important role of topological features (*i.e.* loop/tie/cilia) on mechanical properties by molecular dynamics (MD) simulation. It has been found that an increase in stress transmitters such as tie molecules and bridging entanglements, increases the yielding stress and decreases the generation of voids.

Experimental results have shown that in the lamellar domain the chains interact more strongly than in the amorphous phase, which makes high yielding stress because of difficulty for chain sliding in the crystallite. This suggests that the intermolecular interactions would be stronger when the polymer chains (or chain fragments) get aligned and crystallize. However, the existing MD simulations [21,26,27,123] keep the same interaction potential in both crystalline and amorphous domains, which makes these models not sufficiently realistic. Specifically, these simulation models reached much lower yielding stress in the tensile test than experimental results. In this chapter, we have built a more realistic semicrystalline polymer model with a larger well depth of Lennard-Jones potential for the crystalline phase than the amorphous phase. The validity of this model is confirmed through the promoted stability and elevated yielding stress in the process of tensile test. The evolution of molecular topology and crystalline morphology is monitored during mechanical deformation.

6.2 Dynamical changing Lennard-Jones potential during deformation

The FENE-LJ potential is used here in the current chapter, as described in chapter 2. However, all the simulation details are identical as explained in chapter 2 except the ε_{LJ} of equation (1.2). In this chapter, different ε_{LJ} are used for crystal phase and amorphous phase respectively ($\varepsilon_{LJ}(crystal)$>$\varepsilon_{LJ}(amorph)$). However, during mechanical deformation of the semicrystalline polymer, the beads belonging to crystalline or amorphous phases are not static, which means that the beads may crystalize or melt in this process. Dynamically changing the LJ potential of the polymer atoms based on their phase attribution (crystal or amorphous) during the tensile test would perfectly solve the problem. Lammps software [84] that we have used to perform our molecular dynamics simulations fails to perform this. However, Lammps allows to be invoked as a library from C++ program. So the scenario is illustrated in Figure 6-1: (1) invoke Lammps for MD simulation from C++ program, (2) acquire simulation information from Lammps (like atom coordinates, bonds information, *etc*.) to C++ program, (3) analyze the information in C++ program to determine the phase attribution of all the atoms using our Hierarchical clustering method (explained in section 2.3), (4) return these phase attribution information to Lammps and continue MD running, (5) repeat steps 1~4 periodically. With a good knowledge of the source code of Lammps and parallel programming, we have realized this algorithm and developed this interface C++ code, and tested to be well running.

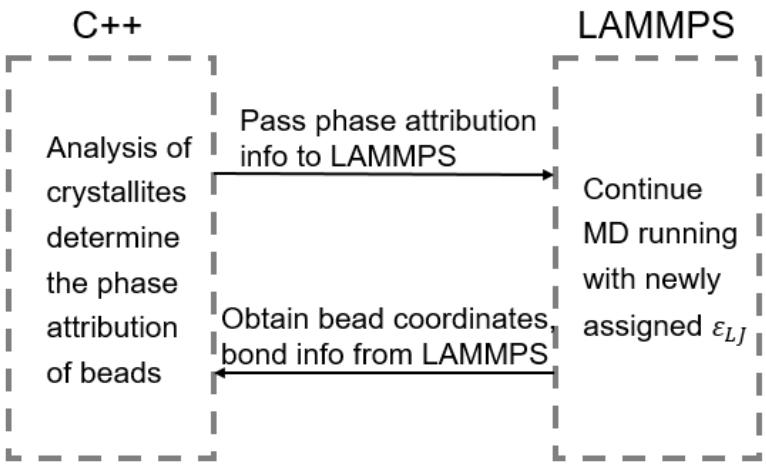

Figure 6-1 Diagram illustrating the C++ interface invoking LAMMPS as a library.

We have done a test of this C++-LAMMPS interface on the semi-crystalline polymer model of system LC50 as explained in section 3.2.1, consisting of 100 long chains (chain length is 500 beads) and 500 short chains (chain length is 100 beads), which makes 50% of weight fraction of long chain content.

6.3 Results and Discussion

In Figure 6-2, we have tested several different possibilities of $\varepsilon_{LJ}(crystal)$, which equals to $1.0\varepsilon_u$, $2.0\varepsilon_u$, $10.0\varepsilon_u$, whereas $\varepsilon_{LJ}(amorph)$ equals to $1.0\varepsilon_u$ in all cases. It is shown that the elevated $\varepsilon_{LJ}(crystal)$ results in a higher yield stress in the mechanical deformation. Clearly, choosing a rational multiple is essential to build the realistic model. Experimentally, it is possible to obtain the yield stress of a pure amorphous polymer, nevertheless it is not possible to access the yield stress of a pure perfect crystalline polymer. This suggests that direct relation of yield stress between pure amorphous domain and perfect crystal is inaccessible in experiment. One possible solution is to build the relation $\varepsilon_{LJ}(crystal) = x \cdot \varepsilon_{LJ}(amorph)$ to fit the experimental yield stress of semicrystalline polymers. For example take the experimental yield stress-strain curves of a polymer at two different initial crystallinities (e.g. X_{c1}, X_{c2}), build two simulation systems with crystallinities X_{c1}, X_{c2}, perform tensile test on these two systems and adjust x to make the yield strain stress curves fit with the experimental results. This test would

consume a lot of time, and for now we use $\varepsilon_{LJ}(crystal) = 10 \cdot \varepsilon_{LJ}(amorph)$ to test the feasibility of this proposal.

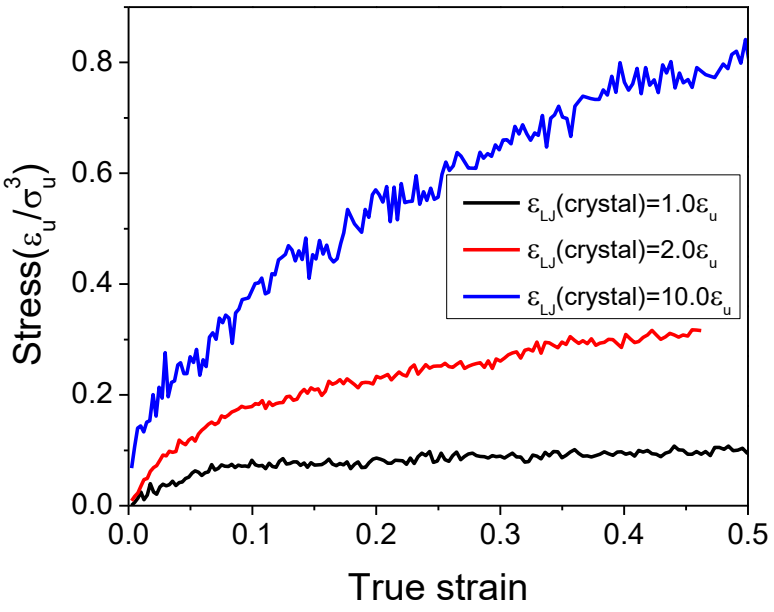

Figure 6-2 Stress-strain curves of system LC50 at temperature 2.0 ε_u/k_B, with a deformation rate is $10^{-5}\tau_u^{-1}$, at various epsilons of Lennard-Jones potential for the crystalline phase, $\varepsilon_{LJ}(amorph)$=1.0ε_u.

In Figure 6-3, we have performed mechanical deformation on system LC50 at temperature 2.0 ε_u/k_B (T_g= 2.0 ε_u/k_B) with the deformation rate is $10^{-5}\,\tau_u^{-1}$, and $\varepsilon_{LJ}(crystal)$=10.0$\varepsilon_u$. The samples are deformed in the z-direction. Over the entire range of deformation, crystallinity decreases slightly and then increases back to the initial level, as shown in Figure 6-3a. In Figure 6-3b, the true strain-stress curve has been plotted. An elastic regime is observed at low deformations, followed with a stress plateau before entering the strain-hardening regime at very large deformations.

Figure 6-3c shows the number of amorphous segments during deformation. The number of loop segments maintains and fluctuates at the similar level. Whereas tie segments also maintain at the same level in the elastic regime and the stress plateau, and then turn to increase when the deformation enters the strain-hardening regime. Figure 6-4 shows the conformations of the simulation system at different stages of deformation. At low strains, the folded chains align

partially in the direction of tensile stress. At high deformations in the strain-hardening regime, chains are partially unfolded and chain segments in amorphous and crystalline phases are stretched and aligned as a result of tensile stress. From strain $\varepsilon = 1.0$ to $\varepsilon = 1.5$, evident fragmentation of the large crystalline domains can be observed, which also explains the increase of the tie segments.

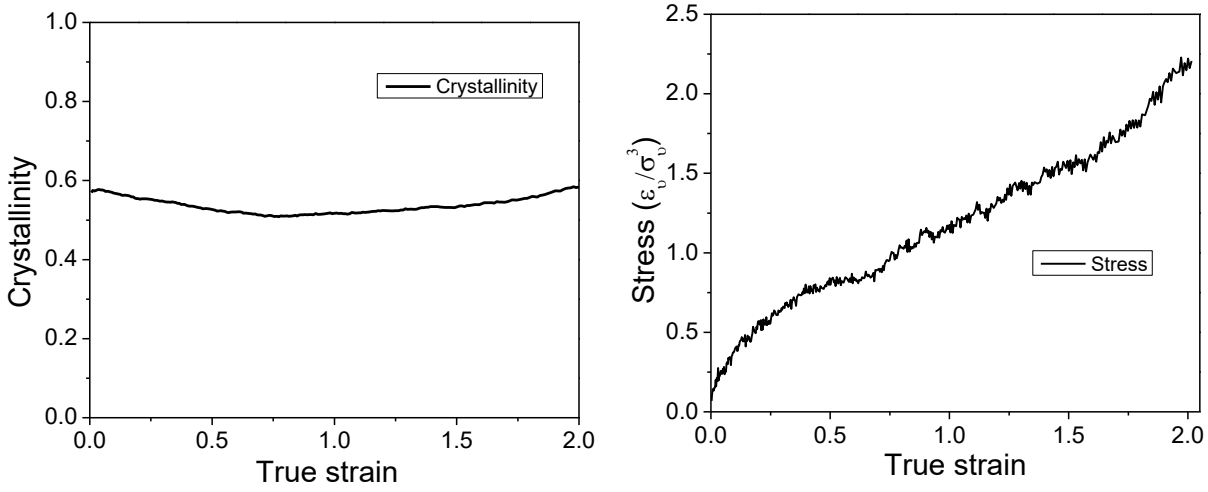

Figure 6-3 (a) Crystallinity of system LC50 as a function of true strain at temperature 2.0 ε_u/k_B, deformation rate is $10^{-5}\,\tau_u^{-1}$. (b) Strain-stress curve. (c) Number of segments as a function of true strain.

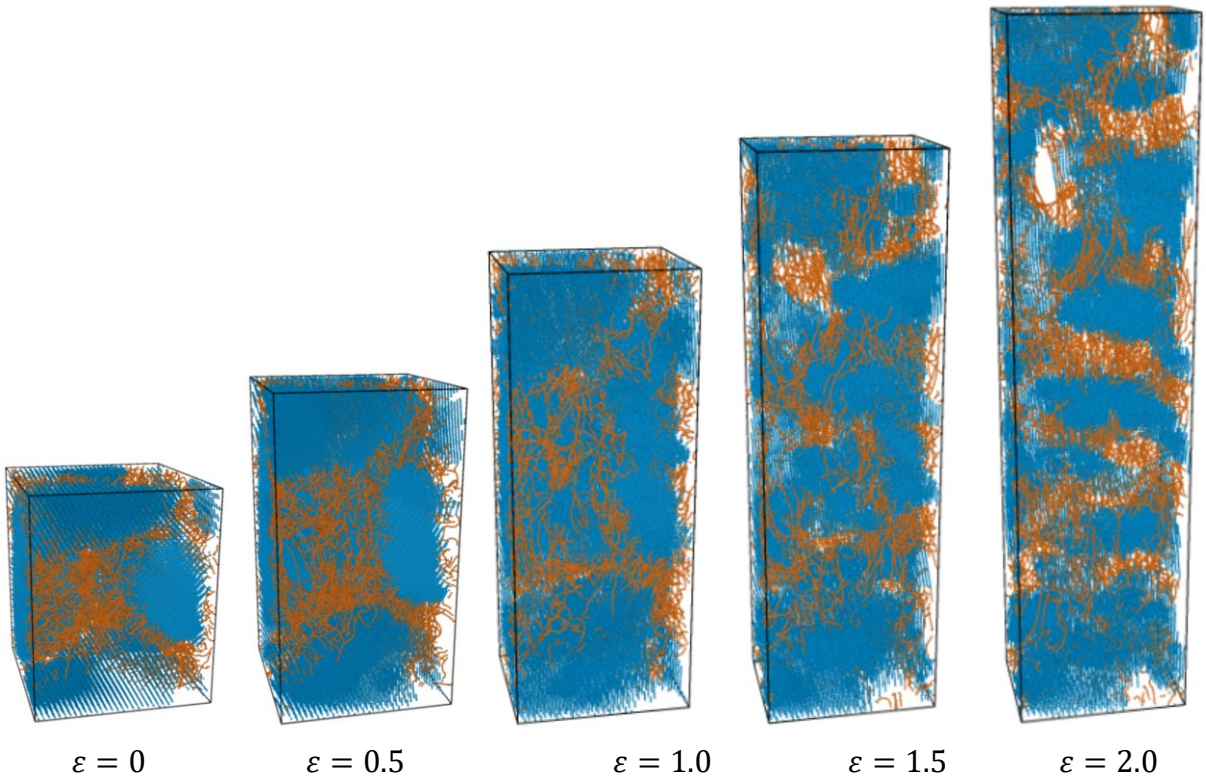

Figure 6-4 Snapshots of the deformed semicrystalline system taken at different strain levels.

6.4 Perspectives

In this chapter, we only perform some relatively simple tests of the idea adapting different LJ potentials for crystalline and amorphous phases of semicrystalline polymers. A more realistic model had been built mimicking the mechanical deformation of semicrystalline polymers. With this model, we will monitor the molecular topology (*i.e.* loop/tie/cilia) and entanglements during polymer deformation and obtain more insights of the correlation between microstructure and mechanical properties in the future.

Chapter 7

Conclusions and perspectives

Contents

7.1 Conclusions

In this thesis, the nucleation and crystal growth of uni and bimodal molecular weight distribution polymers are investigated using coarse grained molecular dynamics (CG-MD) simulations. A coarse grained (CG) model with optimized Lennard-Jones potential, developed in a previous article of our research group [1], is employed in this work. This CG model provides an angular force for chain aligning and is favorable for homogeneous nucleation.

We have found that the incubation time of nucleation decreases with rising weight fraction of long chains, and that the long-chain content has opposite effects on nucleation in the perspective of interfacial free energy and chain segment diffusion. Interfacial free energy decreases with weight fraction of long chains, which we attribute to the competition of chain-folded and chain-extended nucleation. We have provided insights into how bimodal MWD polymer promotes both nucleation and processability, which has been rarely addressed before. In addition, the molecular topology of semi-crystalline systems has been quantitatively accessed. It has been proved that the number of loop and tie segments increases with rising weight fraction of long chain content.

A Growing Probability Method has been proposed to calculate the critical size of nucleus over a range of temperatures. The interfacial free energy is calculated using a cylinder model and found to decrease with temperature. We have calculated the free energy barrier and

activation energy of diffusion, and compared the nucleation rate with classical nucleation theory, which proves the validity of CNT. The simulation has been performed on a bimodal system and a unimodal system with equivalent average molecular weight. Compared to unimodal polymers, the bimodal system exhibits higher nucleation rate. We attribute the promoted nucleation rate of bimodal system to its lower energy barrier resulted from the intramolecular nucleation mode of its long chain content; the high mobility of the short chains does not contribute a lot but may promote the crystal growth rate instead.

Through the primitive path analysis, the entanglement evolution has been continuously monitored during crystallization. We have proved that the crystallization process is correlated to chain disentangling, and shown a quantitative correlation between disentanglement degree and the crystallinity. With the advantage of molecular simulation, we have described polymer crystallization as a process of chain disentangling on the interface of crystal and melted phases in the manner of chain sliding diffusion. Lamellar thickness also displays a linear relation with the degree of disentanglement at all referred temperatures, and the temperature dependence of lamellar thickness is simply a result of temperature dependence of chain sliding diffusion. Bimodal system exhibits a higher lamellar thickness than unimodal system with the same average molecular weight, also because low molecular weight component enhances lamellar thickness because of high sliding mobility. Our observations support Hikosaka's sliding diffusion theory. Compared with unimodal system, the bimodal system reaches a larger lamellar thickness at all temperatures due to the promotion of short chain component.

Observing topological features and entanglements is difficult in experiments. Our observations with MD simulation provides a quantitative proof to the long-term debate of molecular topology, disentanglement and lamellar thickening, which is sensitive to bimodality as a result of high chain sliding mobility of the short chain component. The important role of

molecular topology, entanglements and chain sliding diffusion sheds a light on deeper understanding of polymer crystallization.

7.2 Perspectives

Topological features and entanglement in semicrystalline polymers are believed to play an important role in the mechanical properties. Nevertheless, direct experimental measurement of the molecular topology is not easy, especially during deformation. However, there are already a few frontier researches [21,26,27,123] that have addressed the effect of molecular topology on mechanical properties by molecular dynamics simulation. It has been found that an increase in stress transmitters, which are molecular networks, such as tie segments and bridging entanglements, increases the yielding stress and decreases the generation of voids. As expected, bridging entanglements are stretched, and these persistent bridging entanglements behave similarly to tie segments during deformation. However, the evolution of molecular topology in the process of semicrystalline polymer deformation would be also very interesting, and it has never been investigated to the author's knowledge. Further work on this point can enhance the molecular understanding of the mechanical properties of bimodal MWD semi-crystalline polymers. In chapter 6, we have already built a first step towards a more realistic model for mechanical deformation adopting elevated weak bond potential for crystalline phase compared with the amorphous phase. Further work will be done based on this model.

References

(1) Morthomas, J.; Fusco, C.; Zhai, Z.; Lame, O.; Perez, M. Crystallization of Finite-Extensible Nonlinear Elastic Lennard-Jones Coarse-Grained Polymers. *Phys. Rev. E* **2017**, *96* (5), 52502.

(2) Nishi, M.; Hikosaka, M.; Ghosh, S. K.; Toda, A.; Yamada, K. Molecular Weight Dependence of Primary Nucleation Rate of Polyethylene I. An Extended Chain Single Crystal. *Polymer J.* 1999, pp 749–758.

(3) Long, Y.; Shanks, R. A.; Stachurski, Z. H. Kinetics of Polymer Crystallisation. *Prog. Polym. Sci.* **1995**, *20* (4), 651–701.

(4) Song, S. J.; Wu, P. Y.; Ye, M. X.; Feng, J. C.; Yang, Y. L. Effect of Small Amount of Ultra High Molecular Weight Component on the Crystallization Behaviors of Bimodal High Density Polyethylene. *Polymer (Guildf).* **2008**, *49* (12), 2964–2973.

(5) G. W. Ehrenstein; Richard P., T. *Polymeric Materials: Structure, Properties, Applications*; Hanser Verlag, 2001.

(6) Humbert, S.; Lame, O.; Vigier, G. Polyethylene Yielding Behaviour: What Is behind the Correlation between Yield Stress and Crystallinity? *Polymer (Guildf).* **2009**, *50* (15), 3755–3761.

(7) Humbert, S.; Lame, O.; Chenal, J. M.; Rochas, C.; Vigier, G. New Insight on Initiation of Cavitation in Semicrystalline Polymers: In-Situ SAXS Measurements. *Macromolecules* **2010**, *43* (17), 7212–7221.

(8) Guo, Q. *Polymer Morphology : Principles, Characterization, and Processing*.

(9) Bunn, C. W. The Crystal Structure of Long-Chain Normal Paraffin Hydrocarbons. The “Shape” of the CH2 Group. *Trans. Faraday Soc.* **1939**, *35* (0), 482–491.

(10) Natta, G.; Corradini, P. General Considerations on the Structure of Crystalline

Polyhydrocarbons. *Nuovo Cim. Ser. 10* **1960**, *15* (1 Supplement), 9–39.

(11) Bunn, C. W. Crystal Structure of Polyvinyl Alcohol [6]. *Nature* **1948**, *161* (4102), 929–930.

(12) Bunn CW, Garner EV, B. W. The Crystal Structures of Two Polyamides ('Nylons'). *Proc. R. Soc. London. Ser. A. Math. Phys. Sci.* **1947**, *189* (1016), 39–68.

(13) Mark, J. E. *Methods of X-Ray and Neutron Scattering in Polymer Science*; Oxford University Press New York, 2000; Vol. 739.

(14) Seguela, R. Critical Review of the Molecular Topology of Semicrystalline Polymers: The Origin and Assessment of Intercrystalline Tie Molecules and Chain Entanglements. *J. Polym. Sci. Part B Polym. Phys.* **2005**, *43* (14), 1729–1748.

(15) Huang, Y. L.; Brown, N. DEPENDENCE OF SLOW CRACK-GROWTH IN POLYETHYLENE ON BUTYL BRANCH DENSITY - MORPHOLOGY AND THEORY. *J. Polym. Sci. Part B-Polymer Phys.* **1991**, *29* (1), 129–137.

(16) Garcia, R. A.; Carrero, A.; Martin, C.; Dominguez, C. Effects of the Structural Components on Slow Crack Growth Process in Polyethylene Blends. Composition Intervals Prediction for Pipe Applications. *J. Appl. Polym. Sci.* **2011**, *121* (6), 3269–3276.

(17) Kumar, V.; Locker, C. R.; In 't Veld, P. J.; Rutledge, G. C. Effect of Short Chain Branching on the Interlamellar Structure of Semicrystalline Polyethylene. *Macromolecules* **2017**, *50* (3), 1206–1214.

(18) Nilsson, F.; Gedde, U. W.; Hedenqvist, M. S. Modelling the Relative Permittivity of Anisotropic Insulating Composites. *Compos. Sci. Technol.* **2011**, *71* (2), 216–221.

(19) Gautam, S.; Balijepalli, S.; Rutledge, G. C. Molecular Simulations of the Interlamellar Phase in Polymers: Effect of Chain Tilt. *Macromolecules* **2000**, *33* (24), 9136–9145.

(20) Nilsson, F.; Lan, X.; Gkourmpis, T.; Hedenqvist, M. S.; Gedde, U. W. Modelling Tie Chains and Trapped Entanglements in Polyethylene. *Polymer (Guildf).* **2012**, *53* (16),

3594–3601.

(21) Lee, S.; Rutledge, G. C. Plastic Deformation of Semicrystalline Polyethylene by Molecular Simulation. *Macromolecules* **2011**, *44*, 3096–3108.

(22) Makke, A.; Lame, O.; Perez, M.; Barrat, J.-L. Influence of Tie and Loop Molecules on the Mechanical Properties of Lamellar Block Copolymers. *Macromolecules* **2012**, *45* (20), 8445–8452.

(23) Humbert, S.; Lame, O.; Séguéla, R.; Vigier, G. A Re-Examination of the Elastic Modulus Dependence on Crystallinity in Semi-Crystalline Polymers. *Polymer (Guildf).* **2011**, *52* (21), 4899–4909.

(24) Xiong, B. J.; Lame, O.; Chenal, J. M.; Men, Y. F.; Seguela, R.; Vigier, G. Critical Stress and Thermal Activation of Crystal Plasticity in Polyethylene: Influence of Crystal Microstructure and Chain Topology. *Polymer (Guildf).* **2017**, *118*, 192–200.

(25) Che, J.; Locker, C. R.; Lee, S.; Rutledge, G. C.; Hsiao, B. S.; Tsou, A. H. Plastic Deformation of Semicrystalline Polyethylene by X-Ray Scattering: Comparison with Atomistic Simulations. *Macromolecules* **2013**, *46*, 5279–5289.

(26) Kim, J. M.; Locker, R.; Rutledge, G. C. Plastic Deformation of Semicrystalline Polyethylene under Extension, Compression, and Shear Using Molecular Dynamics Simulation. *Macromolecules* **2014**, *47*, 2515–2528.

(27) Higuchi, Y.; Kubo, M. Deformation and Fracture Processes of a Lamellar Structure in Polyethylene at the Molecular Level by a Coarse-Grained Molecular Dynamics Simulation. *Macromolecules* **2017**, *50* (9), 3690–3702.

(28) Hu, W. The Physics of Polymer Chain-Folding. *Phys. Rep.* **2018**, *747*, 1–50.

(29) Patlazhan, S.; Remond, Y. Structural Mechanics of Semicrystalline Polymers Prior to the Yield Point: A Review. *J. Mater. Sci.* **2012**, *47* (19), 6749–6767.

(30) Moyassari, A.; Gkourmpis, T.; Hedenqvist, M. S.; Gedde, U. W. Molecular Dynamics

Simulations of Short-Chain Branched Bimodal Polyethylene: Topological Characteristics and Mechanical Behavior. *Macromolecules* **2019**, *52* (3), 807–818.

(31) García, R. A.; Carrero, A.; Martín, C.; Domínguez, C. Effects of the Structural Components on Slow Crack Growth Process in Polyethylene Blends. Composition Intervals Prediction for Pipe Applications. *J. Appl. Polym. Sci.* **2011**, *121* (6), 3269–3276.

(32) Bartczak, Z. Effect of Chain Entanglements on Plastic Deformation Behavior of Linear Polyethylene. *Macromolecules* **2005**, *38* (18), 7702–7713.

(33) Schrauwen, B. A. G.; Janssen, R. P. M.; Govaert, L. E.; Meijer, H. E. H. Intrinsic Deformation Behavior of Semicrystalline Polymers. *Macromolecules* **2004**, *37* (16), 6069–6078.

(34) Haward, R. N. Strain Hardening of Thermoplastics. *Macromolecules* **1993**, *26* (22), 5860–5869.

(35) Monasse, B.; Queyroy, S.; Lhost, O. Molecular Dynamics Prediction of Elastic and Plastic Deformation of Semi-Crystalline Polyethylene. *Int. J. Mater. Form.* **2008**.

(36) Sides, S. W.; Grest, G. S.; Stevens, M. J.; Plimpton, S. J. Effect of End-Tethered Polymers on Surface Adhesion of Glassy Polymers. *J. Polym. Sci. Part B Polym. Phys.* **2004**.

(37) Mowry, S. W.; Rutledge, G. C. Atomistic Simulation of the Ac-Relaxation in Crystalline Polyethylene. *Macromolecules* **2002**, *35* (11), 4539–4549.

(38) Nakagawa, K.; Ishida, Y. Annealing Effects in Poly(Vinylidene Fluoride) as Revealed by Specific Volume Measurements, Differential Scanning Calorimetry, and Electron Microscopy. *J. Polym. Sci. Part A-2 Polym. Phys.* **1973**.

(39) Arous, M.; Amor, I. Ben; Kallel, A.; Fakhfakh, Z.; Perrier, G. Crystallinity and Dielectric Relaxations in Semi-Crystalline Poly(Ether Ether Ketone). *J. Phys. Chem. Solids* **2007**, *68* (7), 1405–1414.

(40) Séguéla, R. Dislocation Approach to the Plastic Deformation of Semicrystalline Polymers: Kinetic Aspects for Polyethylene and Polypropylene*. *J. Polym. Sci. Part B Polym. Phys.* **2002**, *40* (6), 593–601.

(41) Suresh, G.; Jatav, S.; Geethu, P. M.; Rephung, Y.; Ramachandra Rao, M. S.; Satapathy, D. K. Poly(Vinylidene Fluoride)-Formvar Blends: Dielectric, Miscibility and Mechanical Studies. *J. Phys. D. Appl. Phys.* **2018**, *51* (6), 065604.

(42) Rekik, H.; Ghallabi, Z.; Royaud, I.; Arous, M.; Seytre, G.; Boiteux, G.; Kallel, A. Dielectric Relaxation Behaviour in Semi-Crystalline Polyvinylidene Fluoride (PVDF)/TiO2 Nanocomposites. *Compos. Part B Eng.* **2013**, *45* (1), 1199–1206.

(43) Hoffman, J. D.; Weeks, J. J. Rate of Spherulitic Crystallization with Chain Folds in Polychlorotrifluoroethylene. *J. Chem. Phys.* **1962**, *37* (8), 1723–1741.

(44) Yi, P.; Locker, C. R.; Rutledge, G. C. Molecular Dynamics Simulation of Homogeneous Crystal Nucleation in Polyethylene. *Macromolecules* **2013**, *46* (11), 4723–4733.

(45) Kampmann, R.; Wagner, R. Kinetics of Precipitation in Metastable Binary Alloys-Theory and Application to Cu--1. 9 At% Ti and Ni-14 At% Al. In *Decomposition of Alloys: the Early Stages*; Elsevier, 1984; pp 91–103.

(46) Shen, H. W.; Xie, B. H.; Yang, W.; Yang, M. B. Thermal and Rheological Properties of Polyethylene Blends with Bimodal Molecular Weight Distribution. *J. Appl. Polym. Sci.* **2013**, *129* (4), 2145–2151.

(47) Nikoubashman, A.; Howard, M. P. Equilibrium Dynamics and Shear Rheology of Semiflexible Polymers in Solution. *Macromolecules* **2017**, *50* (20), 8279–8289.

(48) Vlassopoulos, D.; Harmandaris, V. A.; Mavrantzas, V. G.; Theodorou, D. N.; Kröger, M.; Ramirez, J.; Öttinger, H. C. Crossover from the Rouse to the Entangled Polymer Melt Regime: Signals from Long, Detailed Atomistic Molecular Dynamics Simulations, Supported by Rheological Experiments. *Macromolecules* **2003**, *36* (Md), 1376–1387.

(49) Rouse, P. E. A Theory of the Linear Viscoelastic Properties of Dilute Solutions of Coiling Polymers. *J. Chem. Phys.* **1953**, *21* (7), 1272–1280.

(50) De Gennes, P. G. Reptation of a Polymer Chain in the Presence of Fixed Obstacles. *J. Chem. Phys.* **1971**, *55* (2), 572–579.

(51) Ibhadon, A. O. Crystallization Regimes and Reptation in Polypropylene Molecular Weight Fractions. *J. Appl. Polym. Sci.* **1999**.

(52) Hoffman, J. D.; Lauritzen, J. I. Crystallization of Bulk Polymers with Chain Folding-Theory of Growth of Lamellar Spherulites. *J. Res. Natl. Bur. Stand. (1934).* **1961**, No. 4, 297--+.

(53) Lauritzen, JI and Hoffman, J. D. Theory of Formation of Polymer Crystals with Folded Chains in Dilute Solution. *J. Res. Natl. Bur. Stand. (1934).* **1960**, *64* (1), 73102.

(54) Jiang, X.; Reiter, G.; Hu, W. How Chain-Folding Crystal Growth Determines the Thermodynamic Stability of Polymer Crystals. *J. Phys. Chem. B* **2016**, *120* (3), 566–571.

(55) Luo, C.; Sommer, J.-U. Growth Pathway and Precursor States in Single Lamellar Crystallization: MD Simulations. *Macromolecules* **2011**, *44*, 1523–1529.

(56) Yamamoto, T. Molecular Dynamics Simulations of Polymer Crystallization in Highly Supercooled Melt: Primary Nucleation and Cold Crystallization. *J. Chem. Phys.* **2010**, *133*, 34904.

(57) Welch, P.; Muthukumar, M. Molecular Mechanisms of Polymer Crystallization from Solution. *Phys. Rev. Lett.* **2001**, *87* (21), 218302-1-218302–218304.

(58) Muthukumar, M. Modeling Polymer Crystallization. *Advances in Polymer Science*. 2005.

(59) Strobl, G. From the Melt via Mesomorphic and Granular Crystalline Layers to Lamellar Crystallites: A Major Route Followed in Polymer Crystallization? *Eur. Phys. J. E* **2000**.

(60) Mullin, N.; Hobbs, J. K. Direct Imaging of Polyethylene Films at Single-Chain Resolution with Torsional Tapping Atomic Force Microscopy. *Phys. Rev. Lett.* **2011**,

107 (19), 197801.

(61) Lorenzo, A. T.; Müller, A. J. Estimation of the Nucleation and Crystal Growth Contributions to the Overall Crystallization Energy Barrier. *J. Polym. Sci. Part B Polym. Phys.* **2008**, *46* (14), 1478–1487.

(62) Hubert, L.; David, L.; Séguéla, R.; Vigier, G.; Corfias-Zuccalli, C.; Germain, Y. Physical and Mechanical Properties of Polyethylene for Pipes in Relation to Molecular Architecture. II. Short-term Creep of Isotropic and Drawn Materials. *J. Appl. Polym. Sci.* **2002**, *84* (12), 2308–2317.

(63) Zhang, S.; Zhao, N.; Wu, Y.; Dong, Q.; Wang, Q.; Tang, Y.; Yu, Y.; Da, J.; He, X.; Cheng, R. Short Chain Branches Distribution Characterization of Ethylene/1-Hexene Copolymers by Using TREF+ 13C-NMR and TREF+ SC Methods. In *Macromolecular Symposia*; Wiley Online Library, 2012; Vol. 312, pp 63–71.

(64) Krishnaswamy, R. K.; Yang, Q.; Fernandez-Ballester, L.; Kornfield, J. A. Effect of the Distribution of Short-Chain Branches on Crystallization Kinetics and Mechanical Properties of High-Density Polyethylene. *Macromolecules* **2008**, *41* (5), 1693–1704.

(65) Lenzi, M. K.; Cunningham, M. F.; Lima, E. L.; Pinto, J. C. Producing Bimodal Molecular Weight Distribution Polymer Resins Using Living and Conventional Free-Radical Polymerization. *Ind. Eng. Chem. Res.* **2005**, *44* (8), 2568–2578.

(66) Li, W.; Guan, C.; Xu, J.; Chen, Z. R.; Jiang, B. B.; Wang, J. D.; Yang, Y. R. Bimodal/Broad Polyethylene Prepared in a Disentangled State. *Ind. Eng. Chem. Res.* **2014**, *53* (3), 1088–1096.

(67) Krumme, A.; Lehtinen, A.; Viikna, A. Crystallisation Behaviour of High Density Polyethylene Blends with Bimodal Molar Mass Distribution 1. Basic Characteristics and Isothermal Crystallisation. *Eur. Polym. J.* **2004**, *40* (2), 359–369.

(68) Krumme, A.; Lehtinen, A.; Viikna, A. Crystallisation Behaviour of High Density

Polyethylene Blends with Bimodal Molar Mass Distribution 2. Non-Isothermal Crystallisation. *Eur. Polym. J.* **2004**, *40* (2), 371–378.

(69) Zuo, F.; Keum, J. K.; Yang, L.; Somani, R. H.; Hsiao, B. S. Thermal Stability of Shear-Induced Shish-Kebab Precursor Structure from High Molecular Weight Polyethylene Chains. *Macromolecules* **2006**, *39* (6), 2209–2218.

(70) Yang, L.; Somani, R. H.; Sics, I.; Hsiao, B. S.; Kolb, R.; Fruitwala, H.; Ong, C. Shear-Induced Crystallization Precursor Studies in Model Polyethylene Blends by in-Situ Rheo-SAXS and Rheo-WAXD. *Macromolecules* **2004**, *37* (13), 4845–4859.

(71) He, X. L.; Wang, Y. H.; Wang, Q. T.; Tang, Y.; Liu, B. P. Effects of Addition of Ultra-High Molecular Weight Polyethylene on Tie-Molecule and Crystallization Behavior of Unimodal PE-100 Pipe Materials. *J. Macromol. Sci. Part B-Physics* **2016**, *55* (10), 1007–1021.

(72) Shen, H. W.; Luan, T.; Xie, B. H.; Yang, W.; Yang, M. B. Rheological Behaviors and Molecular Weight Distribution Characteristics of Bimodal High-Density Polyethylene. *J. Appl. Polym. Sci.* **2011**, *121* (3), 1543–1549.

(73) Moyassari, A.; Mostafavi, H.; Gkourmpis, T.; Hedenqvist, M. S.; Gedde, U. W.; Nilsson, F. Simulation of Semi-Crystalline Polyethylene: Effect of Short-Chain Branching on Tie Chains and Trapped Entanglements. *Polymer (Guildf).* **2015**, *72*, 177–184.

(74) Luo, C.; Kröger, M.; Sommer, J. U. Entanglements and Crystallization of Concentrated Polymer Solutions: Molecular Dynamics Simulations. *Macromolecules* **2016**, *49* (23), 9017–9025.

(75) Luo, C.; Sommer, J. U. Role of Thermal History and Entanglement Related Thickness Selection in Polymer Crystallization. *ACS Macro Lett.* **2016**.

(76) Luo, C.; Sommer, J. U. Frozen Topology: Entanglements Control Nucleation and Crystallization in Polymers. *Phys. Rev. Lett.* **2014**, *112* (19).

(77) Luo, C.; Sommer, J. U. Disentanglement of Linear Polymer Chains toward Unentangled Crystals. *ACS Macro Lett.* **2013**, *2* (1), 31–34.

(78) Shen, H. W.; Xie, B. H.; Yang, W.; Yang, M. B. Non-Isothermal Crystallization of Polyethylene Blends with Bimodal Molecular Weight Distribution. *Polym. Test.* **2013**, *32* (8), 1385–1391.

(79) Takeuchi, H. Structure Formation during the Crystallization Induction Period of a Short Chain-Molecule System: A Molecular Dynamics Study. *J. Chem. Phys.* **1998**, *109*, 5614.

(80) Fujiwara, S.; Sato, T. Molecular Dynamics Simulation of Structural Formation of Short Polymer Chains. *Phys. Rev. Lett.* **1998**, *80*, 991.

(81) Kremer, K.; Grest, G. S. Dynamics of Entangled Linear Polymer Melts: A Molecular-dynamics Simulation. *J. Chem. Phys.* **1990**, *92* (8), 5057–5086.

(82) Barrat, J.-L.; Baschnagel, J.; Lyulin, A. Molecular Dynamics Simulations of Glassy Polymers. *Soft Matter* **2010**, *6*, 3430.

(83) Hoy, R. S.; Robbins, M. O. Strain Hardening of Polymer Glasses: Effect of Entanglement Density, Temperature, and Rate. *J. Polym. Sci. Part B Polym. Phys.* **2006**, *44* (24), 3487–3500.

(84) Plimpton, S. Fast Parallel Algorithms for Short-Range Molecular Dynamics. *J. Comput. Phys.* **1995**, *117* (1), 1–19.

(85) Perez, M.; Lame, O.; Leonforte, F.; Barrat, J.-L. Polymer Chain Generation for Coarse-Grained Models Using Radical-like Polymerization. *J. Chem. Phys.* **2008**, *128* (23), 234904.

(86) Morgane, M.; Zhai, Z.; Perez, M.; Lame, O.; Fusco, C.; Chazeau, L.; Makke, A.; Marque, G.; Morthomas, J. Polymer Chain Generation for Coarse-Grained Models Using Radical-Like Polymerization. *Commun. Comput. Phys.* **2018**, *24* (3), 885–898.

(87) Vyazovkin, S.; Sbirrazzuoli, N. Isoconversional Analysis of Calorimetric Data on

Nonisothermal Crystallization of a Polymer Melt. *J. Phys. Chem. B* **2003**, *107* (3), 882–888.

(88) Strebel, J. J.; Moet, A. The Effects of Annealing on Fatigue Crack Propagation in Polyethylene. *J. Polym. Sci. Part B Polym. Phys.* **1995**, *33* (13), 1969–1984.

(89) Huang, Y. L.; Brown, N. The Effect of Molecular Weight on Slow Crack Growth in Linear Polyethylene Homopolymers. *J. Mater. Sci.* **1988**, *23* (10), 3648–3655.

(90) Humbert, S.; Lame, O.; Chenal, J.-M.; Seguela, R.; Vigier, G. Memory Effect of the Molecular Topology of Lamellar Polyethylene on the Strain-Induced Fibrillar Structure. *Eur. Polym. J.* **2012**, *48* (6), 1093–1100.

(91) Brown, N.; Ward, I. M. The Influence of Morphology and Molecular Weight on Ductile-Brittle Transitions in Linear Polyethylene. *J. Mater. Sci.* **1983**, *18* (5), 1405–1420.

(92) Seguela, R. On the Natural Draw Ratio of Semi-Crystalline Polymers: Review of the Mechanical, Physical and Molecular Aspects. *Macromol. Mater. Eng.* **2007**, *292* (3), 235–244.

(93) Liu, Z. H.; Wang, C. S.; Wang, X. Q.; Huang, N. X.; Filippini-Fantoni, R. Monte Carlo Technique to Simulate Amide Interchange Reactions, 3 - Influence of Amide Interchange Reactions on Molecular Weight Distribution. *Macromol. Theory Simulations* **2005**, *14* (3), 164–171.

(94) Tobita, H. Bimodal Molecular Weight Distribution Formed in the Emulsion Polymerization of Ethylene. *J. Polym. Sci. Part a-Polymer Chem.* **2002**, *40* (20), 3426–3433.

(95) Tobita, H. Bimodal Molecular Weight Distribution Formed in Emulsion Polymerization with Long-Chain Branching. *Polym. React. Eng.* **2003**, *11* (4), 855–868.

(96) Deiber, J. A.; Peirotti, M. B.; Gappa, A. The Linear Viscoelastic Relaxation Modulus Related to the MWD of Linear Homopolymer Blends. *J. Elastomers Plast.* **1997**, *29* (4),

290–313.

(97) Wedekind, J.; Strey, R.; Reguera, D. New Method to Analyze Simulations of Activated Processes. *J. Chem. Phys.* **2007**, *126* (13), 134103.

(98) Anwar, M.; Berryman, J. T.; Schilling, T. Crystal Nucleation Mechanism in Melts of Short Polymer Chains under Quiescent Conditions and under Shear Flow. *J. Chem. Phys.* **2014**, *141* (12), 124910.

(99) Harmandaris, V. A.; Mavrantzas, V. G.; Theodorou, D. N. Atomistic Molecular Dynamics Simulation of Polydisperse Linear Polyethylene Melts. *Macromolecules* **1998**, *31* (22), 7934–7943.

(100) Yamamoto, T. Molecular Dynamics Simulation of Polymer Ordering. II. Crystallization from the Melt. *J. Chem. Phys.* **2001**, *115*, 8675.

(101) Kong, Y.; Hay, J. N. The Measurement of the Crystallinity of Polymers by DSC. *Polymer (Guildf).* **2002**, *43* (14), 3873–3878.

(102) Li, Z.; Zhang, W.; Feng, L. Y.; Shen, X. T.; Mai, Y. Y. Role of the Amorphous Morphology in Physical Properties of Ultra High Molecular Weight Polyethylene. *Polym. Plast. Technol. Eng.* **2014**, *53* (11), 1194–1204.

(103) Triandafilidi, V.; Rottler, J.; Hatzikiriakos, S. G. Molecular Dynamics Simulations of Monodisperse/Bidisperse Polymer Melt Crystallization. *J. Polym. Sci. Part B Polym. Phys.* **2016**, *54* (22), 2318–2326.

(104) Kocic, N.; Lederhofer, S.; Kretschmer, K.; Bastian, M.; Heidemeyer, P. Nucleation Parameter and Size Distribution of Critical Nuclei for Nonisothermal Polymer Crystallization: The Influence of the Cooling Rate and Filler. *J. Appl. Polym. Sci.* **2015**, *132* (6).

(105) Kashchiev, B. D.; Heinemann, B. *Nucleation – Basic Theory with Applications Guide to Capital Cost Estimating*; Butterworth Heinemann: Oxford ;Boston, 2000.

(106) Achilias, D. S.; Papageorgiou, G. Z.; Karayannidis, G. P. Isothermal and Nonisothermal Crystallization Kinetics of Polypropylene Terephthalate. *J. Polym. Sci. Part B Polym. Phys.* **2004**, *42* (20), 3775–3796.

(107) Hu, W.; Frenkel, D. Polymer Crystallization Driven by Anisotropic Interactions. *Advances in Polymer Science*. 2005, pp 1–35.

(108) Flory, P. J. Thermodynamics of Crystallization in High Polymers. IV. A Theory of Crystalline States and Fusion in Polymers, Copolymers, and Their Mixtures with Diluents. *J. Chem. Phys.* **1949**, *17* (3), 223–240.

(109) Zachmann, H. G. Der Einfluß Der Konfigurationsentropie Auf Das Kristallisations- Und Schmelzverhalten von Hochpolymeren Stoffen. *Kolloid-Zeitschrift und Zeitschrift für Polym.* **1967**, *216*, 180–191.

(110) Zachmann, H. G. Statistische Thermodynamik Des Kristallisierens Und Schmelzens von Hochpolymeren Stoffen. *Kolloid-Zeitschrift und Zeitschrift für Polym.* **1969**, *231* (1–2), 504–534.

(111) Hoffman, J. D.; Miller, R. L. Kinetics of Crystallization from the Melt and Chain Folding in Polyethylene Fractions Revisited: Theory and Experiment. *Polymer (Guildf).* **1997**, *38* (13), 3151–3212.

(112) Meyer, H.; Müller-Plathe, F. Formation of Chain-Folded Structures in Supercooled Polymer Melts. *J. Chem. Phys.* **2001**, *115*, 7807.

(113) Hu, W.; Frenkel, D.; Mathot, V. B. F. Intramolecular Nucleation Model for Polymer Crystallization. *Macromolecules* **2003**, *36* (21), 8178–8183.

(114) Hu, W.; Frenkel, D.; Mathot, V. B. F. Free Energy Barrier to Melting of Single-Chain Polymer Crystallite. *J. Chem. Phys.* **2003**, *118* (8), 3455–3457.

(115) Ghosh, S. K.; Hikosaka, M.; Toda, A. Power Law of Nucleation Rate of Folded-Chain Single Crystals of Polyethylene. *Colloid Polym. Sci.* **2001**, *279* (4), 382–386.

(116) Kikutani, T.; Kawano, R.; Okui, N.; Umemoto, S.; Hayashi, R. Molecular Weight Dependence of Primary Nucleation Rate of Poly(Ethylene Succinate). *J. Macromol. Sci. Part B* **2003**, *42* (3), 421–430.

(117) Chen, X.; Carbone, P.; Cavalcanti, W. L.; Milano, G.; Müller-Plathe, F. Viscosity and Structural Alteration of a Coarse-Grained Model of Polystyrene under Steady Shear Flow Studied by Reverse Nonequilibrium Molecular Dynamics. *Macromolecules* **2007**, *40* (22), 8087–8095.

(118) Byutner, O.; Smith, G. D. Temperature and Molecular Weight Dependence of the Zero Shear-Rate Viscosity of an Entangled Polymer Melt from Simulation and Theory. *J. Polym. Sci. Part B-Polymer Phys.* **2001**, *39* (23), 3067–3071.

(119) Kraack, H.; Deutsch, M.; Sirota, E. B. N-Alkane Homogeneous Nucleation: Crossover To Polymer Behavior. *Macromolecules* **2000**, *33* (16), 6174–6184.

(120) Gee, R. H.; Fried, L. E. Ultrafast Crystallization of Polar Polymer Melts. *J. Chem. Phys.* **2003**, *118*, 3827.

(121) Sun, Y.; Matsumoto, M.; Haruki, M.; Kihara, S. I.; Takishima, S. Molecular Weight Dependence of the Crystallization of the Polycarbonate Induced by Supercritical CO2. *J. Supercrit. Fluids* **2016**, *113*, 144–149.

(122) Rastogi, S.; Lippits, D. R.; Höhne, G. W. H.; Mezari, B.; Magusin, P. C. M. M. The Role of the Amorphous Phase in Melting of Linear UHMW-PE; Implications for Chain Dynamics. *J. Phys. Condens. Matter* **2007**, *19* (20), 205122.

(123) Yeh, I.-C.; Andzelm, J. W.; Rutledge, G. C. Mechanical and Structural Characterization of Semicrystalline Polyethylene under Tensile Deformation by Molecular Dynamics Simulations. *Macromolecules* **2015**, *48*, 4228–4239.

(124) Sun, X.; Shen, H. W.; Xie, B. H.; Yang, W.; Yang, M. B. Fracture Behavior of Bimodal Polyethylene: Effect of Molecular Weight Distribution Characteristics. *Polymer (Guildf).*

2011, *52* (2), 564–570.

(125) Fujiwara, S.; Sato, T. Molecular Dynamics Simulation of Structure Formation of Short Chain Molecules. *J. Chem. Phys.* **1999**, *110*, 9757.

(126) Moyassari, A.; Gkourmpis, T.; Hedenqvist, M. S.; Gedde, U. W. Molecular Dynamics Simulation of Linear Polyethylene Blends: Effect of Molar Mass Bimodality on Topological Characteristics and Mechanical Behavior. *Polymer (Guildf).* **2019**, *161*, 139–150.

(127) Wu, T.; Yu, L.; Cao, Y.; Yang, F.; Xiang, M. Effect of Molecular Weight Distribution on Rheological, Crystallization and Mechanical Properties of Polyethylene-100 Pipe Resins. *J. Polym. Res.* **2013**, *20* (10), 271.

(128) Jabbari-Farouji, S.; Rottler, J.; Lame, O.; Makke, A.; Perez, M.; Barrat, J.-L. Plastic Deformation Mechanisms of Semicrystalline and Amorphous Polymers. *ACS Macro Lett.* **2015**, *4*, 147–150.

(129) Gee, R. H.; Lacevic, N.; Fried, L. E. Atomistic Simulations of Spinodal Phase Separation Preceding Polymer Crystallization. *Nat. Mater.* **2006**, *5*, 39–43.

(130) Uhlmann, D. R.; Kritchevsky, G.; Straff, R.; Scherer, G. Crystal Nucleation in Normal Alkane Liquids. *J. Chem. Phys.* **1975**, *62* (12), 4896–4903.

(131) Oliver, M. J.; Calvert, P. D. Homogeneous Nucleation of N-Alkanes Measured by Differential Scanning Calorimetry. *J. Cryst. Growth* **1975**, *30* (3), 343–351.

(132) Hoffman, J. D. The Relationship of C∞ to the Lateral Surface Free Energy σ: Estimation of C∞ for the Melt from Rate of Crystallization Data. *Polymer (Guildf).* **1992**, *33* (12), 2643–2644.

(133) Hoffman, J. D.; Roitman, D. B. Relationship between the Lateral Surface Free Energy and the Chain Structure of Melt-Crystallized Polymerst. *Macromolecules* **1992**, *25*, 2221–2229.

(134) Milner, S. T. Polymer Crystal-Melt Interfaces and Nucleation in Polyethylene. *Soft Matter* **2011**, *7* (6), 2909–2917.

(135) Zhai, Z.; Morthomas, J.; Fusco, C.; Perez, M.; Lame, O. Crystallization and Molecular Topology of Linear Semicrystalline Polymers: Simulation of Uni- and Bimodal Molecular Weight Distribution Systems. *Macromolecules* **2019**, acs.macromol.9b00071.

(136) Zhang, W.; Larson, R. G. Direct All-Atom Molecular Dynamics Simulations of the Effects of Short Chain Branching on Polyethylene Oligomer Crystal Nucleation. *Macromolecules* **2018**, *51* (13), 4762–4769.

(137) Hu, Y.; Shao, Y.; Liu, Z.; He, X.; Liu, B. Effect of Short-Chain Branching on the Tie Chains and Dynamics of Bimodal Polyethylene: Molecular Dynamics Simulation. *Eur. Polym. J.* **2018**, *103*, 312–321.

(138) Qi, S.; Yan, D. Nucleation in Polydisperse Polymer Mixtures. *J. Chem. Phys.* **2008**, *129* (20), 204902.

(139) Bai, X.-M.; Li, M. Calculation of Solid-Liquid Interfacial Free Energy: A Classical Nucleation Theory Based Approach. *J. Chem. Phys.* **2006**, *124* (12), 124707.

(140) Müller, A. J.; Michell, R. M.; Lorenzo, A. T. Isothermal Crystallization Kinetics of Polymers. In *Polymer Morphology*; John Wiley & Sons, Inc: Hoboken, NJ, USA, 2016; pp 181–203.

(141) Kornfield, J. A.; Kumaraswamy, G.; Issaian, A. M. Recent Advances in Understanding Flow Effects on Polymer Crystallization. *Ind. Eng. Chem. Res.* **2002**, *41* (25), 6383–6392.

(142) Nele, M.; Pinto, J. C. Molecular-Weight Multimodality of Multiple Flory Distributions. *Macromol. Theory Simulations* **2002**, *11* (3), 293–307.

(143) Maus, A.; Saalwächter, K. Crystallization Kinetics of Poly(Dimethylsiloxane) Molecular-Weight Blends - Correlation with Local Chain Order in the Melt? *Macromol.*

Chem. Phys. **2007**, *208* (19–20), 2066–2075.

(144) Hubert, L.; David, L.; Séguéla, R.; Vigier, G.; Degoulet, C.; Germain, Y. Physical and Mechanical Properties of Polyethylene for Pipes in Relation to Molecular Architecture. I. Microstructure and Crystallisation Kinetics. *Polymer (Guildf).* **2001**, *42* (20), 8425–8434.

(145) DesLauriers, P. J.; Cole, N.; Lamborn, M. C.; White, C. G.; Lavine, B. K. Chemometric Methods for Estimating the Strain Hardening Modulus in Polyethylene Resins. *Appl. Spectrosc.* **2018**, *72* (3), 463–475.

(146) Ko, M. J.; Waheed, N.; Lavine, M. S.; Rutledge, G. C. Characterization of Polyethylene Crystallization from an Oriented Melt by Molecular Dynamics Simulation. *J. Chem. Phys.* **2004**, *121* (6), 2823–2832.

(147) Ramos, J.; Vega, J. F.; Martínez-Salazar, J. Molecular Dynamics Simulations for the Description of Experimental Molecular Conformation, Melt Dynamics, and Phase Transitions in Polyethylene. *Macromolecules* **2015**, *48* (14), 5016–5027.

(148) Yeh, I. C.; Lenhart, J. L.; Rutledge, G. C.; Andzelm, J. W. Molecular Dynamics Simulation of the Effects of Layer Thickness and Chain Tilt on Tensile Deformation Mechanisms of Semicrystalline Polyethylene. *Macromolecules* **2017**, *50* (4), 1700–1712.

(149) Men, Y.; Rieger, J.; Strobl, G. Role of the Entangled Amorphous Network in Tensile Deformation of Semicrystalline Polymers. *Phys. Rev. Lett.* **2003**, *91* (9).

(150) Jabbari-Farouji, S.; Rottler, J.; Lame, O.; Makke, A.; Perez, M.; Barrat, J.-L. Correlation of Structure and Mechanical Response in Solid-like Polymers. *J. Phys. Condens. Matter* **2015**, *27*, 194131.

(151) Kröger, M. Shortest Multiple Disconnected Path for the Analysis of Entanglements in Two- and Three-Dimensional Polymeric Systems. *Comput. Phys. Commun.* **2005**, *168* (3), 209–232.

(152) Miyamoto, Y.; Tanzawa, Y.; Miyaji, H.; Kiho, H. Concentration Dependence of Lamellar Thickness of Isotactic Polystyrene at High Supercoolings. *J. Phys. Soc. Japan* **2005**, *58* (6), 1879–1882.

(153) Hikosaka, M. Unified Theory of Nucleation of Folded-Chain Crystals and Extended-Chain Crystals of Linear-Chain Polymers. *Polymer (Guildf).* **1987**, *28* (8), 1257–1264.

(154) Hikosaka, M. Unified Theory of Nucleation of Folded-Chain Crystals (FCCs) and Extended-Chain Crystals (ECCs) of Linear-Chain Polymers: 2. Origin of FCC and ECC. *Polymer (Guildf).* **1990**, *31* (3), 458–468.

(155) Cosgrove, T. Diffusion in Bimodal and Polydisperse Polymer Systems: 1. Bimodal Solutions of Protonated and Deuterated Polymers. *Polymer (Guildf).* **2002**, *36* (17), 3335–3342.

(156) Hikosaka, M.; Amano, K.; Rastogi, S.; Keller, A. Lamellar Thickening Growth of an Extended Chain Single Crystal of Polyethylene. 1. Pointers to a New Crystallization Mechanism of Polymers. *Macromolecules* **2002**, *30* (7), 2067–2074.

(157) Lippits, D. R.; Rastogi, S.; Talebi, S.; Bailly, C. Formation of Entanglements in Initially Disentangled Polymer Melts. *Macromolecules* **2006**, *39* (26), 8882–8885.

(158) Lippits, D. R.; Rastogi, S.; Höhne, G. W. H.; Mezari, B.; Magusin, P. C. M. M. Heterogeneous Distribution of Entanglements in the Polymer Melt and Its Influence on Crystallization. *Macromolecules* **2007**, *40* (4), 1004–1010.

(159) Foteinopoulou, K.; Karayiannis, N. C.; Mavrantzas, V. G.; Kröger, M. Primitive Path Identification and Entanglement Statistics in Polymer Melts: Results from Direct Topological Analysis on Atomistic Polyethylene Models. *Macromolecules* **2006**, *39* (12), 4207–4216.

(160) Sukumaran, S. K.; Grest, G. S.; Kremer, K.; Everaers, R. Identifying the Primitive Path Mesh in Entangled Polymer Liquids. *J. Polym. Sci. Part B Polym. Phys.* **2005**, *43* (8),

917–933.

(161) Hoffman, J. D. Theoretical Aspects of Polymer Crystallization with Chain Folds: Bulk Polymers. *Polym. Eng. Sci.* **1964**, *4* (4), 315–362.

(162) Rastogi, S.; Lippits, D. R.; Peters, G. W. M.; Graf, R.; Yao, Y.; Spiess, H. W. Heterogeneity in Polymer Melts from Melting of Polymer Crystals. *Nat. Mater.* **2005**, *4* (8), 635–641.

(163) Qin, H.; Li, F.; Wang, D.; Lin, H.; Jin, J. Organized Molecular Interface-Induced Noncrystallizable Polymer Ultrathin Nanosheets with Ordered Chain Alignment. *ACS Nano* **2016**, *10* (1), 948–956.

(164) Keshavarz, M.; Engelkamp, H.; Xu, J.; Braeken, E.; Otten, M. B. J.; Uji-I, H.; Schwartz, E.; Koepf, M.; Vananroye, A.; Vermant, J.; et al. Nanoscale Study of Polymer Dynamics. *ACS Nano* **2016**, *10* (1), 1434–1441.

(165) Verho, T.; Paajanen, A.; Vaari, J.; Laukkanen, A. Crystal Growth in Polyethylene by Molecular Dynamics: The Crystal Edge and Lamellar Thickness. *Macromolecules* **2018**, *51* (13), 4865–4873.

(166) Lacevic, N.; Fried, L. E.; Gee, R. H. Heterogeneous Directional Mobility in the Early Stages of Polymer Crystallization. *J. Chem. Phys.* **2008**, *128* (1).

FOLIO ADMINISTRATIF

THESE DE L'UNIVERSITE DE LYON OPEREE AU SEIN DE L'INSA LYON

NOM : ZHAI

DATE de SOUTENANCE : 30/09/2019

Prénoms : Zengqiang

TITRE : Molecular dynamics simulation of uni and bi-modal semicrystalline polymers: nucleation, chain topology and microstructure

NATURE : Doctorat

Numéro d'ordre : 2019LYSEI069

Ecole doctorale : ED34 Matériaux

Spécialité : Matériaux

RESUME : Semicrystalline polymers (such as polyethylene, polylactic acid, polyamide, etc.) are used in a wide range of application (such as automotive, pipes, gearing, etc.) due to promoted mechanical properties. There is strong link between the mechanical properties and microstructure of semicrystalline polymer. However, these microstructure cannot be access quantitatively in experiment. Thus, the crystallization mechanism of polymers and the dependence of microstructure remain relatively unclear and controversy.
In this thesis, we have performed the homogeneous crystallization of polymers using a coarse-grained molecular dynamics (CG-MD) model published in our previous article, which favors chain alignment and crystallization. The main objective of this thesis is to use CG-MD simulation technique to provide more insights of the homogeneous nucleation and crystal growth behavior of bimodal and unimodal MWD polymers, the influence of bimodality on the molecular topology (loop, tie, cilia) and entanglement concentration, the chain disentanglement process and its influence on lamellar thickening as well the temperature dependence.

MOTS-CLÉS : Semicrystalline polymer, molecular topology, bimodal molecular weight distribution, degree of entanglement, chain sliding diffusion, lamellar thickening

Laboratoire (s) de recherche : MATEIS, INSA de Lyon

Directeur de thèse : Olivier LAME
Co-directeur de thèse : Michel PEREZ

Président de jury :

Composition du jury :

BARRAT, Jean-Louis	Professeur	Université Grenoble Alpes	Rapporteur
BASCHNAGEL, Jörg	Professeur	Université de Strasbourg	Rapporteur
SOMMER, Jens-Uwe	Professeur	Technische Universität Dresden	Examinateur
CASTAGNET, Sylvie	Directrice de Recherche	Institut Pprime (CNRS)	Examinatrice
LAME, Olivier	Professeur	INSA-LYON	Directeur de thèse
FUSCO, Claudio	Maître de conférences	INSA-LYON	Encadrant
PEREZ, Michel	Professeur	INSA-LYON	Invité
MORTHOMAS, Julien	Maître de conférences	INSA-LYON	Invité